

PHOTO-INDUCED INTERFACIAL BIOMIMETIC
CATALYSIS ON NANOCRYSTALLINE METAL OXIDE
SEMICONDUCTORS

JAMIE P. VATERS



**Photo-Induced Interfacial Biomimetic Catalysis on
Nanocrystalline Metal Oxide Semiconductors**

By

© **Jamie P. Vaters**

A thesis submitted to the
School of Graduate Studies
in partial fulfillment of the
requirements for the degree of
Master of Science

The Department of Chemistry
Faculty of Science
Memorial University of Newfoundland

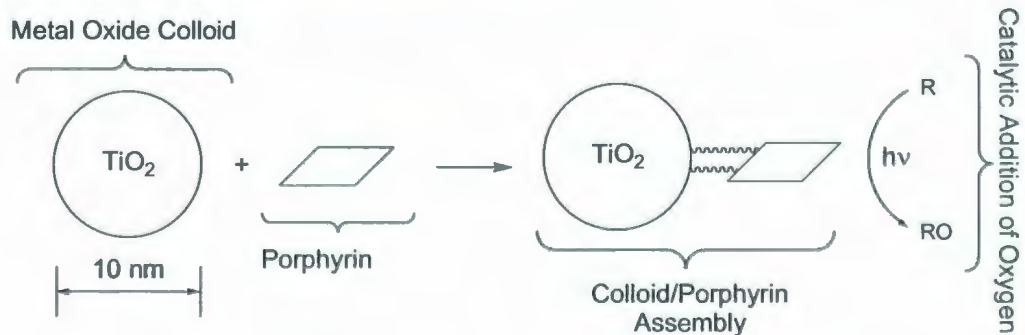
July 2009

St. John's

Newfoundland and Labrador

Abstract

The study of metal oxides (MO_x) materials began in the 1800's but the metal oxides were very difficult to characterize due to their amorphous and intractable nature. New and powerful experimental techniques whose sensitivity is on a nanometer scale have resulted in extraordinary advances in the field of nanotechnology. The characterization of MO_x in terms of size-domain and size-dependent properties has brought about a renaissance and intense interest in metal oxide materials. The versatility of these materials has led to a wide variety of applications from environmental cleanup catalysts to molecular electronics. More specifically, the development of DSSC's (dye sensitized solar cells) where titanium(IV) dioxide films are modified with surface-bound chromophores has shown impressive cost/performance ratios and these are now being used in low-current applications. The work presented in this dissertation includes: the fabrication of surface-derivatized nanoscale TiO_2 colloids for the purpose of photocatalytic insertion of oxygen, similar to that performed via thermally-activated metalloenzymes such as cytochrome P450 and horseradish peroxidase (HRP). The development and characterization of TiO_2 foundations, porphyrin/ TiO_2 assemblies and resulting proof-of-concept biomimetic photocatalysis is discussed. In addition, the preparation of free-standing TiO_2 /Nafion[®] membranes is presented.



Acknowledgements

I would like to thank my supervisor, Dr. David W. Thompson, for giving me the opportunity to work with him and his group. The years I have spent with him and his research group have been filled with enthusiasm, laughter, and friendship.

I want to express my gratitude to the faculty and staff, especially Dr. Graham Bodwell, Dr. D. Jean Burnell, Dr. Peter Pickup, Dr. Raymond Poirier, and Dr. Robert Davis. Your untiring words of advice and encouragement for the duration of my studies are greatly appreciated. The administration here is second to none and I would like to convey my thanks to Linda Corbett, Mary Flinn, Viola Martin, Joan Squires, and Teresa Toope for keeping an eye out for me over the years. Thanks also to Linda Winsor for all her assistance with MS and GC-FID. The amount of support I received from this Department was incredible.

Funding is gratefully acknowledged from NSERC, CFI, IRIF, SGS, and Memorial University of Newfoundland. Contributions of materials and equipment are greatly appreciated from Dr. P. Pickup of Memorial University of Newfoundland (Nafion[®] 112 films), and Dr. G. Meyer of John Hopkins Univeristy (TiO₂ slides).

I would like to convey my thanks and appreciation for the unrelenting support of my family and friends. I thank my brother, Jason, for his help improving the quality of several of the scanned graphs. Finally, I must thank my remarkable wife, Debbie-Lee. Her understanding, patience, and encouragement over the course of my graduate studies were more than I could have ever asked. Thank you.

Table of Contents

Title Page	i
Abstract	ii
Acknowledgements	iii
Table of Contents	iv
List of Tables	vi
List of Figures	vii
List of Schemes	vii
List of Abbreviations and Symbols	xii
Chapter 1 Introduction	1
1.1 Project Overview	2
1.2 Literature Review	5
1.2.1 Properties of Metal Oxide Materials	5
1.2.2 TiO ₂ Membrane Chemistry	16
1.2.3 Metalloenzyme Chemistry	21
1.3 Research Targets	33
Chapter 2 Experimental	36
2.1 General Information	37
2.2 Synthesis	40
2.3 In-Situ Generation of Materials	41
2.4 Photocatalysis	44
Chapter 3 Nanocrystalline Materials	46
3.1 Introduction	47
3.2 Results and Discussion	55
3.2.1 Hydrolytic Synthesis of Anatase TiO ₂	55
3.2.2 Nonhydrolytic Synthesis of Anatase TiO ₂	59
3.2.3 Interconversion of Nanocrystalline Materials	69
3.3 Conclusions	72

Chapter 4	Surface Derivatization of TiO ₂	74
	4.1 Introduction	75
	4.2 Results and Discussion.....	81
	4.2.1 9-Anthracenecarboxylic Acid/TiO ₂ (X) _n Assembly.....	81
	4.2.2 Protoporphyrin IX/TiO ₂ (OH) _n Assembly	87
	4.2.3 Hemin Chloride/TiO ₂ (OH) _n Assembly	98
	4.2.4 Hemin Chloride Dimethyl Ester/TiO ₂ Film	104
	4.3 Conclusions	108
Chapter 5	Biomimetic Catalysis	110
	5.1 Introduction	111
	5.2 Results and Discussion.....	114
	5.2.1 Catalysis via Colloidal TiO ₂ supports	114
	5.2.2 Catalysis via TiO ₂ film supports	122
	5.3 Conclusions	126
Chapter 6	Self-supporting TiO ₂ membranes.....	128
	6.1 Introduction	129
	6.2 Results and Discussion.....	131
	6.2.1 Fabrication.....	131
	6.2.2 Surface Derivatization.....	137
	6.3 Conclusions	139
Chapter 7	Conclusions and Future Work.....	141
	7.1 Introduction	142
	7.2 Conclusions and Future Work.....	142
	7.2.1 Phase 1: Nanocrystalline Materials.....	142
	7.2.2 Phase 2: Surface Derivatization of TiO ₂	144
	7.2.3 Phase 3: Biomimetic Catalysis	147
	7.2.4 Phase 4: Self-Supporting TiO ₂ Membranes	149
References	151

List of Tables

Table 1.1: Selected photochemical applications of TiO ₂	12
Table 1.2: Human P450s.....	27

List of Figures

Figure 1.1:	Overview of research project	3
Figure 1.2:	Bulk structures of rutile and anatase TiO ₂	6
Figure 1.3:	TiO ₂ has been prepared on nanoscale as a) nanotubes b) needles and c) porous foam.....	7
Figure 1.4:	Band gap energies of various semiconductors	8
Figure 1.5:	Indirect band gap excitation	9
Figure 1.6:	Exciton formation with TiO ₂	10
Figure 1.7:	Quantum size effects on valence and conduction band energy states.....	11
Figure 1.8:	The Graetzel Cell	15
Figure 1.9	Porous membranes prepared using TiO ₂ nanowires	18
Figure 1.10:	Active sites for P450 and HRP.....	22
Figure 1.11:	Model of active site of HRP.....	25
Figure 1.12:	Iron porphyrin models.....	30
Figure 1.13:	Component species of biomimetic assemblies.....	33
Figure 1.14:	Biomimetic Assemblies	35
Figure 2.1:	Peak Assignments for 9-anthracenecarboxylic acid	42
Figure 2.2:	¹ H NMR peak reference for protoporphyrin IX/TiO ₂ assembly	43
Figure 3.1:	Solvent-surface interface on TiO ₂	47
Figure 3.2:	TiO ₂ colloids linked via conductive polymers for extended charge separation	49
Figure 3.3:	UV-VIS of colloidal anatase TiO ₂ (OH) _n in nanopure H ₂ O.....	56
Figure 3.4:	Infrared spectrum of TiO ₂ (OH) _n in KBr	57
Figure 3.5:	IR spectra of TiO ₂ (X) _n prepared via nonhydrolytic means in KBr ...	60

Figure 3.6:	Supporting information supplied by Colvin as evidence for the absence of hydroxyl surface groups	61
Figure 3.7:	IR spectrum of nonhydrolytically prepared $\text{TiO}_2(\text{X})_n$ in KBr.....	64
Figure 3.8:	Proposed surface capping agents	66
Figure 4.1:	Surface derivatization of TiO_2 via carboxylate linkage	75
Figure 4.2:	A schematic representation of the biphasic kinetics in the adsorption of 9-9-AcCOOH to TiO_2	76
Figure 4.3:	Porphyrin/ TiO_2 Assemblies	80
Figure 4.4:	^1H NMR of 9-anthracenecarboxylic acid on $\text{TiO}_2(\text{X})_n$	83
Figure 4.5:	^1H NMR of 9-anthracene carboxylic acid on $\text{TiO}_2(\text{X})_n$	84
Figure 4.6:	Surface loading differences among colloids	85
Figure 4.7:	UV-VIS spectra of PPIX, $\text{TiO}_2(\text{OH})_n$, and PPIX/ TiO_2	89
Figure 4.8:	IR of free PPIX and PPIX/ $\text{TiO}_2(\text{OH})_n$ in KBr.....	91
Figure 4.9:	^1H NMR of PPIX/ $\text{TiO}_2(\text{OH})_n$ in DMF- d_7	92
Figure 4.10:	^1H NMR spectra for PPIX and PPIX/ $\text{TiO}_2(\text{OH})_n$	94
Figure 4.11:	Excitation/Emission spectra for PPIX and PPIX/ $\text{TiO}_2(\text{OH})_n$	95
Figure 4.12:	Representation of colloidal $\text{TiO}_2(\text{OH})_n$ with attached PPIX.....	97
Figure 4.13:	UV-VIS of hemin chloride and hemin chloride/ $\text{TiO}_2(\text{OH})_n$	100
Figure 4.14:	IR spectra for hemin chloride and hemin chloride/ $\text{TiO}_2(\text{OH})_n$	101
Figure 4.15:	^1H NMR of hemin chloride and hemin chloride/ $\text{TiO}_2(\text{OH})_n$	102
Figure 4.16:	IR of hemin chloride dimethyl ester/ $\text{TiO}_2(\text{OH})_n$	106
Figure 4.17:	UV-VIS of surface sensitized TiO_2 films.....	108
Figure 5.1:	Porphyryns can form μ -oxo dimers which can inhibit oxygen insertion reactions.....	113

Figure 5.2:	UV-VIS spectra of reaction mixture at 0, 3, and 22 hours.....	115
Figure 5.3:	GC-MS of reaction solution following 22 hours of irradiation.....	116
Figure 5.4:	GC-FID chromatograph of cyclohexene, cyclohexene oxide, and cyclohexanol in DMF	118
Figure 5.5:	GC-FID chromatograph of hexane solution of cyclohexene, cyclohexene oxide, and cyclohexanol.....	119
Figure 5.6:	Hexane extraction of DMF standards solution showed a significant improvement in GC-FID peak resolution.....	120
Figure 5.7:	GC-FID chromatograph of hexane extraction of reaction solution ..	121
Figure 5.8:	Magnified view of GC-FID chromatograph of hexane extraction of reaction mixture	121
Figure 5.9:	UV-VIS spectra of hemin chloride/TiO ₂ slides irradiated at 420 nm.....	124
Figure 5.10:	GC-FID chromatograph of standards in cyclohexene, cyclohexanol, and cyclohexene oxide in toluene.....	125
Figure 5.11:	GC-FID chromatograph of reaction solution following irradiation at 420 nm	125
Figure 6.1:	TiO ₂ self-supporting membranes	129
Figure 6.2:	Proposed application of membranes into biphasic chemistry	130
Figure 6.3:	Arrangement used to incorporate Nafion [®] 112 film onto TiO ₂ membranes.....	133
Figure 6.4:	Incorporation of TiO ₂ , Teflon, Nafion [®] , and Carbowax [®] to form membranes under pressure and heat.....	136
Figure 6.5:	TiO ₂ /Nafion [®] membranes	136
Figure 6.6:	Proposed application of TiO ₂ /Nafion [®] membranes	140
Figure 7.1:	Incorporation of μ -oxo porphyrin dimers onto the surface of TiO ₂	148

List of Schemes

Scheme 1.1:	Exciton formation within a semiconductor following the photon absorption.....	9
Scheme 1.2:	Dye-sensitized semiconductors.....	14
Scheme 1.3:	Transmembrane electron transfer.....	20
Scheme 1.4:	Catalytic mechanism of horseradish peroxidase.....	24
Scheme 1.5:	Hydrogen abstraction-oxygen rebound mechanism for hydroxylation by cytochrome P450.....	27
Scheme 1.6:	Consensus for the catalytic cycle of cytochrome P450.....	28
Scheme 1.7:	The first synthetic model of cytochrome P450.....	29
Scheme 1.8:	Expoxidation via Pacman porphyrins.....	31
Scheme 1.9:	Photo-induced oxidation of iron porphyrin using $\text{Ru}(\text{bpy})_3^{3+}$	32
Scheme 3.1:	Synthesis of CdSe nanocrystallites.....	51
Scheme 3.2:	Mechanism of TiO_2 formation via nonhydrolytic route.....	52
Scheme 3.3:	Synthesis and interconversion of TiO_2 surfaces.....	55
Scheme 3.4:	Hydrolysis of titanium(IV) isopropoxide to yield $\text{TiO}_2(\text{OH})_n$	55
Scheme 3.5:	Photodegradation and reduction of nitric acid on $\text{TiO}_2(\text{OH})_n$	60
Scheme 3.6:	Nonhydrolytic synthesis of $\text{TiO}_2(\text{X})_n$	59
Scheme 3.7:	Extraction of chloride capping agents with $\text{AgNO}_3(\text{aq})$	69
Scheme 3.8:	Attempted modification of hydrolytically prepared TiO_2 capping agents.....	66
Scheme 4.1:	Proposed mechanism for the biphasic kinetics of 9-anthracene carboxylic acid tethering to TiO_2	77
Scheme 4.2:	Preparation of $\text{PPIX}/\text{TiO}_2(\text{OH})_n$	87

Scheme 4.3:	Synthesis of Hemin chloride/TiO ₂ (OH) _n	98
Scheme 4.4:	Preparation of hemin chloride/TiO ₂ (OH) _n	105
Scheme 4.5:	Surface sensitization of TiO ₂ films with hemin chloride dimethyl ester	107
Scheme 5.1:	Proposed mechanism for the catalytic insertion of oxygen through photochemical activation of porphyrin/TiO ₂ assemblies	112
Scheme 5.2:	Epoxidation of cyclohexene with hemin chloride/TiO ₂ assembly	114
Scheme 5.3:	Biomimetic catalyst via glass supported TiO ₂ films	122

List of Abbreviations and Symbols

$^1\Delta\text{O}_2$	singlet oxygen
$^3\Sigma\text{O}_2$	triplet oxygen
9-AcCOOH	9-anthracenecarboxylic acid
b.p.	boiling point
bpy	2,2'-bipyridine
COSY	correlated spectroscopy
δ	chemical shift
d	doublet
DMF	N,N-dimethylformamide
FTIR	fourier transform infrared (spectroscopy)
GC-FID	gas chromatography-flame ionization detector
GC-MS	gas chromatography-mass spectrometry
h	hour(s)
HRP	horseradish peroxidase
IR	infrared (spectroscopy)
LC-MS	liquid chromatography-mass spectrometry
m	multiplet
min	minutes
MOS	metal oxide semiconductor
m.p.	melting point

MS	mass spectrometry
NMR	nuclear magnetic resonance (spectroscopy)
P450	cytochrome P450
PMT	photomultiplier tube
PPIX	protoporphyrin IX
ppm	parts per million
QSE	quantum size effects
s	singlet
SEM	scanning electron microscopy
t	triplet
TEM	transmission electron microscopy
TMS	tetramethylsilane
TOP	trioctylphosphine
TOPO	trioctylphosphine oxide
tpy	2,2':6',2''-terpyridine
UV	ultraviolet
UV-VIS	ultraviolet visible (spectroscopy)
XRD	x-ray diffraction

Chapter 1

Introduction

Chapter 1: Introduction

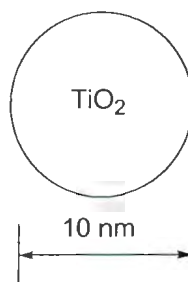
1.1 Project Overview

The core of the work which is described in this thesis is predicated on the assembly, characterization and the use of a nanoscale metal oxide semiconductor, TiO_2 , surface derivatized with biologically-relevant porphyrins. These assemblies were used to mimic the biological activity of two selected metalloenzymes, specifically horseradish peroxidase and cytochrome P450.

The research described consists of four distinct objectives, which are outlined in Figure 1.1. Initially, investigations were conducted into the surface characteristics of nanoscale anatase TiO_2 prepared by well-established sol-gel methodology. This hydrolytic synthetic procedure results in the formation of nanoscale $(\text{TiO}_2)_n$ colloids where the interfacial region is composed of OH groups which limit solubility to aqueous solutions. This is a serious impediment to achieving catalysis in low-polarity nominally weakly binding solvents. Extensive experiments were undertaken to explore the applicability of nonhydrolytic synthesis of anatase TiO_2 with hydrophobic surface groups (i.e. trioctylphosphine oxide, TOPO). Colvin *et al.*¹ had previously reported a synthetic methodology where the products were soluble in heptane. Significant problems with the nonhydrolytic methods were uncovered in this research. The problem was recast in terms of well-known concepts for ligand substitution in transition metal complexes and was applied to TiO_2 .

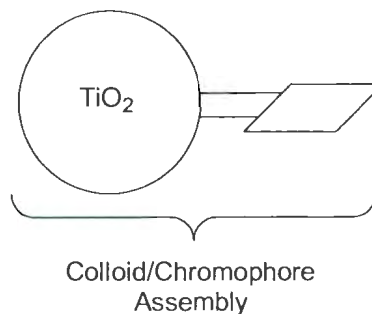
Phase 1:

Preparation of
Nanoscale Materials



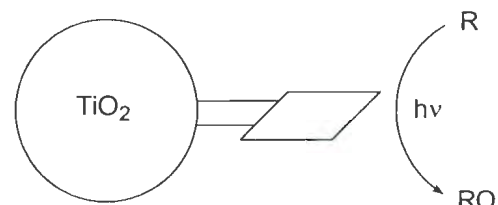
Phase 2:

Construction of
Assemblies



Phase 3:

Biomimetic Catalysis



Phase 4:

Fabrication of Free Standing
 TiO_2 Membranes

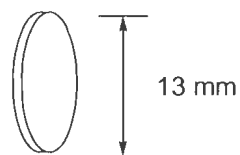


Figure 1.1: Overview of the research project described in this thesis.

The next phase of the project centered on the surface attachment of various chromophores which were characterized by IR, UV-VIS, and most importantly NMR spectroscopy, which was demonstrated as a crucial characterization experiment. This represents one of the most important contributions toward the study of MO_x systems.

Phase 3 involved irradiation of the assemblies which can result in an exchange of electrons between the metal oxide support and the attached molecule, known as interfacial electron transfer. Following this process, the attached molecule may be in a reduced or oxidized state, from which it can be utilized for further chemistry. Using a carboxylate tethering group, several anthracene and porphyrin-based assemblies were prepared using both the hydrolytic and nonhydrolytic preparations of TiO_2 . The assemblies were characterized using the standard spectroscopic techniques listed above.

The porphyrin-based assemblies were used in experiments to define conditions to mimic the catalytic reactions of horseradish peroxidase (HRP) and cytochrome P450 (P450) on semiconductor surfaces. The assemblies were irradiated in the presence of an organic substrate and the products examined for evidence of oxygen insertion. The TiO_2 serves a dual purpose as an electron reservoir and to immobilize the iron porphyrin to inhibit the formation of μ -oxo dimers which often interfere with catalytic models of this type.

The final phase of this project was the development of free-standing TiO_2 membranes. The transfer of electrons through metal oxide membranes from one distinct chemical environment to another holds many possibilities for the extension of this type of chemistry. Using a heated hydraulic press, hybrid membranes were developed incorporating Nafion[®] films on a single side of a disc prepared from powdered anatase TiO_2 . While focus centered on the development and fabrication of these membranes, possible applications and future considerations are also addressed.

Each segment of the project yielded insight into the nature of the TiO₂ nanoparticles in terms of synthesis, modification, mechanistic enzymology, and potential applications. The specific targets of each phase are presented in more detail at the end of this Chapter, following a review of background information and relevant current research.

1.2 Literature Review

The following sections attempt to provide the reader with a general overview of the concepts relevant to the current project. A discussion of the fundamental chemistry behind titanium dioxide are presented with a brief review of current membrane research. Metalloenzyme chemistry of horseradish peroxidase and cytochrome P450 is introduced with emphasis on the mechanisms of oxygen insertion in biological systems. Synthetic models of the two enzymes are also presented.

1.2.1 Properties of Metal Oxide Materials

The study of metal oxides and their chemical properties began very early in the 1800's² and is the foundation for the newly-mature field of nanoscale materials science.

TiO₂ is naturally formed in three distinct bulk structures: brookite, rutile, and anatase. A synthetic structure, known as cotunnite, is synthesized at high pressures and temperatures and is one of the hardest polycrystalline metal oxides known.³ For the

purpose of photochemical activity, the rutile and anatase phases are the primary structures of interest, with brookite exhibiting significantly less photochemical activity. A significant body of photoelectrochemical research exists for the study of rutile TiO_2 in the past⁴ while recent advancements in nanotechnology have prompted an emergence of interest in the anatase form of the metal oxide. Figure 1.2 displays the crystal structures of anatase and rutile TiO_2 .

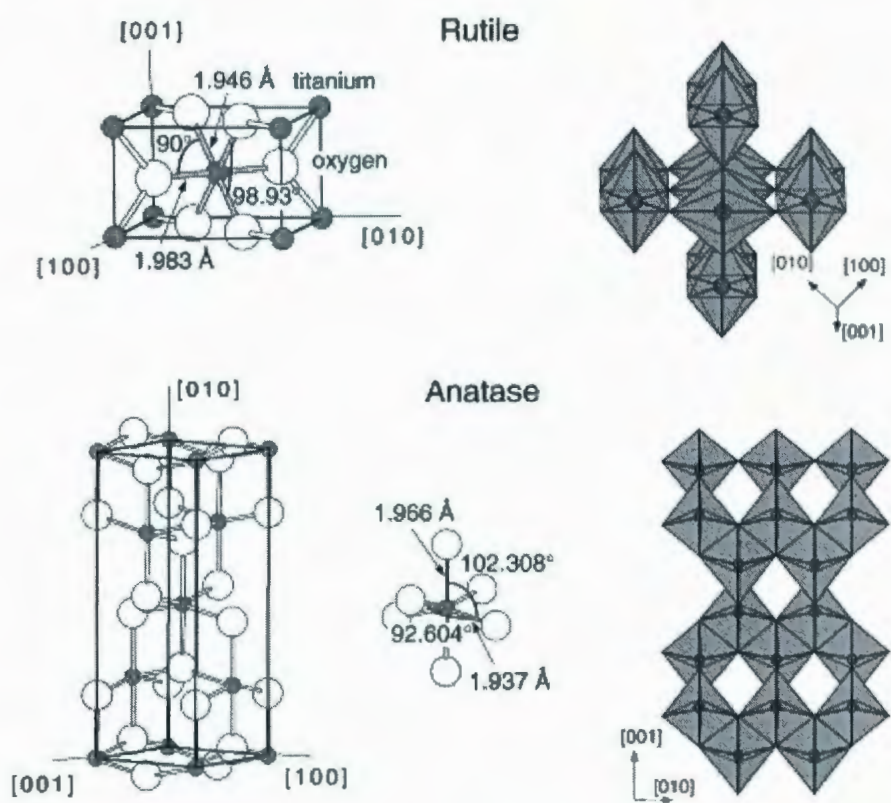


Figure 1.2: Bulk structures of rutile and anatase TiO_2 . Stacking of octahedra shown on right. Adapted from Reference 5.

While the majority pre-1990's research focused on the surface science of bulk crystals, advancements in technology have led to a boom in the preparation of nanoscale titanium dioxide in various forms. Chapter 3 discusses the preparation of colloidal TiO_2

as spherical structures on the order of 7 to 10 nm in diameter. Figure 1.3 displays several other forms that have been recently reported.

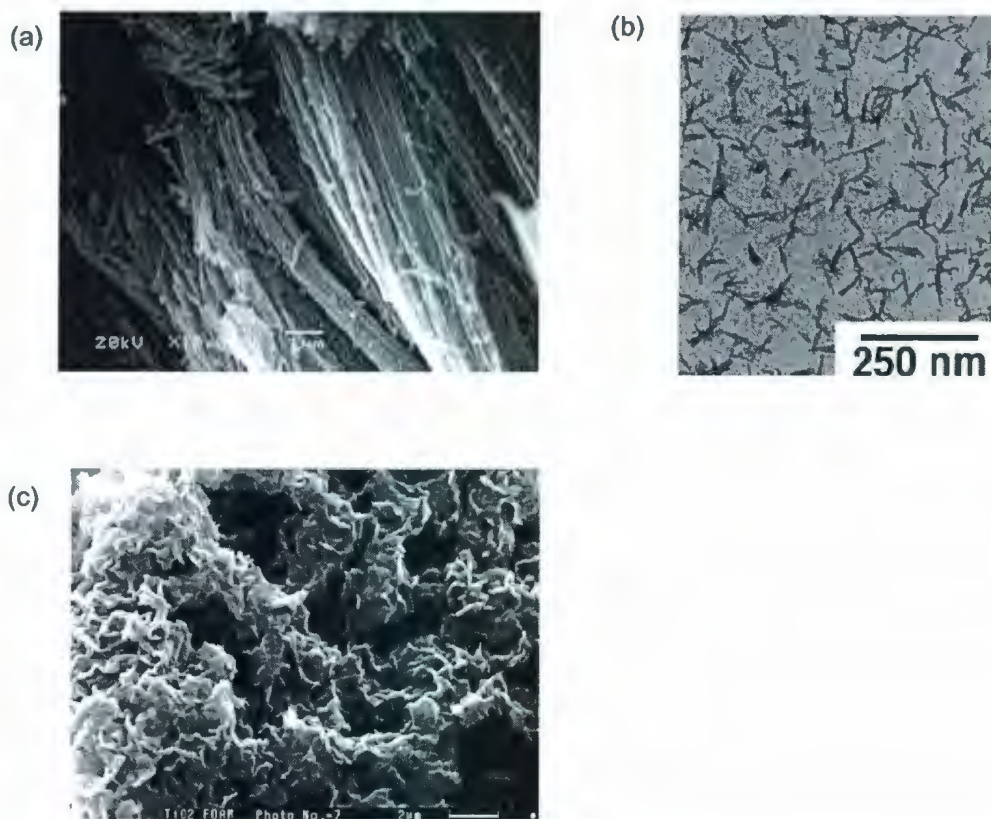


Figure 1.3: TiO₂ has been prepared on nanoscale as (a) nanotubes,⁶ (b) needles⁷ and (c) porous foam.⁸

An excellent review of TiO₂ catalysis, surface science, photochemistry and energetics is provided by Yates *et al.*⁹ Briefly, the semiconductor properties of TiO₂ introduce an energy separation of the valence band and conduction band states. Figure 1.4 shows the bandgap separation and edge positions of TiO₂ as a function of chalcogenide semiconductor-based materials.

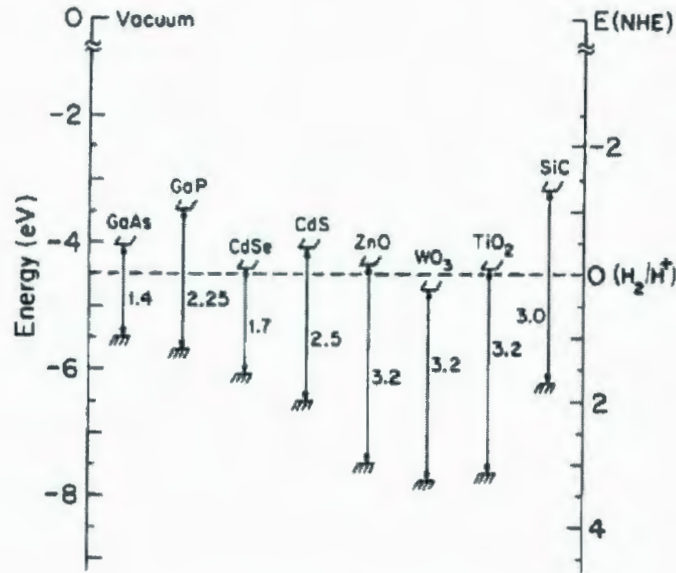
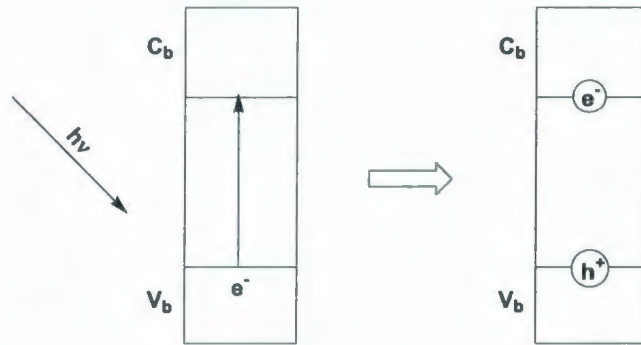


Figure 1.4: Band gap energies of various semiconductors. Adapted from Reference 9.

Absorption of light by these structures results in the promotion of an electron within the semiconductor valence band to the conduction band, known as band gap excitation (Scheme 1.1). The result is the formation of an e^-/h^+ pair known as an exciton, $[e^-_{cb}, h^+_{vb}]$, where the electron is promoted to the conduction band and the imaginary particle, h^+ , a positively charge hole, is left in the valence band. Strictly speaking, the exciton shown in Scheme 1.1 is tightly bound and must dissociate for electron conduction to occur. If the energetics of the systems preclude exciton dissociation, e^-/h^+ recombination occurs. Separation can be sustained on the nanosecond scale¹⁰ before recombination occurs, often emitting a photon.



Scheme 1.1: Exciton formation within a semiconductor following the photon absorption.

It should also be noted that the promotion of a single electron from the valence band to the conduction band is considered to be indirect.^{11,12} The bands are separated in both energy, E , and wavevector, k , as represented in Figure 1.5.

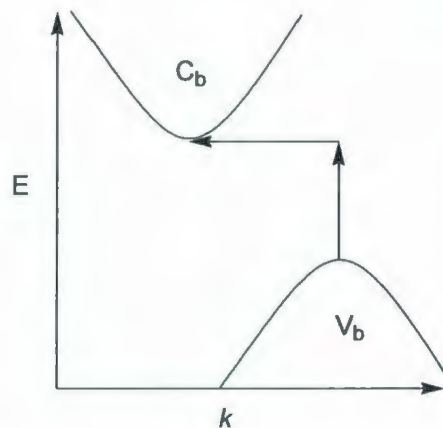


Figure 1.5: Indirect band gap excitation. Conductance and valence bands are separated by in both energy and wavevector. Adapted from Reference 11.

As a result, the energy required for the process is greater than direct band gap excitation. Lattice phonons are required to account for the difference in wavevector.

Aside from the role of the band gap in prolonging charge separation, inconsistencies and defects within the structures serve to extend these recombination lifetimes as well. Vacancies and other structural defects can act as localized areas of energy differences from that of the bulk structure, which serve as charge carrier traps.^{9,13} These defects also play an important role in interactions between the TiO₂ surface and adsorbed molecules.¹⁴ Often, these inconsistencies serve as the active sites for photochemical reactions. Whether by band gap excitation or charge carrier trapping, the prolonged separated state can lead to several different processes as displayed in Figure 1.6.

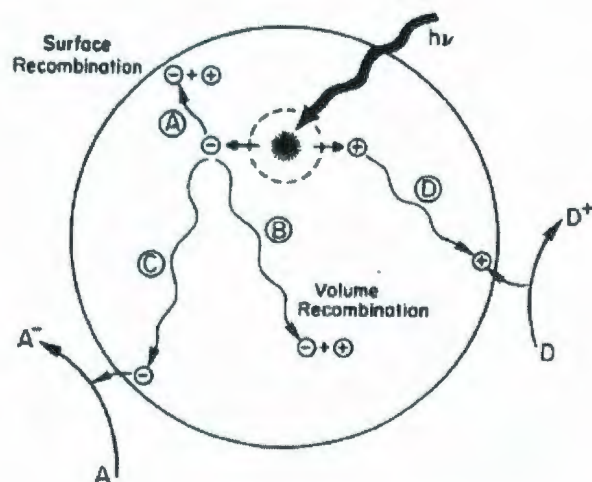


Figure 1.6: Exciton formation with TiO₂ can be followed by (A) recombination at the surface, (B) recombination within the structure, (C) electron migration to the surface followed by substrate reduction, and (D) hole migration to the surface followed by substrate oxidation. Adapted from Reference 9.

An excellent study and discussion of charge-carrier trapping and recombination dynamics is provided by Graetzel *et al.*¹³ and Bahnemann *et al.*¹⁵ while a more recent

review of colloidal semiconductor dynamics has been published by Zhang¹⁶ and Yates.¹⁷ It should be noted that a change in size domain from bulk crystals to nanoscale particles results in a change in the physical and electrochemical properties of the material, known as *quantum size effects* (QSE). In the 5 to 20 nm range, the diameters of the particles themselves are approximately the same size as the wavelengths of the excitons. The continuous and delocalized valence and conduction bands of bulk TiO₂ become localized quantized discrete energy states, (i.e. more molecular-like) as depicted in Figure 1.7.

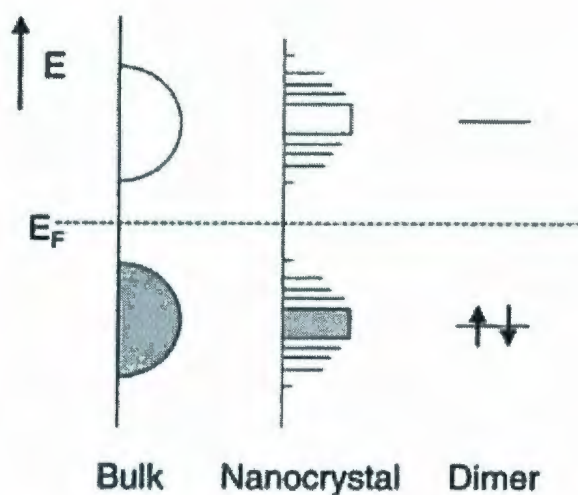


Figure 1.7: Quantum size effects on valence and conduction band energy states. Adapted from Reference 18.

The concepts of conduction bands, valence bands, and band bending are probably not important, as the size of the particle does not result in an interfacial chemical potential. On the nanoscale, a *density of states* exist, as opposed to *bands*. Other QSE include a general increase in gap energies with decreasing size, as well as a decrease in band bending. Band bending describes the difference in energetics between internal

volume of the material and the external surface. With small diameters, internal properties are very similar to those found on the surface.

Bulk and nanoscale TiO₂ has found use in a wide variety of photochemical applications. Early studies included the photolysis of water¹⁹ and nitrogen fixation.²⁰

Table 1.1 provides a simple list of a few of the photochemical applications of TiO₂, in bulk, nanoscale, and modified forms.

Table 1.1: Selected photochemical applications of TiO₂. Adapted from Reference 21

Photocatalytic purification of water and air

Drinking water purification
Wastewater treatment
Killing of microorganisms and pathogens
Destruction of air pollutants/air purification
Conversion or recovery of heavy metal ions/precious metal ions
Photocatalytic reactor engineering
Oil spill remediation
Prevention of algal bloom and algal growth
Photocatalytic oxidation coupled with other treatment processes

Development of photocatalytic materials and coatings

Synthesis of visible light active photocatalytic materials
Photocatalytic materials for self-cleaning, superhydrophilic, and antibacterial function
Coating technology for product developments
Photo-functional composite materials

Solar energy conversion through photocatalysis

Hydrogen production through water splitting
Development of visible light sensitizers and composite materials
Photocatalytic conversion of N₂/CO₂
Nano-structured TiO₂ electrodes for dye-sensitized solar cells
Solar reactor design and development

Photocatalysis for chemicals synthesis and manufacturing

Development of new synthetic method utilizing greener processes and reagents

Photocatalytic metal corrosion prevention

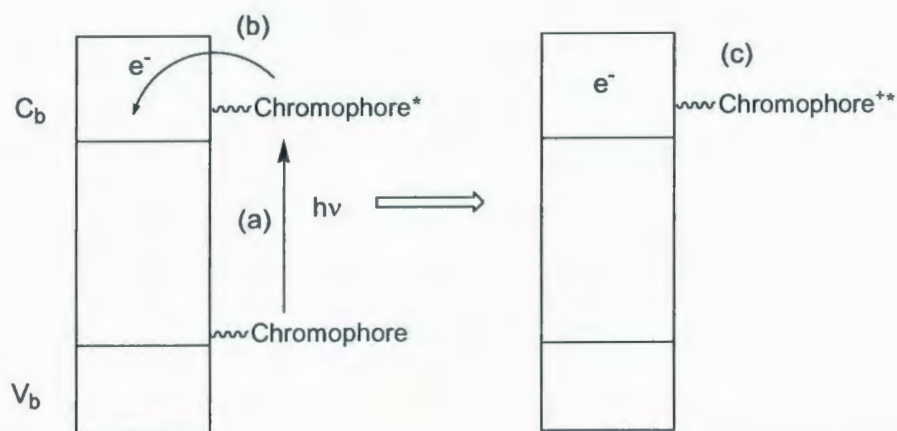
Metal corrosion prevention using a TiO₂ photoanode
Photocatalyst coating on metal surface for corrosion prevention

Photocatalytic lithography

Development of alternative lithographic process utilizing photocatalysis

A compilation of specific photodegradation substrates is provided in a review by Hoffmann *et al.*²² and Diebold,⁵ in which extensive mechanisms and references are provided for the reactions of various hydrocarbons and inorganic compounds. Taoda²³ published a review of many interesting commercial and agricultural applications.

While the absorbance wavelength of the TiO₂ is limited to ~280 nm, the attachment of chromophores extends the light-harvesting properties of the materials. Scheme 1.2 portrays the process followed by the absorption of a photon by an attached dye. Following excitation, an electron is injected into the conducting band of the semiconductor, where $k_{inj} \sim 10 - 20$ fs. Depending on the nature of the chromophore, injection can occur through several different mechanisms. An extensive discussion of charge-transfer in molecular electronics on the nanoscale is provided by Creutz *et al.*²⁴ (including but not limited to TiO₂) and Gundlach *et al.*²⁵ The process of adsorption occurs via tethering groups on the substrate which interact with the surface groups on the semiconductor surface to achieve attachment. In general, the capping agents on the TiO₂ are hydroxyl groups, although it can vary, depending on the synthetic approach under which the oxides are prepared. Tethering groups on the adsorbed molecules include carboxylic acids, phosphoric acids, alcohols, and esters. (See Figure 4.1 on page 75).



Scheme 1.2: Dye-sensitized semiconductors: (a) The attached chromophore absorbs a photon followed by (b) injection of an electron from the excited state of the chromophore into the conduction band of the metal oxide resulting in (c) an oxidized excited state.

In a landmark paper published in 1991 by Graetzel and O'Regan²⁶ it was demonstrated that the surface modification of TiO_2 films with a ruthenium bipyridyl complex could be incorporated into a photochemical cell now collectively known as *Graetzel Cells* having 7 - 10 % efficiency,. A schematic of the cell is exhibited in Figure 1.8. Excitation of the ruthenium complex with light is followed by injection into the TiO_2 , which is attached to a conductive electrode. A counter electrode and sacrificial acceptor complete the circuit.

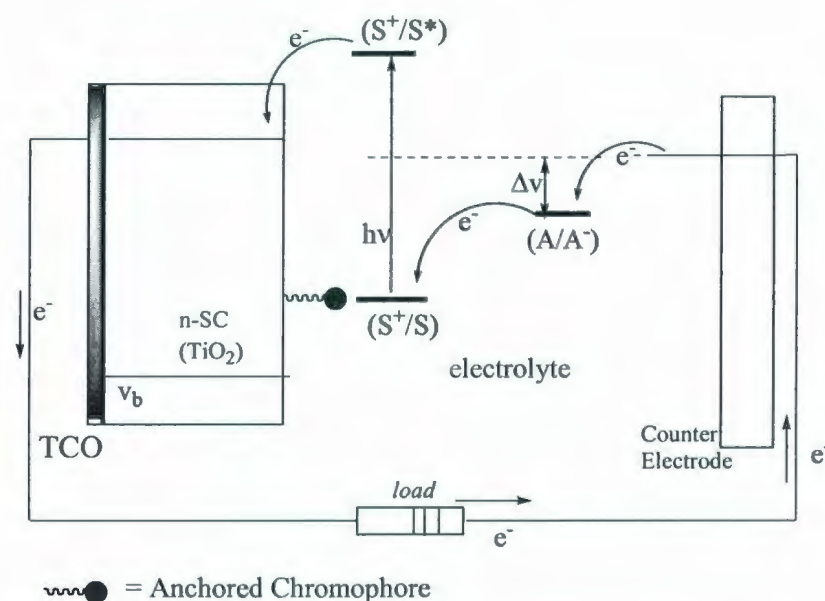


Figure 1.8: The Grätzel Cell. Adapted from References 27 and 26.

The success of these solar cells prompted a boom in research on dye-sensitized metal oxides on both bulk and nanoscale materials, including both electrical and chemical applications. Molecules and ions such as ascorbic acid,²⁸ carotenoids,²⁹ $\text{Fe}(\text{CN})_6^{4-}$,³⁰ $\text{Ru}(\text{2,2'}$ -bipyridine-4,4'-dicarboxylic acid)₃⁴⁻,³¹ DNA³² and porphyrin heterodimers³³ represent only a small sampling of species that have been attached to the surface of metal oxide semiconductors. The adsorption of simple molecules, such as CO_2 and H_2O , on the surface of TiO_2 has also been extensively studied, as well as their acid/base interactions. An excellent resource discussing the surface science and adsorption of various organic molecules on TiO_2 is published by Diebold,⁵ but discussion of nanoscale materials is limited. A detailed review of photo-induced molecule-metal and molecule semiconductor electron transfer is provided by Lindstrom and Zu³⁴ which includes a discussion of rates and energies that are outside the scope of this project. Meyer and

Ardo³⁵ recently published an excellent discussion of surface-sensitized TiO₂ as a key technology in renewable energy research, with extensive discussion of the energetics and kinetics involved.

Of specific interest to the project described in this thesis is the incorporation of porphyrins to the surface of titanium(IV) dioxide. Well-established synthetic methods of these systems have provided an almost limitless assortment of porphyrins for incorporation into metal oxide chemistry. The ring structure of a porphyrin is a versatile scaffold for the incorporation of various metals, tethering sites, and functional groups. Officer *et al.*³⁶ assessed a wide variety of porphyrins that have been used as light-harvesting arrays for solar cells and found 4-*trans*-2'-(2''-(5'',10'',15'',20''-tetraphenylporphyrinato zinc(II)yl)ethen-1'-yl)-1-benzoic acid proving to be one of the most effective. Other applications of porphyrin-sensitized metal oxides include decomposition of organohalide pollutants^{37,38} by irradiation of the TiO₂, initiating a multielectron reduction of the attached porphyrin, the reverse of the process utilized in solar cells.

1.2.2 TiO₂ Membrane Chemistry

As the body of information regarding the nature of the photochemistry of nanoscale metal oxides grows, researchers are finding new and novel methods to incorporate these properties into practical applications. TiO₂ is being integrated into a wide assortment of consumer products such as glassware³⁹ and fabrics.⁴⁰ Upon absorption of light, both of these materials become self-cleaning by photodegradation of

any adsorbed organic material. TiO_2 has found application as a means of sterilizing operating rooms as well. Of particular interest to the research presented here is the development and application of TiO_2 membranes. Chapter 6 reports the fabrication of free-standing membranes for the purpose of transmembrane electron transfer between separate chemical environments. Several examples of current membrane technologies are presented in the following pages.

The photochemical degradation of organic pollutants in an aqueous environment by TiO_2 is one of the most attractive pursuits in materials chemistry. Success has been found by passing the aqueous solution through a porous TiO_2 membrane while it is being irradiated. Porous membranes can be prepared using several techniques with the most popular being a sol-gel approach. In the late 1980's, Anderson *et al.*^{41,42} developed techniques to prepare high-quality TiO_2 membranes, and also examined their photochemical properties. It was also demonstrated that the degree of porosity could be tuned through control of aggregation of TiO_2 .⁴³ A more recent paper by Agoudjil *et al.*⁴⁴ describes the variation of pore diameter and volumes as a function of the temperature of the calcinations process. Zhang *et al.*⁴⁵ have reported the use of TiO_2 nanowire to develop porous membranes, shown in Figure 1.9.

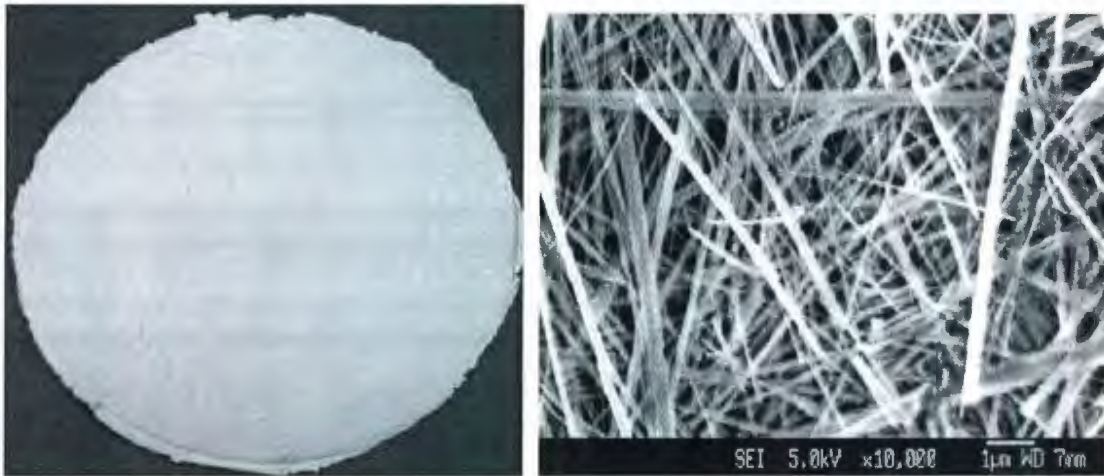


Figure 1.9 Porous membranes prepared using TiO_2 nanowires. SEM image is at high magnification (10,000x). Adapted from Reference 45.

Membranes were prepared via this method with $\sim 0.05 \mu\text{m}$ pore sizes.

Photodegradation of humic acid, a standard test compound, was found to be 93 to 100 % effective. A major benefit of the nanowire preparations over standard sol-gel methods was the absence of membrane fouling. Membrane fouling is one of the major obstacles to efficient treatment of environmental pollutants.⁴⁶ Throughout the filtering process, particulate pollutants tend to build up within the membranes, decreasing the effective pore size and thus increasing the pressure required. Using this approach, Zhang *et al.* detected no evidence for the retention of humic acid, and thus no need for physical or chemical cleaning of the membranes. The amount of literature that exists regarding the preparation and application of TiO_2 sol-gels is too vast to completely address in this report.

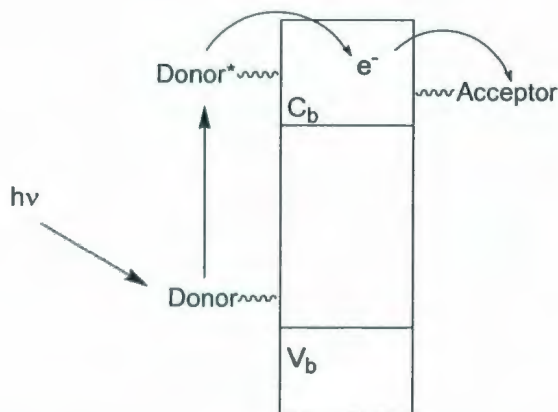
Other ventures in TiO_2 membrane chemistry utilize the photochemical properties of the semiconductor without flow-based filtration. TiO_2 films have been briefly

mentioned in the previous section. In general, these films are transparent TiO₂ sol-gels mounted on a physical support, such as glass or conductive materials. Fujishima and Honda⁴⁷ demonstrated the electrochemical photolysis of water in 1972 using electrodes composed of supported TiO₂ films. Development of these films experienced an enormous boom in research following the success of the aforementioned Graetzel Cells. Many of the applications listed in Table 1.1 use a supported film approach as well.

Both colloidal and film-based TiO₂ were utilized in this project. The preparation of these films is described in the literature by Meyer *et al.*⁴⁸ Briefly, a colloidal solution is prepared from the hydrolysis of titanium(IV) isopropoxide with water in 2-propanol, heated within a sealed flask. Carbowax[®] is added to the viscous white mixture, and the paste is placed on a glass slide or conductive flask, and is sintered at high temperatures. There are several advantages to preparing TiO₂ films in this manner, with one of the primary ones being ease of surface sensitization. The films are simply immersed in a solution of the selected dye for a period of time, are then extracted, and rinsed. The transparency of the films allows for spectroscopic verification of attachment. One of the major difficulties encountered in this project using a colloidal approach was the separation of sensitized and nonsensitized TiO₂ and is further discussed in Chapter 4.

In 1997, Fitzmaurice *et al.*⁴⁹ published several papers describing the attachment to TiO₂ of both an electron donor and an electron acceptor. Membranes were prepared using the sol-gel technique described previously whereby TiO₂ films are attached to glass slides. In contrast to films prepared by Meyer and Graetzel, Fitzmaurice removed the films from the support to yield self-supporting transparent membranes. The resulting

films possessed an area measuring 4 cm^2 and could best be described as fragments obtained during cracking of the sol-gels obtained following drying. Modification of these surfaces consist of an electron donor, bis[(4,4'-dicarboxy-2,2'-bipyridine)(4,4'-dimethyl-2,2'-bipyridine)-ruthenium(II)], and a co-adsorbed electron acceptor, 1-ethyl-1'-[(4-carboxy-3-hydroxyphenyl)methyl]-4,4'-bipyridinium perchlorate. Upon absorption of light by the ruthenium complex, reduction of the viologen is achieved via transmembrane electron transfer, as shown in Scheme 1.3.



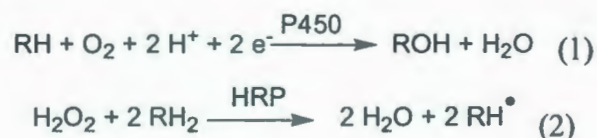
Scheme 1.3: Transmembrane electron transfer. A photon is absorbed, injected into the TiO_2 , followed by reduction of the acceptor molecule on the other side of the membrane. Adapted from Reference 49.

The incorporation of separate donor and acceptor molecules on opposite sides of a TiO_2 membrane led to the fourth phase of this project. Expanding on the concepts demonstrated by Fitzmaurice *et al.* the production of stronger free-standing membranes was pursued. It was intended that these membranes would not only be capable of

selective sensitization and transmembrane electron transfer, but also be able to allow the donor and acceptor molecules to exist in distinctly different chemical environments.

1.2.3 Metalloenzyme Chemistry

The majority of research involving metal oxide surface modification focuses on the development of dye-sensitized solar cells. In contrast, this project is focused on progress towards photochemical oxygen insertion in a similar process to the activity of hemoproteins cytochrome P450 and horseradish peroxidases which can be represented in their simplest forms respectively by equations (1) and (2):



While both enzymes exhibit similar mechanistic pathways, cytochrome P450 shows much higher efficiency in catalyzing oxygen insertion reactions. Horseradish peroxidase is capable of hydroxylation, but its primary role serves to initiate oxidative coupling of various substrates following oxidation by H_2O_2 . Hydroxylation of C-H bonds or the epoxidation of C=C bonds are not only important processes from a strictly biological perspective but also from that of synthetic drug metabolism and energy storage. While the discovery of P450 in 1958⁵⁰ can be considered relatively new compared to the first reports of reactivity of the roots of horseradish by Planche⁵¹ in 1810, an extensive amount of research has been published on both enzymes. A concise

overview of HRP has been published by Gajhede,⁵² while Veitch⁵³ presents the history of HRP with inclusion of recent advances. Omura⁵⁴ provides a brief historical review of cytochrome P450 research and several milestone discoveries from a biochemical perspective. A more complete discussion of the P450s has been compiled by Ortiz de Montellano,⁵⁵ Lewis,⁵⁶ and Denisov *et al.*⁵⁷ All three provide an excellent introduction to the study of P450 for both biochemists and chemists. The research presented in this thesis does not deal directly with the enzymes in any form. These systems are the models on which the porphyrin/TiO₂ assemblies are based. The active heme sites for both of these enzymes are shown in Figure 1.10.

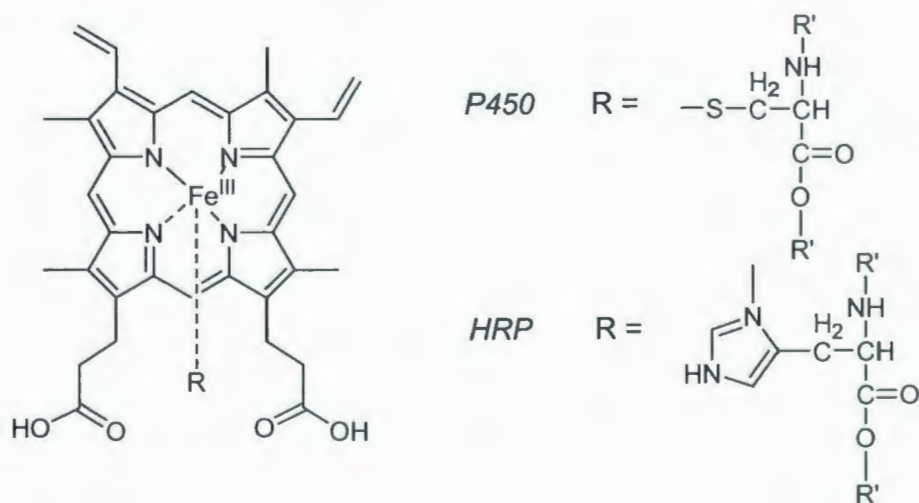


Figure 1.10: Active sites for P450 and HRP.

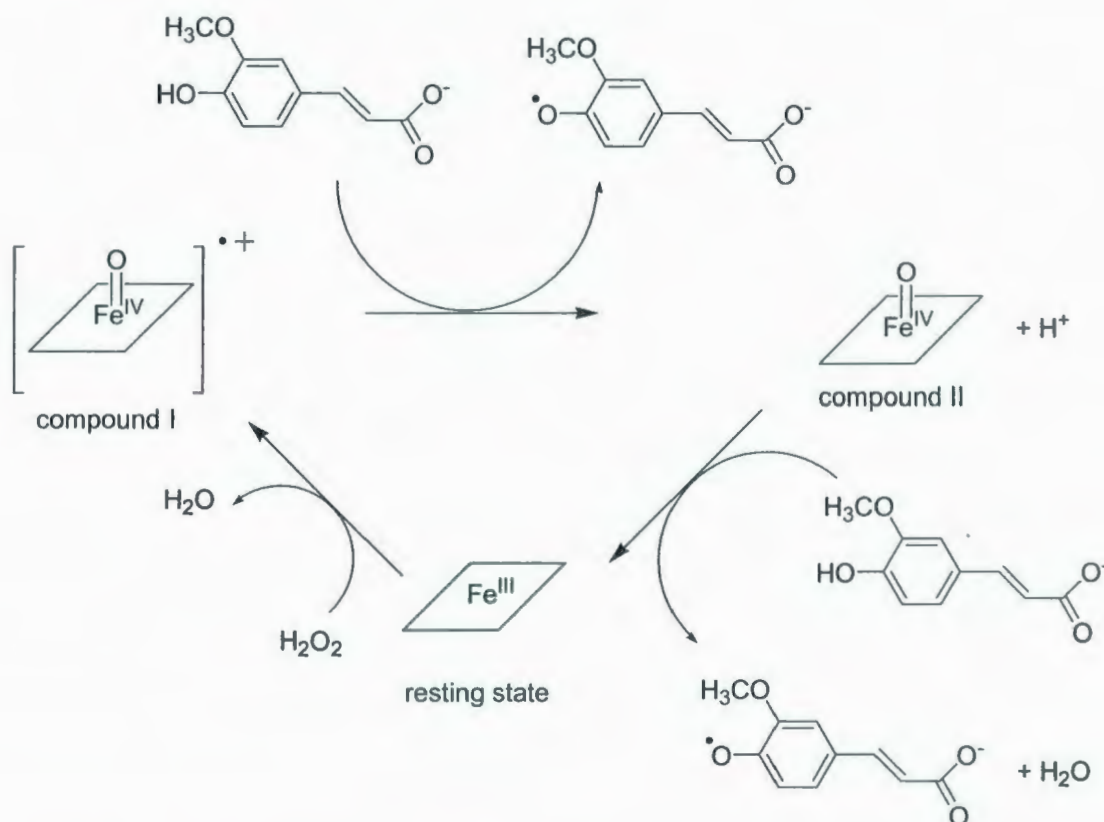
The axial coordination ligand is generally cysteine for P450 and histidine for HRP. These ligands serve an important role in the electron transfer needed for catalysis.

The following sections will provide an overview of the enzyme's functionality, active centers, and proposed mechanistic pathways.

Horseradish Peroxidase

Enzymatic activity of HRP is initiated by the conversion of peroxides to water, followed by further oxidation of organic substrates. While the enzyme is true to its namesake, it is thought that reaction with peroxides is not the primary function within plants. Mittler⁵⁸ has shown that other enzymes, such as ascorbate peroxidase, serve the role of peroxide level regulation. Following reaction with hydrogen peroxide, HRP produces highly reactive radical species which proceed with activities that can vary depending on the biological environment in which the reaction proceeds. These reactive products have made it difficult to determine the exact role the HRP plays within a plant. Scheme 1.4 shows the proposed catalytic mechanism of HRP on 3-(4-hydroxy-3-methoxyphenyl)-2-propenoic acid.

Reaction of the Fe(III) resting state with hydrogen peroxide yields water with an Fe(IV)=O state with a radical cation situated within the porphyrin ring. This reactive state, known as *compound I* or *HRP-I*, is formally two oxidative states above the resting state. Compound I will proceed to oxidize an organic substrate, generating a highly reactive radical species. The resulting state of the enzyme, known as *compound II* or *HRP-II*, is a reactive Fe(IV)=O state that proceeds to repeat the oxidation of another substrate molecule.



Scheme 1.4: Catalytic mechanism of horseradish peroxidase. Hydrogen peroxide is oxidized to water via the Fe(III) resting state, followed by two separate oxidations of a substrate, resulting in the production of reduced compound I and compound II. Adapted from (53).

It should be noted that within this general mechanism there has been much debate and examination of the individual steps. Evidence for a two-step mechanism has been reported by Garcia-Canovas *et al.*⁵⁹ for oxidation via compound II. The production of radical species can lead to the formation of dimers, polymers, or other reactions. Compounds I and II have been extensively studied and modeled within the literature. A comparison of catalytic site intermediates of oxidases and peroxidases is provided by Rich and Iwaki.⁶⁰ In recent years, HRP has been incorporated into various electrochemical biosensors.⁶¹

Compared to cytochrome P450, horseradish peroxidase exhibits limited oxygen insertion activity. It has been shown that it is capable of oxygen transfer from hydrogen peroxide to thioanisoles,⁶² but is not capable, for example, of epoxidation of styrene. Given the proximity of distal His42, Phe41, and Arg38 (Figure 1.11) within the enzyme it is thought that electron transfer in the HRP mechanism occurs at the edge of the porphyrin ring. As such, the Fe(IV)=O species is unable to achieve oxygen transfer as effectively as P450.

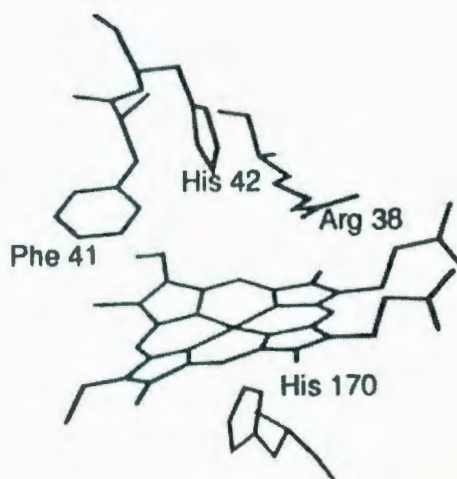


Figure 1.11: Model of the active site of HRP. The proximity of His42 has been shown to limit peroxygenase activity. Adapted from Reference 63.

Ortiz de Monetallano *et al.* have demonstrated the genetic modification of HRP through the replacement of Phe41 with leucine and threonine⁶⁴ or the modification of Arg38 to produce several different mutants with which epoxidation of styrene and various other organic substrates can be achieved.⁶³ O-18 isotope experiments verify that the attached oxygen originated within the H₂O₂. With regard to the oxygen addition of thioanisoles, the oxygen source is generally not the peroxide, but water from the

surrounding solution. Ozaki *et al.*⁶⁵ have demonstrated the activation of molecular oxygen with HRP through the interaction of sodium sulfite in the oxidation of thioanisole.

It should be noted that in the context of this research project, oxygen insertion is the primary goal. HRP is included in this discussion to provide a more complete overview of the mechanisms involved in metalloporphyrin chemistry. While this enzyme exhibits only limited oxygen transfer, the hindrance provided by the surrounding structure would not be an issue for the target assemblies. With respect to the biomimetic assemblies produced here, both HRP and P450 mechanisms were considered as viable pathways.

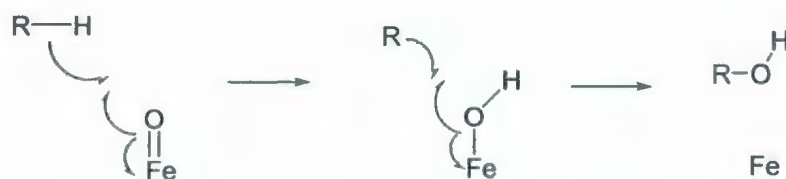
Cytochrome P450

Analogous to the goals of this project, cytochrome P450's primary purpose is the addition of oxygen to various organic substrates to achieve many different roles. With a vast family of P450s found in a wide range of species, the applications of the enzyme are extremely diverse, even within a single organism. Table 1.2 provides a small selection of the P450s found in humans, along with the tissue site and role. Within the liver, cytochrome P450 is one of the primary enzymes responsible for the metabolism of toxins and drugs.

Table 1.2: Human P450s. Adapted from Reference 55.

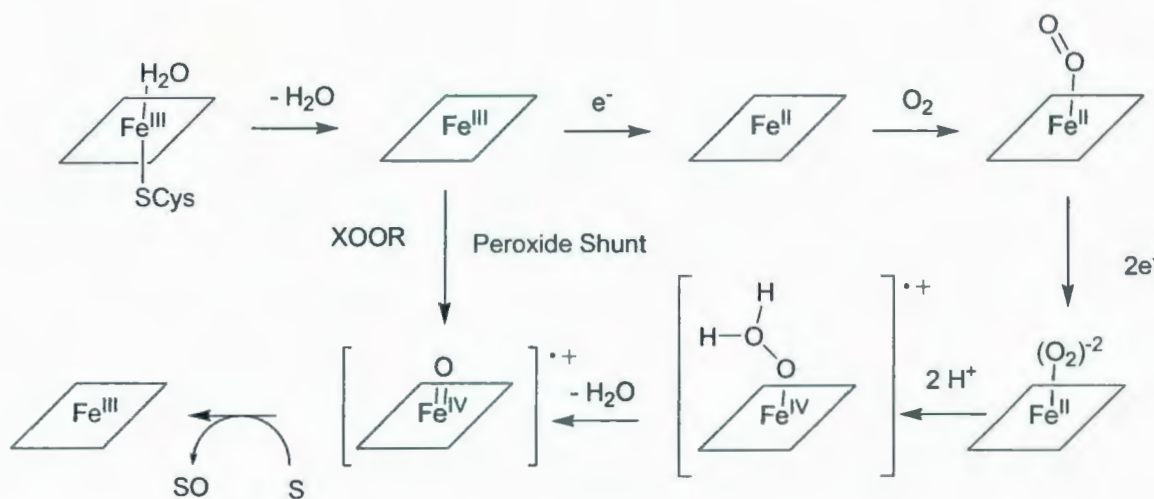
P450	Tissue Site	Typical Reaction
1A1	Lung	Benzo[a]pyrene 3-hydroxylation
1A2	Liver	Caffeine N ³ -demethylation
2A13	Nasal Tissue	Activation of 4-(methylnitrosamino)-1-(3-pyridyl)-1-buranone)
2C9	Liver	Tobutamine methyl hydroxylation
2F1	Lung	3-Methylindole activation
3A4	Liver, Small Intestine	Testosterone 6 β -hydroxylation
4F8	Seminal Vesicles	Prostaglandin ω -2 hydroxylation
5A1	Platelets	Thromboxane A ₂ synthase reaction
7B1	Brain	Dehydroepiandrosterone 7 α -hydroxylation
11B1	Adrenals	Corticoasterone 18-hydroxylation
24A1	Kidney	25-hydroxyvitamin D ₃ 24-hydroxylation
52A1	Liver, testes	Lanosterol 14 α -demethylation

Arimoto⁶⁶ has published an excellent overview of computational techniques for predicting interactions of several different cytochrome P450s with emphasis on drug metabolism. Over the last 50 years, there has been much debate regarding the catalytic mechanisms of these reactions. Early research supported the hydroxylation of the substrate via a hydrogen abstraction-oxygen rebound mechanism as shown in Scheme 1.5.

**Scheme 1.5:** Hydrogen abstraction-oxygen rebound mechanism for hydroxylation by cytochrome P450. Adapted from Reference 67.

Attempts to quantify lifetimes through the use of radical clock methods led to examination of many different P450s with many different substrates. Inconsistencies with the proposed pathways began to appear as it became evident that the mechanism of oxygen insertion is much more complex than first assumed. Evidence was found for the presence of cationic intermediates and multiple reactive states. An excellent discussion of the development of a mechanistic picture of P450 is provided by Newcomb *et al.*⁶⁷

Scheme 1.6 shows one of the currently accepted models, largely attributed to the work of Groves *et al.*^{68,69} and Schwarz *et al.*⁷⁰



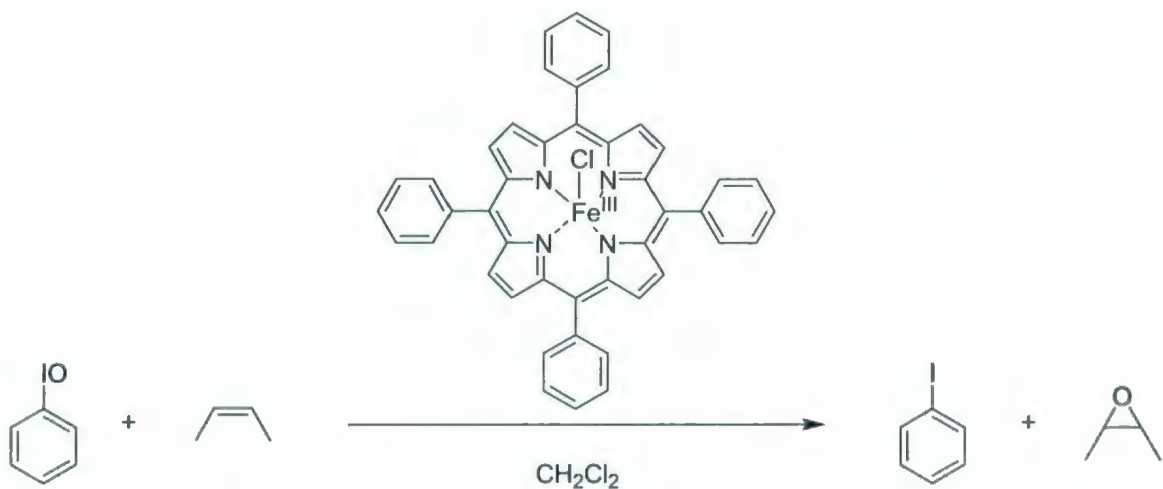
Scheme 1.6: Consensus mechanism for the catalytic cycle of cytochrome P450. Adapted from References 68 and 69.

Initial reduction of the iron(III) center is followed by coordination of molecular oxygen. Further reduction and proton addition leads to the formation of an Fe(IV)=O radical cation intermediate, similar to compound I in HRP. This radical cation reacts

with the substrate to achieve oxygen addition returning the heme to the Fe(III) state to repeat the process again. Synthetic approaches have utilized a peroxide shunt pathway which provides a route to the same reactive intermediate without the incorporation of molecular oxygen. It should be noted that this is a generalized overview of P450 activity. Various combinations of P450s and substrates lend support to this model while other studies provide evidence to discount it.

Synthetic Models

The ease with which P450 and HRP can achieve some of the most difficult reactions in chemistry has led to the development of many different models in search of mechanistic information and chemical applications. The first reported model using a simple iron porphyrin was reported in 1979, again by Groves *et al.*,⁷¹ as shown in Scheme 1.7.



Scheme 1.7: The first synthetic model of cytochrome P450. Iodosylbenzene acts as the oxygen transfer agent⁷¹.

Since that time, a wide assortment of synthetic models have been prepared and shown to effectively mimic the biological activity of P450. A review of metalloporphyrins effective in epoxidation reactions is provided by Collman *et al.*⁷² up to 1993. Recent discussions have been published by Woggon *et al.*^{73,74} In the design of these synthetic models there are several considerations that must be taken into account.

Figure 1.12 shows several examples of P450 models.

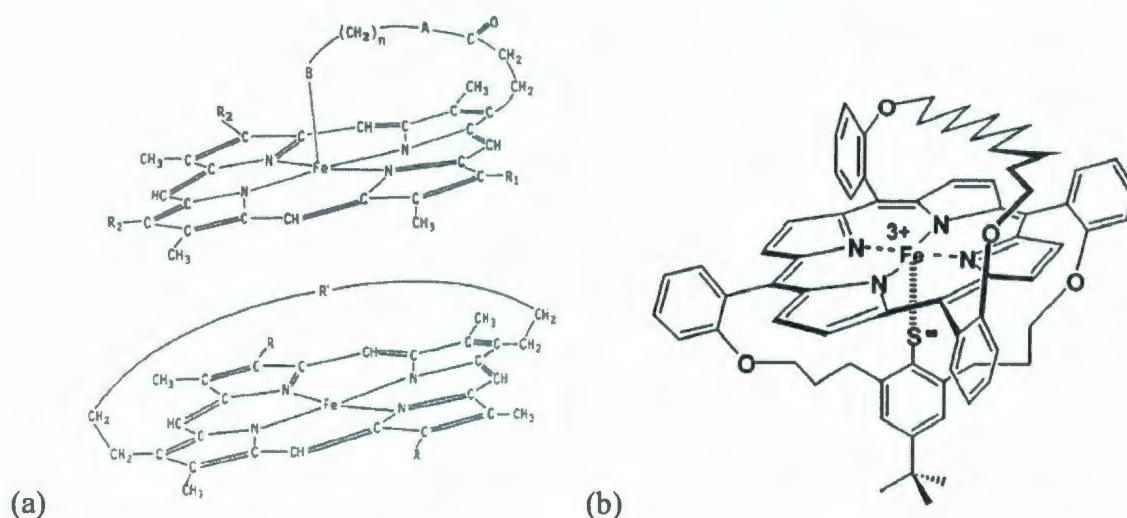
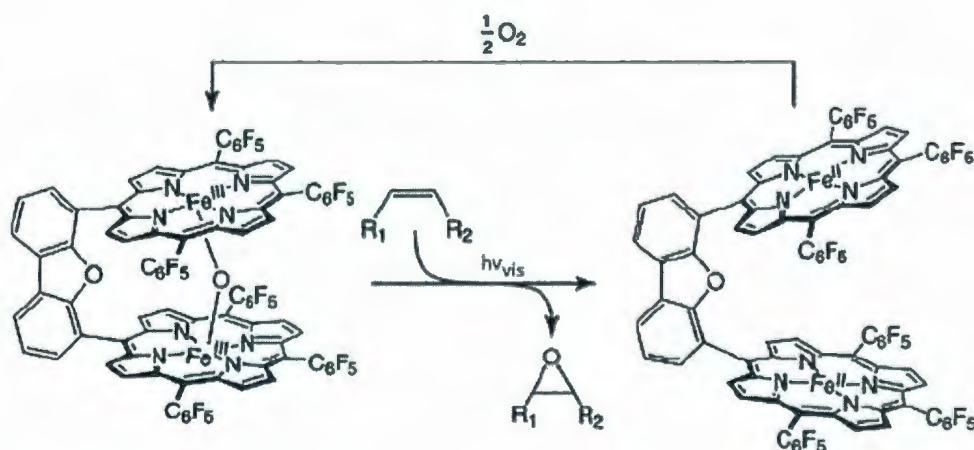


Figure 1.12: Iron porphyrin models used in model cytochrome P450 chemistry: (a) Chelated porphyrins prepared by Traylor *et al.*⁷⁵ (b) Heme thiolate linkage prepared by Woggon *et al.*⁷³

Over the years, the importance of a thiolate or other cysteine-like axial ligand has become apparent. This area in particular has led to substantial investigations through computational approaches. Harris⁷⁶ examines the influence of proximal and distal ligands with the enzymes and models, whereas Visser⁷⁷ provides DFT calculations focused on the effects of thiolate and chloride axial ligands on epoxidation reactions. Common to all three structures in Figure 1.12 is the presence of hydrocarbon chains for the purpose of adding steric bulk to the porphyrins. Without these chains, simulating the

restrictions imposed by the enzyme body, Fe=O porphyrins tend to form μ -oxo dimers. Once these dimers are formed, oxygen insertion reactions are prevented. μ -Oxo dimers are discussed further, in specific relation to the biomimetic assemblies fabricated in this project, in Chapter 5. The nature of the porphyrin heterocycle lends it to modification with an almost limitless combination of substrates. Aside from the prevention of dimerization, ring modification allows for regioselective epoxidation to give stereospecific products.

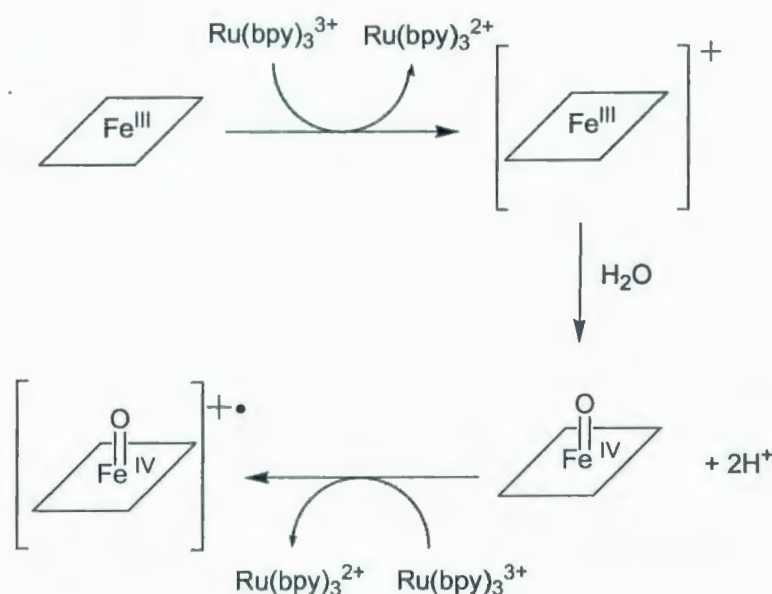
With these considerations in mind, one of the more novel approaches is that of Nocera *et al.*⁷⁸ shown in Scheme 1.8. Termed ‘Pacman porphyrins’, the Fe(III)-O-Fe(III) linkage is irradiated with light to achieve hemolytic cleavage, resulting in Fe(II) and Fe(IV)=O, where the latter proceeds with the epoxidation reaction.



Scheme 1.8: Epoxidation via Pacman porphyrins. Adapted from Reference 78.

These Pacman porphyrins are an example whereby a peroxide pathway is not used to initiate the reactions. Oxygen insertion or C-H bond activation initiated via absorption of photons holds great potential for storing light energy in chemical form, which is the

primary focus of this project. Gray *et al.*^{79,80} have reported the photo-induced oxidation of the iron porphyrin active sites within microperoxidase-8 and HRP (Scheme 1.9). In both cases $[\text{Ru}(\text{bpy})_3]^{2+}$ is irradiated with visible light in the presence of a sacrificial acceptor to produce $[\text{Ru}(\text{bpy})_3]^{3+}$. Using water as an oxygen source, two equivalents of $[\text{Ru}(\text{bpy})_3]^{3+}$ oxidizes the porphyrin ring to the $\text{Fe}(\text{IV})=\text{O}$ radical cation known as compound I.



Scheme 1.9: Photo-induced oxidation of iron porphyrin using $[\text{Ru}(\text{bpy})_3]^{3+}$ ^{79,80}.

More recently, Gray *et al.*⁸¹ have incorporated the ruthenium component directly into modified myoglobin using an alkyl chain attached to the porphyrin ring via an amide group, replacing one of the carboxylic acids. Photoexcitation of the ruthenium prosthetic group again generates the porphyrin radical cation. Analogous methods have been used by Thordarson *et al.*⁸² using a $[\text{Ru}(\text{tby})_2]^{2+}$ tethered to the active site porphyrin of cytochrome C.

Research towards the development of P450 and HRP models continues to produce an astounding display of creativity in design, for the purpose of chemical application and to better understand the mechanism under which these enzymes perform such complicated tasks with ease.

1.3 Research Targets

The primary goal of this project is to achieve photocatalytic oxygen insertion through a mechanism similar to that of the enzymes discussed previously. To accomplish this, a three-phase approach was used, as introduced earlier. Figures 1.13 and 1.14 show the specific components and assemblies used.

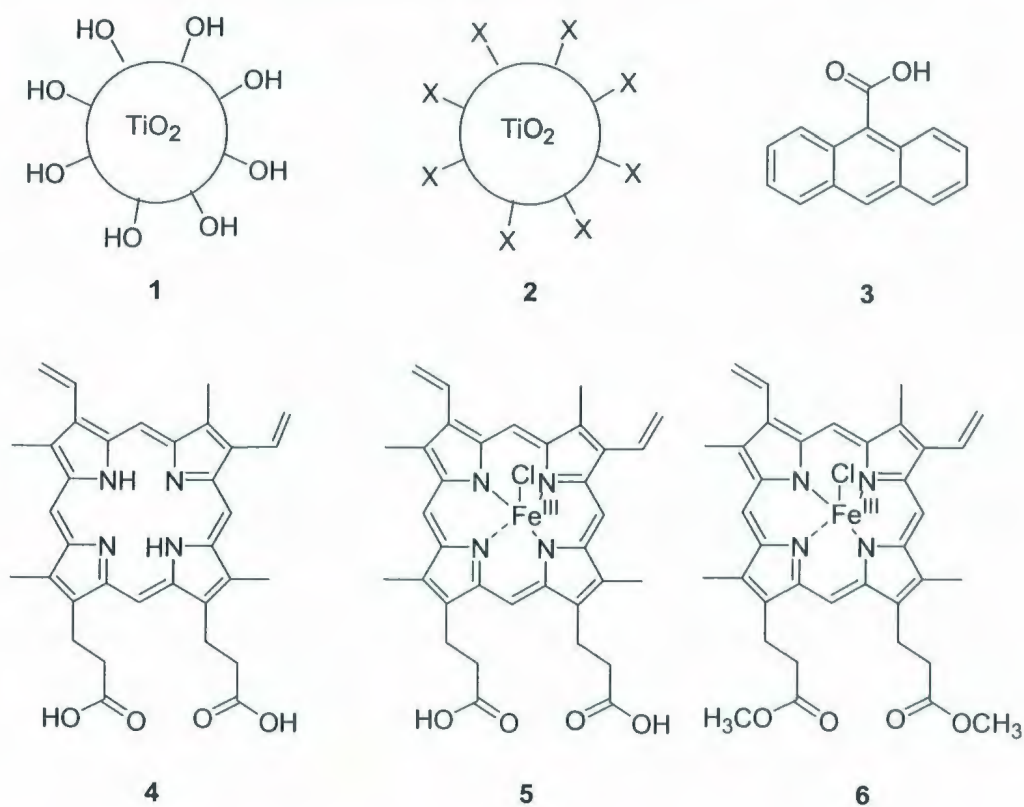


Figure 1.13: Component species of biomimetic assemblies.

Chapter 3 presents the synthesis and analysis of a suitable TiO₂ scaffold.

Nanoscale colloids were prepared via published methods using both hydrolytic and nonhydrolytic approaches to produce nanoscale anatase TiO₂ possessing a hydroxylated surface (1), TiO₂(OH)_n and nonhydroxylated surface (2), TiO₂(X)_n, respectively. These metal oxide materials were further characterized to assess each form for suitability in the next phase of building the biomimetic assemblies. 9-anthracenecarboxylic acid (3) was also utilized to probe the surface-substrate interface between TiO₂ and adsorbed molecules, specifically for TiO₂ prepared via nonhydrolytic means. Chapter 4 describes the fabrication of those assemblies using three similar porphyrins: protoporphyrin IX (4), hemin chloride (5), and hemin chloride dimethyl ester (6).

For the purpose of assessing biomimetic activity, the substrates were attached to the surface of the metal oxides to yield the assemblies shown in Figure 1.14. 7 was prepared from 9-anthracenecarboxylic acid (3) and nonhydrolytically-prepared TiO₂ (2) to assess both the properties of the metal oxide, as well as the potential of ¹H NMR as a spectroscopic tool for these assemblies. Assembly 8 was prepared from the apoporphyrin 4 with 1 for the development of synthetic methods and extraction procedures, as well as to examine the surface-substrate interface. The final assembly 9 was prepared using both porphyrins 5 and 6 using colloidal and film-based TiO₂ to proceed to Phase 3, namely, photocatalytic oxygen insertion.

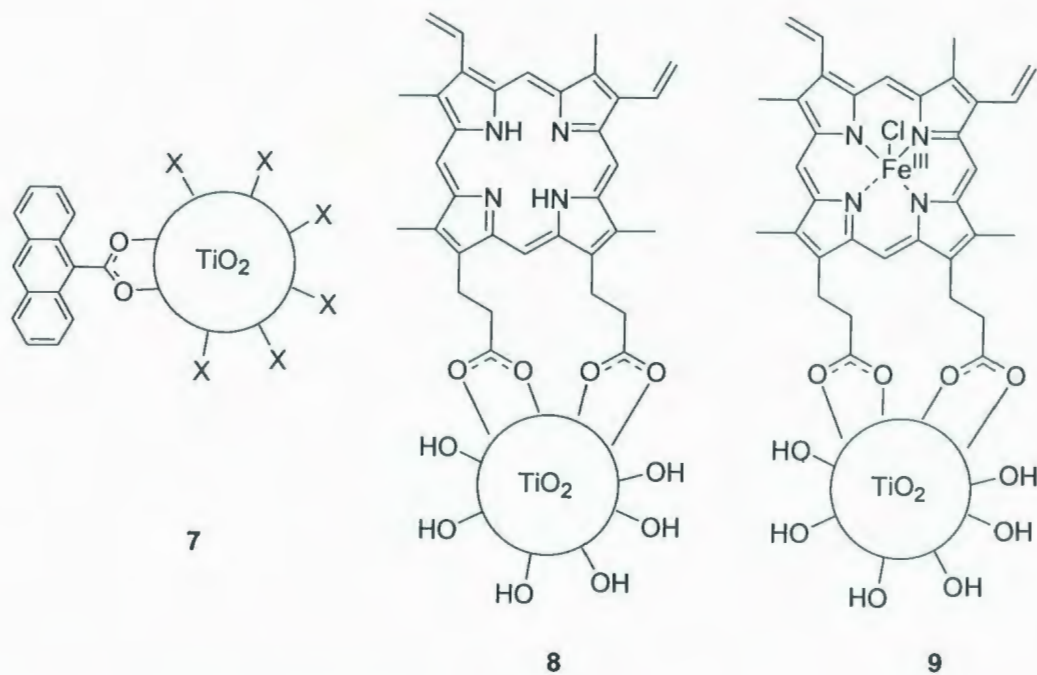


Figure 1.14: Biomimetic Assemblies.

Phase 4 may be considered separately from the main stream of the research. The production of TiO_2 membranes for the role of transmembrane electron transfer across distinct chemical environments was much more mechanical in nature.

Chapter 2

Experimental

Chapter 2 Experimental

2.1 General

Materials: Toluene (99.5%, Caledon) was dried and distilled from calcium hydride and stored over Type 4A molecular sieves. Water was purified using a Barnstead Nanopure II purification system, consisting of distillation followed by filtration through a colloid/organic removal filter (Barnstead D0835), high capacity ion exchange filter (Barnstead D0803), ultra-pure mixed bed filter (Barnstead D0809), and a final organic removal filter (Barnstead D0820). Water purified by this process is referred to as 'nanopure water'. Acetonitrile (99.5%, Caledon), anhydrous diethyl ether (99.0%, Caledon), anhydrous hexane (95+%, Aldrich), *N,N*-dimethylformamide, (DMF, 99.9% biotech grade, Aldrich), titanium(IV) isopropoxide (97%, Aldrich), titanium(IV) tetrachloride (99.9%, Aldrich), trioctylphosphine oxide (TOPO, 99%, Aldrich), heptadecane (99%, Aldrich), hemin chloride (>98%, Fluka Biochemika), chloroform (99.8% spectral grade, Caledon), methanol (Caledon), protoporphyrin IX disodium salt (Aldrich), 9-anthracenecarboxylic acid (9-AcCOOH, 99%, Aldrich), cyclohexene (99%, Caledon), cyclohexanol (donated by Dr. G. Bodwell, purity and manufacturer unknown, pure by ^1H NMR), cyclohexene oxide (98%, Aldrich), poly(ethylene glycol) (Carbowax[®], Aldrich), deuterated chloroform, (CDCl_3 , 0.05% v/v TMS, 99.8% atom D, Cambridge Isotope Laboratories, Inc.), deuterated *N,N*-dimethylformamide, ($\text{DCON}(\text{CD}_3)_2$, 99.5 % atom D, Aldrich) and Nafion[®] (5 % wt in solution of lower aliphatic alcohols and water, Aldrich) were all used as received. TiO_2 films on glass slides were generously donated

by Dr. Gerald J Meyer of John Hopkins University. Nafion 112[®] membranes were generously donated by Dr. P. Pickup of Memorial University of Newfoundland.

Instrumentation:

Ground State Measurements: UV-VIS spectra were obtained using an HP 8452A diode array spectrophotometer, using 1 cm path length quartz or glass cuvettes as required. Fourier Transform Infrared spectra were obtained using a Bruker Tensor 27 FTIR instrument, using KBr discs prepared using ~1% analyte in KBr versus a KBr blank. Signals are reported as wavenumber (cm^{-1}), width, intensity, and assignment. Spectra were processed using OPUS V4.0 software, provided by the manufacturer. NMR spectra were obtained on a Bruker AVANCE 500 MHz spectrometer, (^1H , ^{13}C , and COSY) or a GE Tecmag APOLLO 300MHz (^1H , ^{13}C). Spectra were processed using Acorn NMR's NUTS 2D V5.07 analysis software. The ^1H chemical shifts were measured relative to either a tetramethylsilane signal ($\delta = 0.00$ ppm) for CDCl_3 or the solvent signal ($\delta = 2.75$ ppm) for d_7 -DMF. The ^{13}C NMR chemical shifts were calibrated to the solvent signal ($\delta = 77.23$ ppm) for CDCl_3 and ($\delta = 163.15$ ppm) for d_7 -DMF. Individual ^1H signals are reported as chemical shift, multiplicity (s = singlet; d = doublet; t = triplet; m = multiplet), and coupling constants (Hz). Mass spectra were obtained using an Agilent 1100 series LC/MSD. Gas Chromatograph Flame Ionization Detector (GC-FID) chromatograms were obtained using a Varian 4200 GC-FID. Retention times evaluated using Varian Star Workstation V5.5. GC-FID chromatograms were obtained by the following procedure. After photoexcitation, hexane (2 mL) is added to a sample

of the reaction mixture (3 mL). Water (2 mL) is added, and the mixture capped, shaken, and allowed to separate. Using a glass syringe, a small amount of the hexane layer (2 μL) is extracted and injected into the GC-FID. The injector temperature was held constant at 200 °C. The column was held at 60 °C for 3 minutes. The temperature was increased at a rate of 15 °C/min to a temperature of 100 °C and held for 2 minutes, after which the temperature of the column was increased by 25 °C/min to 160 °C where it was held constant for another 2 minutes. The temperature was increased to 210 °C at a rate of 25 °C/min and held at that temperature for 2 minutes.

Photophysical and Photochemical Measurements: Broadband white light experiments were initiated using a 450 W Xenon arc lamp housed in a water-cooled Products for Research (PRA) Model ALH 220 lamp housing. The unit was powered by a PRA 302 power supply coupled to a PRA model 301 S capacitor bank. Excitation spectra were obtained using a Photon Technology International (PTI) Quantamaster 6000 emission spectrometer. Excitation light was provided by a 175 W USH10 Xenon arc lamp. The emitted light was collected at 90° to the excitation beam and detected by a Hamamatsu R-928 photomultiplier tube (PMT) in a photon counting mode. The PMT was housed in a PRA Pelletier cooled PMT Housing. All measurements were recorded using quartz fluorescence cells (Aldrich). All experiments were performed by measuring the solvent and cell first, and then adding the sample to the solution. The samples were saturated with $\text{N}_2(\text{g})$ by purging the samples for 60 minutes.

2.2 Synthesis:

Hydrolytic Preparation of Anatase Titanium(IV) Dioxide: $\text{TiO}_2(\text{OH})_n$

The synthesis of nanoscale $\text{TiO}_2(\text{OH})_n$ was carried out using the protocols described by Lian *et al.*⁸³ Briefly, a solution of titanium(IV) isopropoxide (5.0 mL, 17 mmol) in isopropanol (95 mL) was added dropwise to nanopure water (900 mL) containing $\text{HNO}_3(\text{aq})$ (pH \sim 2) over 1.5 h at 0 °C. The resulting opaque white mixture was stirred for 15 h at 0 °C. The solvent was removed *in vacuo* to yield white crystals of $\text{TiO}_2(\text{OH})_n$ (1.9g). IR (KBr Pellet) 500 cm^{-1} (broad, intense, ν Ti-O); 1384 cm^{-1} (sharp, intense, ν NO_3^-); 3500-2500 cm^{-1} (broad, medium, ν O-H).

Nonhydrolytic Preparation of Anatase Titanium(IV) Dioxide: $\text{TiO}_2(\text{X})_n$

$\text{TiO}_2(\text{X})_n$ was prepared by a modified synthesis to the previously published procedure by Colvin *et al.*¹ Trioctylphosphine oxide (2.5 g, 6.5 mmol) was added to heptadecane (22.5 mL) in a 3-neck flask equipped with stir bar and condenser. The flask and contents were purged with $\text{N}_2(\text{g})$ for 15 minutes. Titanium(IV) tetrachloride (0.24 mL) was injected, and the mixture heated to reflux at 300 °C. Upon reaching reflux, titanium(IV) isopropoxide (0.65 mL) was immediately added via syringe. The mixture was refluxed for 5 minutes and cooled to room temperature, yielding a white crystalline material. The reaction mixture was centrifuged and the liquid decanted. The precipitate was washed with heptadecane with further centrifugation until washings became clear and colourless. The isolated solid was washed with hexane and filtered to yield TiO_2 as

an off-white powder (142.7 mg). The sample was dried under high vacuum at ~ 200 °C to remove residual solvent. IR (KBr Pellet) 500 cm^{-1} (broad, intense, ν Ti-O).

Hemin Chloride Dimethyl Ester

Following the preparation of Smith,⁸⁴ hemin chloride (64.6 mg) was dissolved in 5% v/v $\text{H}_2\text{SO}_4(\text{aq})/\text{MeOH}(\text{l})$ (20 mL) and stored in the dark and stirred overnight. Addition of $\text{CHCl}_3(\text{l})$ (40 mL) to the reaction mixture and subsequent washings with 2 M $\text{Na}_2\text{CO}_3(\text{aq})$ (2 x 30 mL) to neutralize residual acid was followed by a washing with water (30 mL). The aqueous layers were combined and back-extracted with $\text{CHCl}_3(\text{l})$ (2 x 20 mL). Organic layers were combined and dried over $\text{MgSO}_4(\text{s})$. The solvent was removed *in vacuo*, and dried under high vacuum. Quantitative amounts of the dark purple crystalline solid obtained and stored at 0°C. UV-VIS: $\lambda_{\text{max}} = 394\text{nm}$.

2.3 In-situ Generation of Materials:

$\text{TiO}_2(\text{X})_n$ + 9-Anthracenecarboxylic Acid

Nonhydrolytic $\text{TiO}_2(\text{X})_n$ (61.0 mg) was placed in an NMR tube with $\text{CDCl}_3(\text{l})$ (~ 1 mL). To this, 9-anthracenecarboxylic acid (6.6 mg) was added. This was repeated in reverse order where TiO_2 (10.8mg) was added to an NMR tube containing 9-anthracenecarboxylic acid (7.1 mg) in $\text{CDCl}_3(\text{l})$. ^1H NMR spectra were obtained at various time intervals over a period of 96 hours.

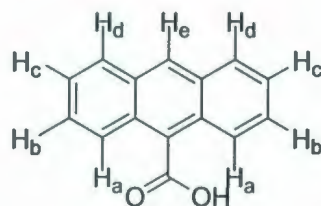


Figure 2.1: Peak assignments for 9-anthracenecarboxylic acid.

9-Anthracenecarboxylic acid: ^1H NMR (CDCl_3 , 300 MHz) δ 7.54 (t, 2H, **H_c**), 7.634 (t, 2H, **H_b**), 8.08 (d, 2H, **H_d**), 8.37 (d, 2H, **H_a**), 8.62 (s, 1H, **H_e**). $\text{TiO}_2(\text{X})_n + 9$ -anthracenecarboxylic acid ^1H NMR (CDCl_3 , 500 MHz) δ 0.56 (broad m), 0.88 (m), 0.99 (broad m), 1.14 (broad m), 1.42 (broad m), 1.84 (broad m), 2.17 (s), 7.35 (t), 7.41 (m), 7.46 (m), 7.52 (broad m), 7.61 (broad m), 7.97 (d), 8.00 (m), 8.05 (broad m), 8.33 (broad m), 8.48 (s), 8.54 (s), 8.59 (broad m), 8.64 (d), 8.99 (d).

$\text{TiO}_2(\text{OH})_n + \text{Protoporphyrin IX}$ Assembly

A suspension of protoporphyrin IX disodium salt (2.9 mg) in nanopure water (5.0 mL) was added via syringe to an aqueous solution of $\text{TiO}_2(\text{OH})_n$ (56.8 mg) in nanopure water (2.0 mL). The burgundy mixture was stirred overnight at room temperature, and the resulting solid was isolated by vacuum filtration, and washed with H_2O (2 x 10 mL). After allowing the solid to dry, DMF was used to extract the product from the filter paper and the solvent removed under reduced pressure yielding a black oil (9.2 mg). Care was taken to isolate samples from light as a precaution. ^1H NMR (DMF-d_7 , 500 MHz) δ 0.89 (m, 4H, $\text{CH}_2\text{CH}_2\text{COO}$), 1.29 (m, 12H, CH_3), 1.55 (m, 4H, $\text{CH}_2\text{CH}_2\text{COO}$), 4.80 (m, 4H, CHCH_2), 8.25 (m, 2H CHCH_2); UV-VIS (DMF , Quartz Cuvette) 268 nm (TiO_2), λ_{max}

406 nm (Soret Band), 506 nm, 540 nm, 574 nm (Q-bands); IR (KBr Pellet) 3442 cm^{-1} , 2929 cm^{-1} , 1671 cm^{-1} , 1384 cm^{-1} , 1054 cm^{-1} ; Emission (JPV3-80) (DMF, aerated) fluorescence = 644 nm; Excitation using 644 nm, (DMF, aerated) fluorescence = 406 nm.

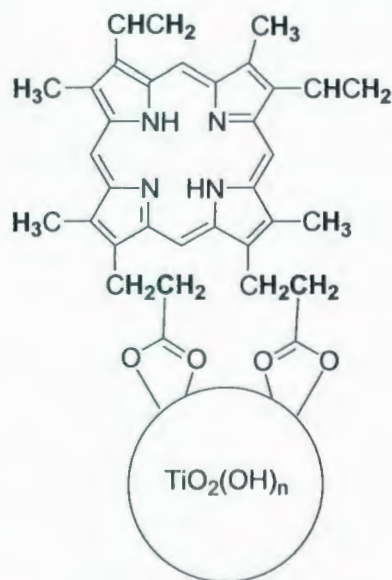


Figure 2.2: Protoporphyrin IX/TiO₂ assembly.

TiO₂(OH)_n + Hemin Chloride Assembly

Hydrolytically-prepared TiO₂ (111.0 mg) was combined with hemin chloride (21.8 mg) in 3% v/v DMF/H₂O (10 mL) and stirred at room temperature for 15 h. A black solid was isolated by gravity filtration. The black solid was extracted from the filter paper with pure DMF, yielding a burgundy solution. The DMF was removed under reduced pressure, and the resulting black solid washed with diethyl ether to remove any remaining DMF, yielding a black solid (68.3 mg). UV-VIS (DMF, Quartz Cuvette) 272 nm (TiO₂), λ_{max} 394nm (Soret Band), 510 nm, 542 nm, 642nm (Q-bands); IR (KBr Pellet) 663 cm^{-1} , 1023 cm^{-1} , 1470 cm^{-1} , 1658 cm^{-1} , 2439 cm^{-1} , 2780 cm^{-1} , 3024 cm^{-1} .

TiO₂(OH)_n + Hemin Chloride Dimethyl Ester Assembly

Hydrolytically-prepared TiO₂ (406.1 mg) was combined with hemin chloride dimethyl ester (25.6 mg) in CHCl₃ (15 mL) in a pear shaped flask. The dark purple mixture was stirred in the dark for 96 h. The solid was isolated from the purple solution by centrifuge and the mother liquor decanted. The precipitate was washed with CHCl₃(l) (10 mL portions) until the washings became colourless. Any residual solvent was removed under reduced pressure yielding a beige solid (364.4 mg).

TiO₂(OH)_n Films (Glass Slides) + Hemin Chloride Dimethyl Ester Assembly

TiO₂ films (clear, colourless) on glass slides were immersed in a dilute solution of hemin chloride dimethyl ester in acetonitrile. The vial was sealed with a rubber septum and stored in the dark overnight. The films were removed from the solution, rinsed with chloroform, and allowed to dry. Tethering was evidenced by a change in the colour of the films, from transparent and colourless, to transparent orange. The modified films were stored in the dark. UV-VIS (glass slide) λ_{max} 394 nm.

2.4 Photocatalysis

Broad Band Excitation: The hemin chloride/TiO₂ assembly (1.0 mg) was combined with cyclohexene (41.8 mg) in DMF (9.0 mL) to give a burgundy solution. NaOH(aq) (1.0 mL, 9×10^{-4} mol/L) was added. After ~ 10 min a dark brown precipitate formed. The mixture was stirred and irradiated with white light overnight, yielding a transparent

yellow solution. The reaction was followed by UV-VIS spectrometry. Products were analyzed using LC-MS, UV-VIS, and GC-FID through comparison of retention times with standards.

Soret Band Excitation: Cyclohexene (3 μL) was added to a quartz cuvette containing aerated toluene (3 mL). A glass slide coated with a film of hydrolytic TiO_2 in Carbowax[®] previously derivatized with hemin chloride dimethyl ester was placed diagonally in the quartz cuvette. A rubber septum was placed on top of the cuvette to prevent contamination of the sample. This apparatus was then placed in the PTI fluorimeter. The assembly was then irradiated at 420 nm for 278 minutes. Small portions of the toluene solution were removed at various time intervals throughout the experiment for analysis. The experiment was halted at various times to analyze the TiO_2 assembly by UV-VIS as irradiation progressed. The toluene solution was analyzed for reactants and products using the GC-FID.

Chapter 3

Nanocrystalline Materials

Chapter 3 Nanocrystalline Materials

3.1 Introduction

The first step towards the development of the target catalytic assemblies was the selection, preparation, and characterization of the metal oxide semiconductor scaffold. Titanium(IV) dioxide can be prepared by several different procedures, with each method influencing the structural characteristics and electrochemical properties of the particles formed. Nanoscale anatase TiO_2 was required for its electrochemical properties as discussed in Chapter 1. In addition, it was decided to use the nanoparticles in colloidal form, as opposed to sol-gel film, for ease of characterization by NMR, which cannot be accomplished in films. The final consideration is the surface structure of the colloids. The interfacial region, as shown in Figure 3.1, between the metal oxide surface and bulk solution is important in terms of its influence over solubility and tethering interactions with substrate molecules coupled to the field effects, such as dielectric properties.

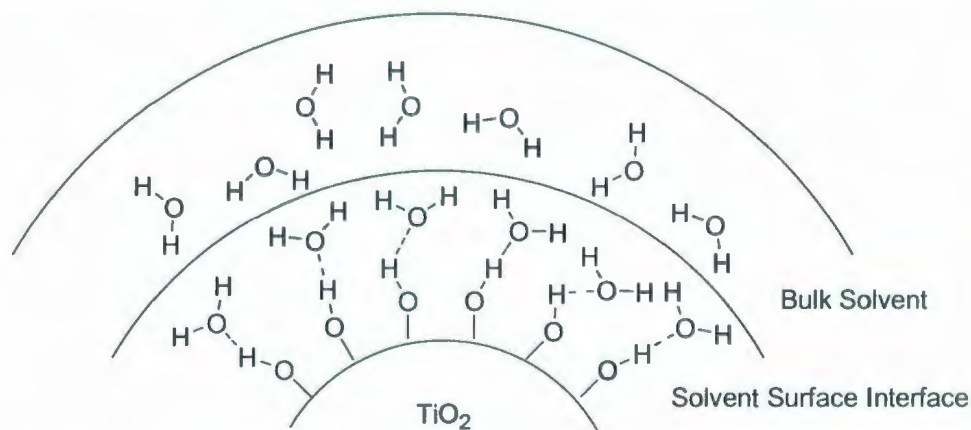


Figure 3.1: Solvent-surface interface on TiO_2 . Static electric fields, charge distribution within the particles, defect sites, and the coordination of solvent molecules play important roles in the interfacial region.

Two synthetic methods, as well as attempted modifications of existing capping agents, were chosen and studied. As discussed in Chapter 1, TiO₂ is found in three different forms: anatase, rutile, and brookite. While all are capable of absorbing light and achieving band gap excitation, anatase is the form most often used for photochemical applications.⁹ In unmodified form, anatase TiO₂ has the ability to absorb light at 270 nm, resulting in production of an exciton. This exciton is an electron/hole pair [e^-_{cb}, h^+_{vb}] where the electron is promoted into the conduction band resulting in a positively charged hole in the valence band. This hole can migrate to the surface of the particle where it can be utilized in a variety of reactions, as discussed in Chapter 1. For the purpose of this project, it is the extension of band gap excitation to interfacial electron transfer that makes TiO₂ a viable foundation for the catalytic assembly. Although band gap excitation is a useful process it offers access to a limited portion of the electromagnetic spectrum and little control over the highly reactive excited electron and positively charged hole pair. Through modification of the surface of the TiO₂ particles, band gap excitation can be used indirectly to accept electrons from attached chromophores through a process referred to as interfacial electron transfer. Chromophores attain excited states through direct absorption of light, followed by injection of the high-energy electrons into the conduction band of TiO₂. TiO₂ acts as an electron sink leaving the donor compound in an oxidized excited state. It is this reactive state that is the core of the target catalysts.

In the photochemical applications of TiO₂ some of the more common methods employ the use of films, sol-gels, or some other fixed medium. The utilization of TiO₂ in these forms often involves the use of an additive to perform the role of binding agent

in order to increase the strength and practicality of the films. One of the goals of this project is to better characterize the surface structure of the nanoparticles, including identification and interconversion of capping agents, and investigation into the tethering interactions of various molecules. With this in mind, the semiconductor was prepared in colloidal form. This form, free of any interference from additives, would provide additional clarity when it comes to looking into the surface structure and interactions with various chromophores. Aside from surface characterization, unhindered colloids possess a certain amount of mobility which may prove useful in the assembly of different materials. Retention of the colloidal mobility in solution may be useful in the development of nanoparticles linked via conductive polymers, which may hold possibility for excited states with extended charge separation, shown below.

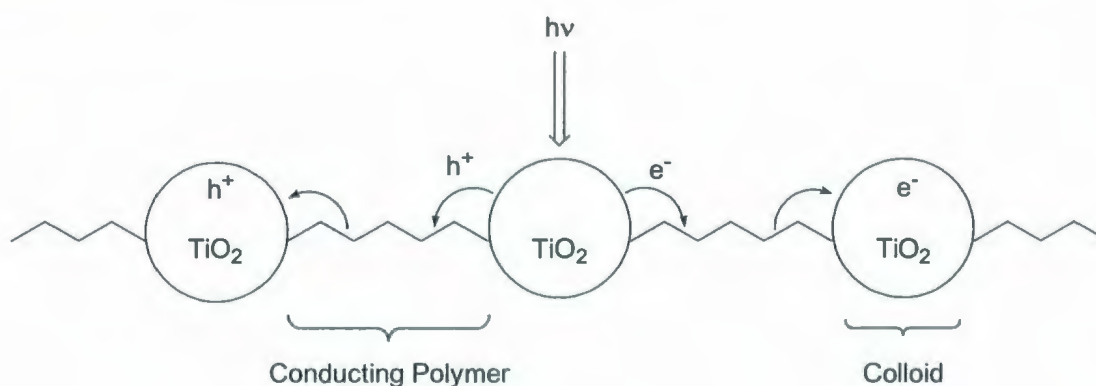


Figure 3.2: TiO_2 colloids linked via conductive polymers for extended charge separation.

Although outside of the scope of this project, the possibility of fabricating this type of assembly in the future emphasizes the importance of building the initial phase of

research around a form of TiO_2 that is versatile and applicable in the long term.

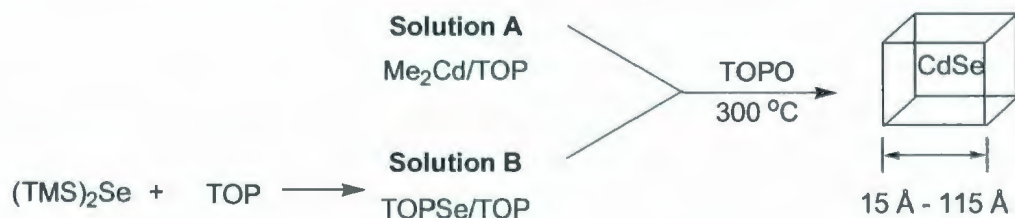
Restriction of the nanoparticles would not allow for the mobility needed for the assembly of these types of structures.

The surface structure of the TiO_2 nanoparticles depends primarily on the synthetic approach used to make them. The surface is comprised of the terminal ends of the Ti-O-Ti grids that compose the internal structure of the nanoparticles. The functional groups that terminate the chains are referred to as capping agents. The method of preparation determines exactly what groups are present on the surface of the colloids. These capping agents govern the interactions that the particles have with any surrounding molecules. Solubility and tethering of chromophores to the semiconductor are influenced by the identity of the capping agents. The two procedures chosen for the production of the TiO_2 particles provide different capping agents. The first, via hydrolysis of a titanium alkoxide results in hydroxyl functional groups on the surface of the nanoparticles. This method is widely used and established. The particles formed are easily dispersed in water.

The second reaction proceeds through the thermal decomposition of molecular precursors but in a nonaqueous medium. Developed by Colvin *et al.*¹ this approach utilizes the thermal decomposition of molecular precursors in the presence of a passivating agent at high temperatures to produce the metal oxide semiconductors. The primary focus of this project was the development of material without the hydroxyl surface groups formed in aqueous-based routes. Briefly, a titanium halide (TiF_4 , TiCl_4 , TiBr_4 , TiI_4) is added to a TOPO/heptadecane mixture, and is heated to 300 °C. A titanium alkoxide ($\text{Ti}(\text{OCH}_3)_4$, $\text{Ti}(\text{OCH}_2\text{CH}_3)_4$, $\text{Ti}(\text{OPr}^i)_4$, $\text{Ti}(\text{OBu}^t)_4$) was then rapidly

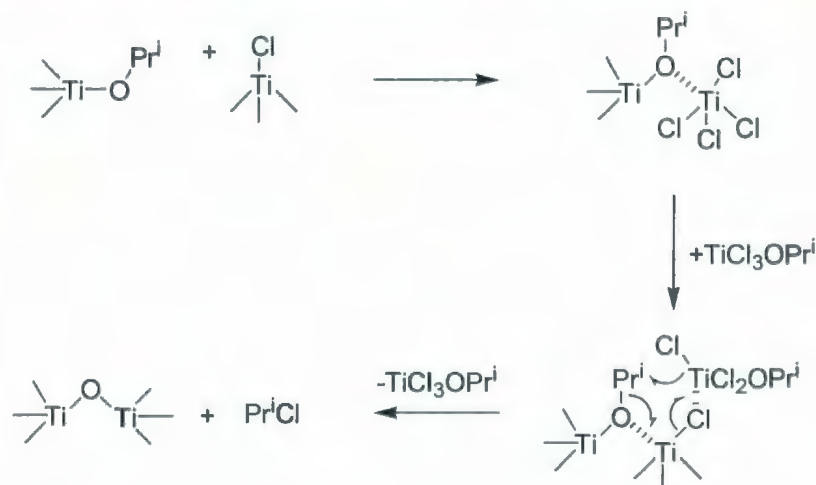
injected into the hot solution. High reactant concentrations resulted in the formation of a precipitate and low concentrations formed clear orange solutions. Precipitates were isolated by centrifugation and were washed with acetone. Reports of low yields were attributed to retention of material by the reaction solution, as evidenced by partial precipitation upon the addition of acetone.

The product is described as nanoscale anatase TiO_2 on the order of 3 to 10 nm in diameter, with a high degree of crystalline perfection. In place of hydroxyl capping agents, it is proposed that the passivating agent, trioctylphosphine oxide, is coordinated to the surface and is responsible for the exhibited high dispersibility in hydrocarbon solvents. The absence of hydroxyl groups in the product is supported by FTIR spectroscopy of the reaction solution. Trace amounts of water are observed but Colvin asserts the amount is much less than the amount required to completely cover the particle surfaces. This procedure was developed based on methods previously reported for the fabrication of group II-VI semiconductor clusters. Murray *et al.*⁸⁵ used rapid thermal decomposition of molecular precursors in the production of CdS, CdSe, and CdTe semiconductor nanocrystallites. Scheme 3.1 shows a simplified summary of the approach used by Murray *et al.*



Scheme 3.1: Synthesis of CdSe nanocrystallites. Adapted from Reference 86.

Two separate solutions were prepared. The first, solution A, was prepared by the addition of dimethylcadmium to trioctylphosphine (TOP). Solution B, the source of Se, involves the preparation of a stock solution of TOPSe, through the addition of bis(trimethylsilyl)sulfide to a volume of TOP. This stock solution is then added to an additional volume of TOP. This mixture of solution A and B is quickly injected into TOPO at 300 °C. Murray's group isolated crystals that range in size from 15 Å to 115 Å by extraction of aliquots of the reaction mixture at specific time intervals in the growth process. The growth rate of the crystals can be controlled by varying the reaction temperature. In addition, the group developed size-selective precipitation methods for the nanocrystallites. Following this approach, Colvin's group extended the methodology to include metal oxides. The mechanism of reaction is provided by Vioux.⁸⁶ Scheme 3.2 shows the reaction of the titanium(IV) isopropoxide group with TiCl₄ to form the Ti-O-Ti chains that compose the semiconductor nanocrystals. Initially, the oxygen within the metal alkoxide coordinates to the titanium present in the tetrachloride.



Scheme 3.2: Mechanism of TiO₂ formation via nonhydrolytic route.

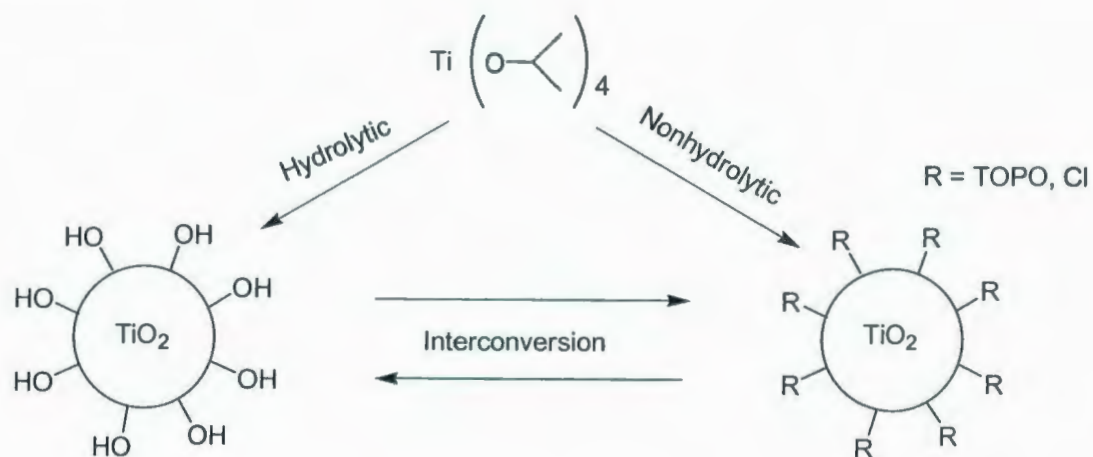
Coordination with $\text{TiCl}_3\text{OPr}^i$, another intermediate within the cycle leads to a rearrangement reaction in which a new Ti-O bond is formed. The byproduct of this reaction, which provides support for this mechanism, is 2-chloropropane. This cycle continues as more Ti-O bonds are formed, and the particles grow.

The synthetic preparation proposed by Colvin differs from Murray's in that heptadecane, $\text{C}_{17}\text{H}_{36}$, is used as the solvent. This allows for the use of high temperatures (b.p. $303\text{ }^\circ\text{C}$) which are needed for the thermal decomposition of the molecular precursors. TOPO is present as a passivating agent to slow the development of the nanocrystallites and control the growth. In addition to its role as a passivating agent TOPO is reported to be the alternate surface capping agent. The presence of 2-chloropropane isolated within a liquid nitrogen trap attached in order to capture any byproducts vaporized during the reaction is supplied as evidence of a mechanism analogous to that proposed by Murray.

The prospect of creating nanoscale anatase TiO_2 which could be soluble in organic solvents was appealing enough to justify an investigation into the practicality of this reaction. A review of the paper and its supporting information did raise several questions. Primary interest centered on the identification of the capping agents. Colvin provides evidence for the absence of OH but the support offered for the presence of TOPO could be considered to be weak. The conjecture that TOPO is attached to the surface of the particles is based solely on the fact that the particles exhibit solubility in organic solvents. The only portion of the IR spectrum provided is an isolated range focused on the hydroxyl stretching frequency. It would stand to reason if TOPO were

present on the surface of the particles it would be substantial enough to exhibit a P=O stretch in the IR spectra. In addition, data provided from mass spectrometry experiments of the by-products of the reaction, exhibits a peak at $m/z = 18$ (possibly H₂O) which is not addressed in Colvin's paper. This raises questions concerning the susceptibility of the particles to the adherence of water. The paper did not refer to any special precautions taken to isolate the samples from atmospheric water. The majority of the spectroscopic evidence was based on solutions of the metal oxide. XRD and TEM were obtained from the solid material, but corresponding data confirming the absence of hydroxyl groups following isolation from the liquid phase for these materials, was not provided.

Both the hydrolytic and nonhydrolytic preparations of TiO₂ were examined. In addition, the attempted interconversion of the hydroxyl capping agents to produce a material with alternate capping agents while still using the hydrolysis of a titanium alkoxide as a starting point was performed. Interconversion of the capping moieties on the nonhydrolytically-prepared TiO₂ to hydroxyl groups was also achieved. Scheme 3.3 presents an overview of the reactions studied.



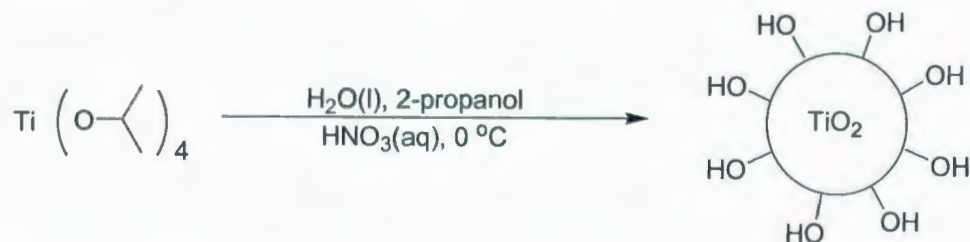
Scheme 3.3: Synthesis and interconversion of TiO_2 surfaces.

Henceforth, titanium(IV) dioxide prepared via hydrolytic and nonhydrolytic methods are noted using the notation $\text{TiO}_2(\text{OH})_n$ and $\text{TiO}_2(\text{X})_n$ respectively.

3.2 Results and Discussion

3.2.1 Hydrolytic Preparation of Anatase Titanium(IV) Dioxide

Following the procedure outlined by Lian *et al.*⁸³ the synthesis of anatase nanocrystalline TiO_2 via the hydrolysis of titanium(IV) isopropoxide is outlined below.



Scheme 3.4: Hydrolysis of titanium(IV) isopropoxide to yield $\text{TiO}_2(\text{OH})_n$.

Titanium(IV) isopropoxide in 2-propanol was added dropwise to an acidified ($\text{HNO}_3(\text{aq})$, $\text{pH} \sim 2$) solution of nanopure water at 0°C . The resulting white opaque solution was then stirred for 15 h at 0°C . After removal of solvents *in vacuo*, a colourless crystalline solid was obtained. The reliability of this reaction makes it appealing to produce the semiconductor supports for the catalyst. It proved to be easily reproducible and reliable. The high yield and relatively large scale (1 – 2 grams) which could be obtained was useful as a starting point for this project. XRD analysis by Hughes⁸⁷ verified the presence of anatase as the major component with a small amount of rutile present. It was found to be dispersible in water but not in all of the organic solvents which were tested.

The sample was analyzed by UV-VIS not only to verify the formation of $\text{TiO}_2(\text{OH})_n$, but also as a spectroscopic reference for future experiments.

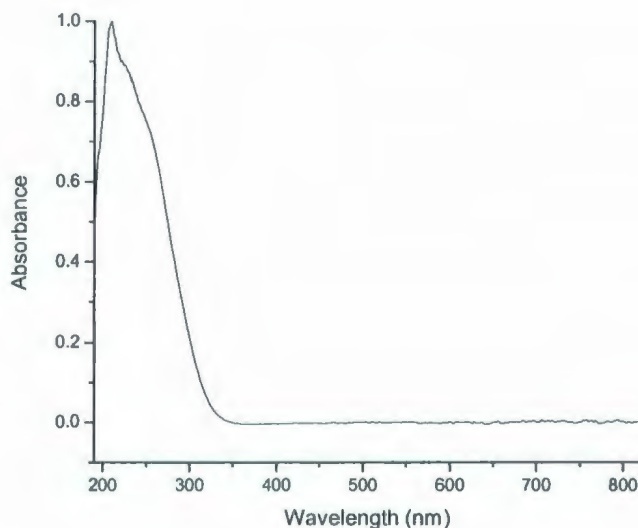


Figure 3.3: UV-VIS of colloidal anatase $\text{TiO}_2(\text{OH})_n$ in nanopure H_2O .

An IR spectrum was also obtained, and it displayed the characteristic Ti-O stretch ($\sim 500 - 800 \text{ cm}^{-1}$) and O-H stretch ($\sim 3200 \text{ cm}^{-1}$) frequencies. The sharp peak at $\sim 1400 \text{ cm}^{-1}$ indicates the presence of residual nitrates from the nitric acid used to produce the acidic reaction conditions necessary.

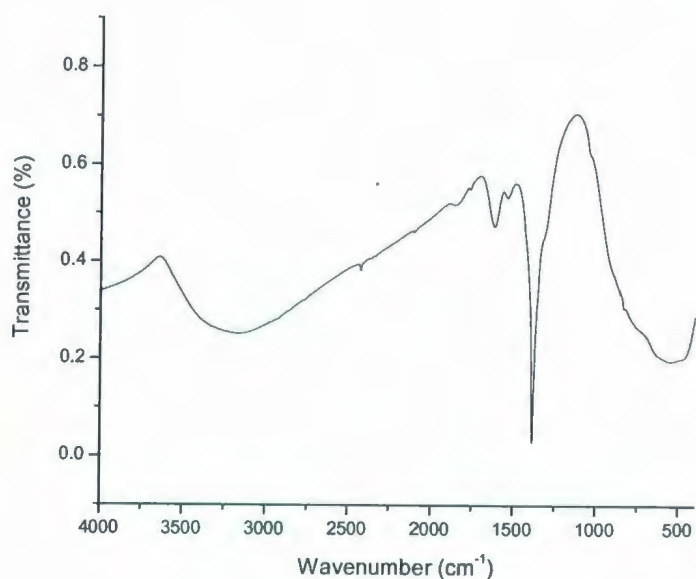
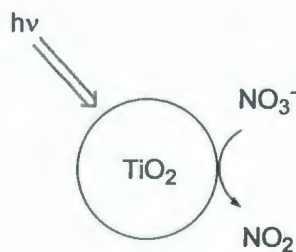


Figure 3.4: Infrared spectrum of $\text{TiO}_2(\text{OH})_n$ in KBr.

Although this reaction proved reliable and reproducible, on occasion a slight yellow discoloration was present in the isolated solid following removal of solvent. In addition, prolonged storage in a sealed sample vial at times resulted in the development of a reddish-brown gas above the solid. The source of this discoloration was hypothesized to be the nitric acid used in the acidification of the reaction solution, as seen in the IR spectrum. Depending on the strength of the vacuum applied to the rotary evaporator, it is possible that removal of the acid (b.p. $120.5 \text{ }^\circ\text{C}$) was incomplete. If

adsorption and/or retention of the nitric acid by $\text{TiO}_2(\text{OH})_n$ occurred, it is possible the nitric acid was being reduced via photochemical activation of the semiconductor. Samples where formation of the reddish-brown gas was evident were generally stored without protection from light.



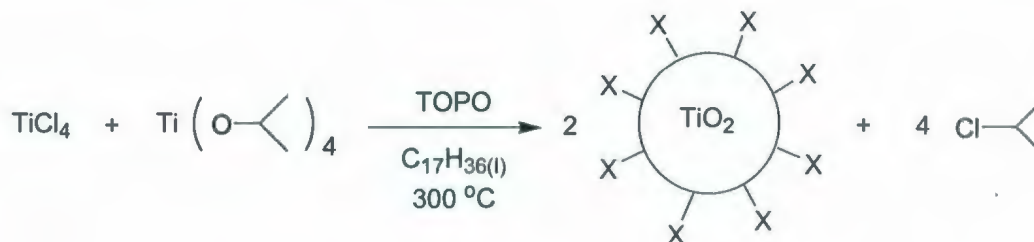
Scheme 3.5: Photodegradation and reduction of nitric acid on $\text{TiO}_2(\text{OH})_n$.

Although the effect that the presence of HNO_3 on the surface of TiO_2 has on the energetics of the metal oxide is not clear, removal of this impurity was considered important in order to avoid interference with any future reactions. Following solvent removal, samples were stored in vacuum desiccators for several days under high vacuum. This proved successful in extending the shelf life of the samples and eliminating the formation of the gas, taken as evidence for the removal of nitric acid from the solid TiO_2 .

This reaction proved to be an excellent means for the production of large amounts of starting material, with consistent results. The solids obtained exhibited extended shelf life and could be used with no noticeable spectroscopic differences over several months.

3.2.2 Nonhydrolytic Preparation of Anatase Titanium(IV) Dioxide

Following the procedure outlined by Colvin,¹ the synthesis of nanocrystalline anatase titanium(IV) dioxide was attempted.



Scheme 3.6: Nonhydrolytic synthesis of $\text{TiO}_2(\text{X})_n$.

The first attempt at repeating this synthesis followed the information provided by the published paper. Trioctylphosphine oxide (2.5 g) was added to a flask containing heptadecane (22.5 mL). Titanium(IV) chloride (0.24 mL) was added creating a yellow mixture. A condenser was attached and the mixture was placed under a static atmosphere of nitrogen, was stirred and heated to the point of reflux at $300\text{ }^\circ\text{C}$. At this point, the TOPO had dissolved, giving a clear orange solution. Titanium(IV) isopropoxide (0.65 mL) was injected into the hot solution. Vaporization of the injected liquid was instantaneous and the reaction vessel became filled with a white vapor. Formation of a precipitate was evident. After 5 minutes, heating was discontinued and the reaction mixture was allowed to cool to room temperature. Isolation of the solid from the non-volatile heptadecane was achieved through centrifugation. Repeated acetone washings

followed by further centrifugation were used to remove any residual heptadecane. The grey-white solid obtained was dried *in vacuo* (142 mg).

Initial analysis showed promise for the formation of TiO_2 . While UV-VIS spectroscopic data was supportive for the formation of $\text{TiO}_2(\text{X})_n$, IR spectroscopy exhibited evidence for the presence of hydroxyl groups ($3500 - 2500 \text{ cm}^{-1}$). Spectra appeared nearly identical to that of TiO_2 prepared via hydrolytic means, with the exception of the NO_3^- peak seen earlier.

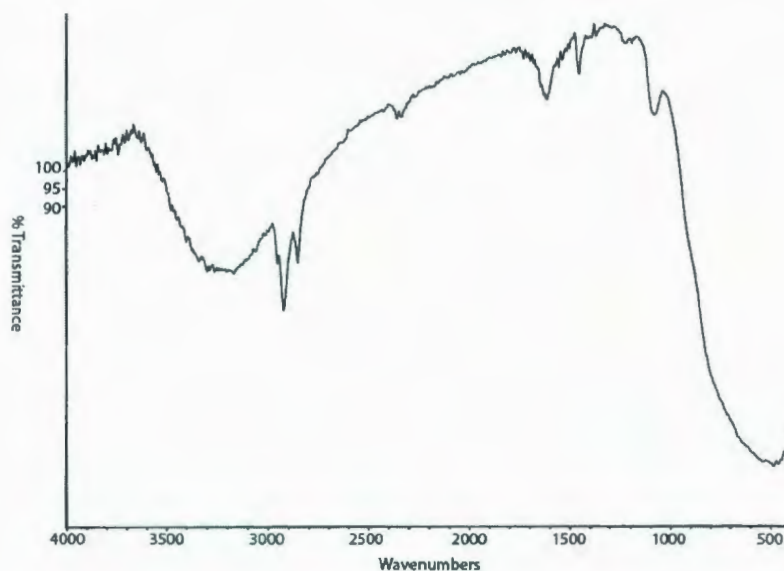


Figure 3.5: IR spectra of $\text{TiO}_2(\text{X})_n$ prepared via nonhydrolytic means in KBr.

The C-H stretch (2900 cm^{-1}) evident is attributed to either residual heptadecane or possibly TOPO capping agents. These results indicate that the thermal decomposition of molecular precursors successfully produced TiO_2 , but failed to produce a material having no hydroxyl groups present. The question remains as to whether the incorporation of the

hydroxyl groups occurred within the synthetic process, or were adsorbed during the isolation procedures. The O-H stretch may therefore not indicate hydroxyl capping agents, but possibly adsorbed atmospheric water.

In Colvin's publication, support for the absence of hydroxyl groups is provided via IR of the reaction solution, shown in the Figure 3.6. The lower part of the figure shows the reaction solution following the addition of 3 μL of water, the amount calculated to cover the surface of the colloids.

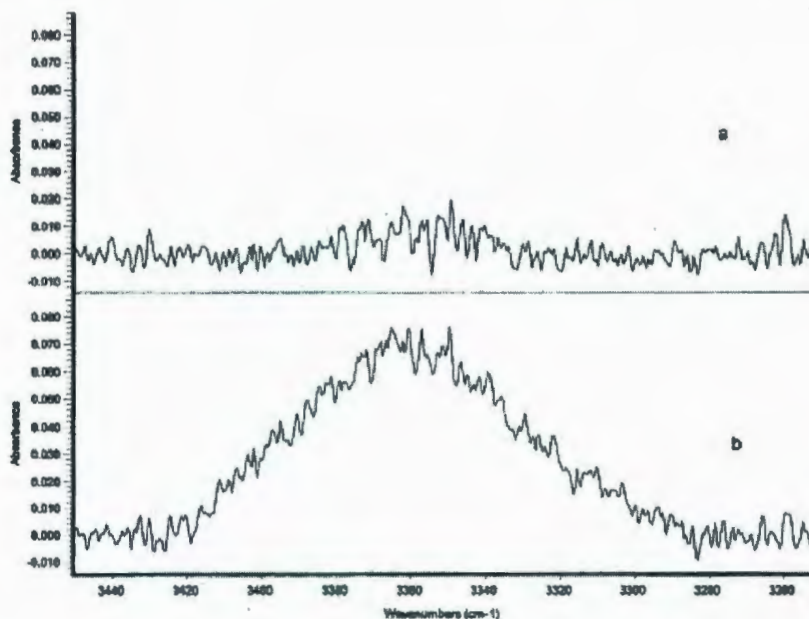


Figure 3.6: Supporting information supplied by Colvin as evidence for the absence of hydroxyl surface groups. Adapted from Reference 1.

While these results support Colvin's conclusions for the reaction solution, no unambiguous direct evidence is provided to show the material was not only synthesized

without any hydroxyl groups on the surface of the nanoparticles but also remained so through isolation and storage.

The main objective in pursuing this route is to enable production of TiO_2 colloids without hydroxyl capping agents, and that are dispersible in organic media. After several attempts, it was clear that in our hands, the synthesis of $\text{TiO}_2(\text{X})_n$ outlined by Colvin was not reproducible. Given the initial failures, focus shifted towards modification of the synthetic method. Several different approaches were attempted. Closed and open systems were considered, as well under dynamic and static atmospheres of nitrogen. Given the volatility of the reactants, retention of the materials was examined, while still allowing for the elimination of byproducts.

Injection of titanium(IV) isopropoxide into the base of the heated reaction mixture results in a vigorous vaporization which often resulted in the ejection of glass stoppers from the reaction vessel. Retention of these volatile reactants would be best achieved using a closed system, but for safety reasons, caution was taken to ensure the system remained open, with pressure release through the nitrogen line possible. The reaction apparatus consisted of glassware heated via an oil bath at $300\text{ }^\circ\text{C}$ and any dramatic increase in pressure would likely have an undesirable outcome. Supporting the assumption that the system remained open in Colvin's procedure is her description of the removal of haloalkane byproducts via vaporization at high temperature. With this in mind, several reactions were attempted using an open system under a dynamic flow of nitrogen vented through a cooled trap (0°C) with the absence of a condenser to allow for the free flow of any produced vapors. Under these conditions, the formation of a

precipitate following the injection of titanium(IV) isopropoxide did occur, but it disappeared following cooling of the reaction mixture to room temperature. This redispersion of the precipitate is taken as evidence for the reduction of reactant concentrations as correlated to reports from Colvin regarding the absence of precipitate when lower reactant concentrations are initially added to the reaction. The injection of volatile components into the heated reaction solution (300 °C) under a dynamic flow of nitrogen would aid in the removal of unwanted byproducts but also enhances the loss of starting material. To test this theory, the same reaction mixture was once again heated to the point of reflux, and additional equivalents of titanium(IV) isopropoxide and TiCl_4 were then added. Before the addition of these reactants however the precipitate reappeared at ~ 180 °C. The white solid did not redissolve following cooling to room temperature. Following similar isolation procedures mentioned previously, TiO_2 prepared via nonhydrolytic means was isolated. Unfortunately, the IR spectra still showed the presence of an O-H stretch (3500 to 2500 cm^{-1}).

Following several different variations of the synthetic method which only afforded the same results, focus shifted towards the isolation procedures. Various solvents were tried in attempts to aid in the removal of heptadecane and to avoid any introduction of water to the formed TiO_2 . Various anhydrous solvents were substituted in the isolation attempts with no noticeable difference. In a final effort to remove any residual heptadecane, the isolated white solid was placed under high vacuum (~ 2 mmHg) at 200 °C for 1.5 hours. The resulting IR spectrum obtained showed not only success in

the removal of heptadecane, but also no O-H stretching absorption could be detected. (See Figure 3.7).

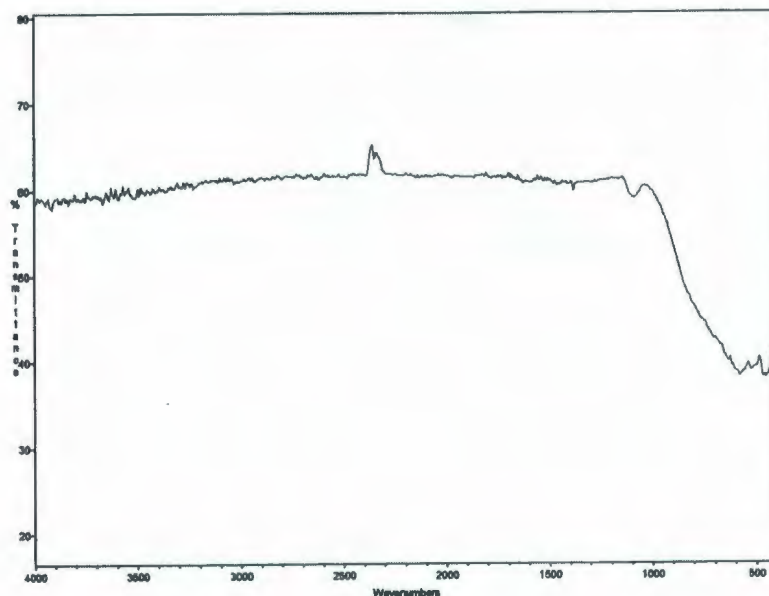


Figure 3.7: IR spectrum of nonhydrolytically prepared $\text{TiO}_2(\text{X})_n$ in KBr.

The spectrum shown in Figure 3.7 represents the successful isolation of TiO_2 having no hydroxyl capping agents. This technique was also proved valuable for the removal of any residual heptadecane. In Chapter 4, the surface sensitization of this material with 9-anthracenecarboxylic acid believed to be the first application of its kind using this synthetic approach is described.

The primary objective of the nonhydrolytic route was to obtain TiO_2 colloids that would be dispersible in organic solvents. In contrast to reported results, the isolated

material could not be redispersed in any of the organic solvents on hand. It should be noted that at various times prior to isolation of the solid, the precipitate was dispersible in chloroform and hexanes. Removal of the solvent to isolate the solid resulted in a loss of this property. Colvin proposed that the passivating agent, TOPO, is coordinated to the surface, allowing for solubility of the capped TiO_2 in hydrocarbon solvents. However, the IR spectrum of isolated TiO_2 shown previously show no evidence for the presence of a $\text{P}=\text{O}$ stretch. While the coordination of TOPO to the surface of the TiO_2 may have been responsible for its dispersibility seen prior to the isolation step, the subsequent removal of solvents must have also remove any attached TOPO as well.

Attention then shifted to identification of the capping agents. It was proposed that a chloride capping agent could be a possibility. Scheme 3.2 shown earlier shows the proposed mechanism for the thermal decomposition of titanium(IV) isopropoxide in the presence of titanium(IV) chloride to form the metal oxide particles. Briefly, Ti-O-Ti chains are proposed to form through the coordination of the TiCl_4 to the oxygen of the isopropoxide. Removal of the attached isopropoxide and chloride groups is achieved following coordination with similar intermediates, leaving the Ti-O-Ti chain. The reactions are assumed to go to completion as by-products propene, chloropropanes, and diisopropyl ether, for example, are eliminated via vaporization.

If this assumption is invalid, it is reasonable to suggest that chloride ions may be attached to the terminal ends of the Ti chains on the surface of the colloids. A simple $\text{AgNO}_3(\text{aq})$ test was performed (Scheme 3.7). A small amount of the isolated TiO_2 was added to deionized water. The resulting opaque solution was then combined with a

$\text{AgNO}_3(\text{aq})$ solution, producing a white precipitate. Following irradiation under UV light, the white precipitate turned black in colour, suggesting the presence of $\text{AgCl}(\text{s})$. This test supports the possibility of chloride capping agents (Figure 3.8). While it does not exclude the presence of TOPO as a capping agent, it lends support for the inclusion of chloride on the surface. It also introduced the concept of interconversion of surface groups occurring after the synthesis of the materials. The removal of the chloride capping agent results in a vacant site on the surface of the colloid. In aqueous solution, the most logical replacement to fill such a vacancy is expected to be some form of water, or more specifically, hydroxide ions. The treatment of capping agents as interchangeable ligands led to investigations which were addressed in Section 3.2.3.

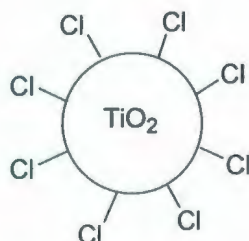


Figure 3.8: Proposed surface capping agents.

The successful fabrication of TiO_2 through nonhydrolytic methods and the characterization of the surface groups showed promise for the use of this material as the foundation for the biomimetic catalyst developed in the approaching phases of the project. There were still many problems that ultimately prevented its incorporation into the catalyst. Upon formation, the precipitate is a colourless solid. Throughout the

isolation procedures (centrifugation, washing, drying) a progressive change to a dark gray was normally seen. Final removal of the solvent *in vacuo* generally resulted in the isolation of a black solid. The cause of this change was not determined, but several possibilities exist. Photochemical degradation of any adsorbed organic material, such as TOPO, may be plausible. Care was taken to isolate the material from light, but a greater emphasis may have to be placed on this in future experiments. The TiO₂ itself may be unstable, however IR spectra taken over time, indicated that the Ti-O stretch remained.

On a practical level, the quantity of TiO₂ isolated through this procedure was approximately 100 – 160 mg, and often less. Given the difficulties encountered at this point, increasing the scale of the reaction was not considered. Changing the scale by a substantial amount may introduce particle size and crystallinity issues.

Repeated attempts to fabricate TiO₂ via the methods published by Colvin were met with moderate success. A paper published by Lian *et al.*⁸⁸ used the same approach with a few small modifications. Lian prepared TiO₂ nanocrystals via a modified version of Colvin's preparation and compared crystallinity to nanoparticles prepared via hydrolysis. Although the process followed the same method of thermal decomposition, different proportions of reactants as well as a slightly lower temperature were used. In this synthesis, TiCl₄ (0.44 mL) was added to heptadecane (24 mL) with TOPO (5.0 g). The reaction mixture was then heated to 270 °C as opposed to the 300 °C in the Colvin preparation. At this point Ti(OC₃H₇)₄ (1.19 mL) was rapidly injected into the mixture. Lian does not mention the formation of a precipitate upon injection. After allowing the reaction to cool, reagent-grade acetone was added to initiate precipitation of the

nanocrystals, however these TiO₂ nanocrystals were reported to be redispersable in heptane.

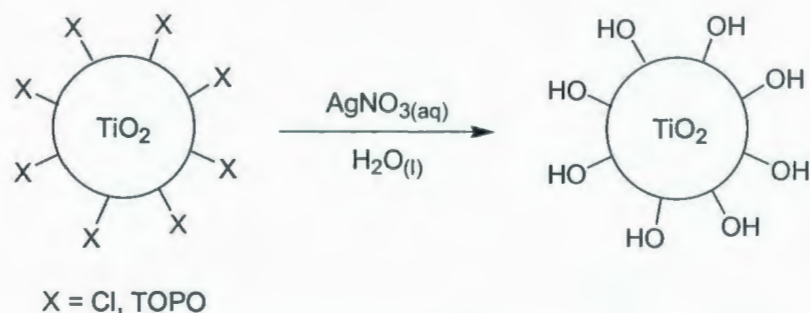
Using the same apparatus as previous experiments, another attempt was made to produce the nanocrystals using Lian's modifications. At 270 °C, just below the reflux temperature, addition of the Ti(OC₃H₇)₄ resulted in vaporization, however bumping of the reaction solution was much less pronounced. In contrast to previous experiments, therefore, formation of a precipitate did not occur. Addition of acetone to the cooled solution did not immediately initiate precipitation, but a small amount was formed after leaving the reaction solution for ~ 36 hours at room temperature. The white solid was isolated via centrifuge and washed with acetone to remove residual heptadecane. Throughout isolation, the colour of the solid progressed from white to gray with time. This method yielded a small amount of TiO₂(X)_n (7.2 mg). Such a small yield compared to previous experiments led to the re-examination of the heptadecane layer originally decanted from the precipitated solid. It was thought that any additional TiO₂, if formed, might still be dissolved within the reaction solution. A copious amount of acetone (50 mL) was added to the orange solution and checked for precipitate formation periodically over a few days. No formation of solid, however, was evident. If TiO₂ was present in the solution, it could not be precipitated after the addition of acetone.

The many complications and questions raised by investigations into the preparation of TiO₂ soluble in organic media prepared via nonhydrolytic methods led to the utilization of different means to prepare a foundation for the target catalyst in this project. Studies regarding this synthetic method continued within the research group to

ascertain whether or not an approach could be found that provided usable TiO_2 in which the capping agents, surface structure, and solvent solubilities could be reliably determined. For this project, the decision was made to abandon the nonhydrolytic synthesis in favor of the established hydrolytic route used more commonly in the preparation of TiO_2 colloids.

3.2.3 Interconversion of Nanocrystalline Materials

Although Colvin's method was abandoned, the goal of producing organic solvent-soluble TiO_2 nanoparticles remained. In the process of surface characterization of these materials, the identification and extraction of chloride capping agents attached to the surface proposed an alternate route towards the modification of the surface.

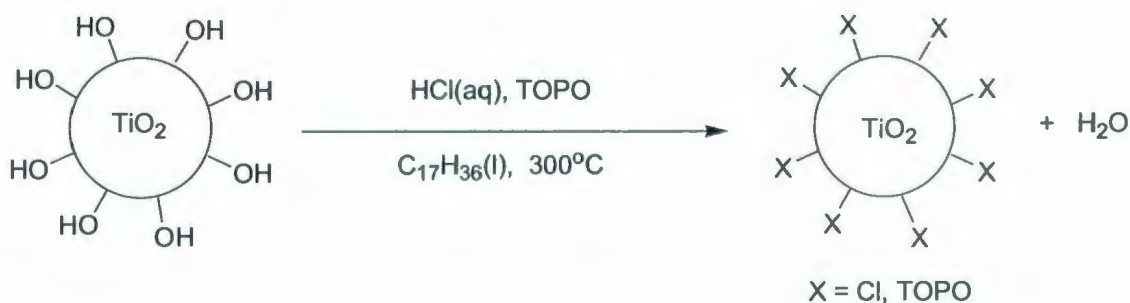


Scheme 3.7: Extraction of chloride capping agents with $\text{AgNO}_3(\text{aq})$.

As previously discussed, TiO_2 produced via nonhydrolytic methods was mixed with a solution of $\text{AgNO}_3(\text{aq})$ in an effort to identify the capping agents. The formation of $\text{AgCl}(\text{s})$ confirmed the presence of chloride in the material. Following the extraction

of the chlorides from the surface of the colloids, the particles became soluble in aqueous solution. Incorporation of hydroxyl groups onto the surface would be the most plausible explanation. Alternately, adsorption of water to the surface of the colloids may also take place in the absence of AgNO_3 . Regardless, this simple experiment led to the consideration of capping agents as interchangeable ligands, coordinated to titanium on the surface of the colloids.

Starting with TiO_2 prepared via hydrolysis, which gave high yields, stability, and consistent results, an attempt to replace the surface hydroxyl groups was made (Scheme 3.8).



Scheme 3.8: Attempted modification of hydrolytically prepared TiO_2 capping agents.

In this interconversion reaction conditions were chosen to mirror those that existed at the point of formation of nonhydrolytic TiO_2 . The solvent, temperature, and presence of TOPO were replicated. In addition, concentrated HCl(aq) was added to aid in the removal of hydroxides from the surface of the TiO_2 , as well as provide a source of chloride ions. TiO_2 (202.6 mg) prepared via hydrolysis was combined with TOPO (1.0 g) in heptadecane (25 mL). A Dean-Stark water trap with condenser was attached to the

reaction vessel followed by the addition of concentrated HCl(aq) (1.0 mL). The cloudy white mixture was then stirred and heated to 300 °C. The colour of the mixture turned from white to yellow to brown as the temperature increased. In contrast to previous experience with TOPO and heptadecane, the solid did not dissolve as the temperature increased. At high temperatures, the reaction mixture proved to be of similar volatility to that of previous experiments. After several minutes at high temperature, the heat was removed and the mixture was left to cool. The brown mixture was then transferred to an appropriate vessel and centrifuged. The result of this process was the formation of a mixture of three distinct components: a clear orange layer atop a viscous black oil with a brown solid on the bottom of the centrifuge tube. The liquid layers were decanted from the solid, and the solid was rinsed with hexane and chloroform to remove any residual heptadecane and oil that remained. The brown solid (113.6 mg) was dried under high vacuum.

In an effort to determine if the original capping agents had been replaced, an IR spectrum was obtained. This spectrum shows similar peaks to that of the starting material, verifying the presence of hydroxyl groups with the isolated solid. It is interesting to note that only 113.6 mg of TiO₂ was recovered, indicating that some portion of the added TiO₂ may have achieved solubility within the heptadecane. In hindsight, acetone should have been added to the heptadecane supernatant liquid in an attempt to precipitate any dissolved solids. Unfortunately, this was not considered at the time. Focus was placed on the isolated solid, and not the heptadecane solution.

3.3 Conclusions

The development of nanoscale colloids was an important first step towards the fabrication of the target porphyrin – metal oxide catalyst. Several interesting results were obtained from each synthetic approach examined, as outlined below.

The production of $\text{TiO}_2(\text{OH})_n$ colloids through hydrolysis of titanium(IV) isopropoxide with water was successful. This well-established approach yielded relatively large quantities of stable TiO_2 , determined by previous group members to be primarily anatase.⁸⁷ Additional purification methods were developed to aid in the removal of residual nitric acid. Identity was verified through UV-VIS and IR spectroscopy. The colloids which were produced however did not exhibit any dispersibility in organic solvents that were tested. Attempts to replace the hydroxyl surface groups with chloride, or TOPO using reaction conditions similar to those used to produce nonhydrolytically-prepared TiO_2 were unsuccessful, but attempts were limited and were not studied in any great detail. Further modification of reaction conditions and use of alternate reactants might show promise in future work.

The majority of the research in this phase focused on the production of organic-soluble $\text{TiO}_2(\text{X})_n$ nanocrystals prepared through nonhydrolytic means. While isolation of $\text{TiO}_2(\text{X})_n$ without any hydroxyl surface groups was achieved, yields were low and the stability of the product was suspect. In contrast to results published by Colvin *et al.* no evidence was seen for the presence of TOPO coordinated to the surface of the material following isolation of the sample, and redispersal in organic solvents was not achieved. It is important to note that one of the primary discrepancies between this work and that of

Colvin's is the isolation of $\text{TiO}_2(\text{X})_n$ in solid form. The techniques used in the isolation of the sample from the involatile heptadecane may have resulted in the removal of TOPO located on the surface of the colloids. Hence, following isolation, dispersibility into organic solvent was lost. The small amounts of the materials recovered may indicate that retention of the metal oxides within the reaction solvent occurred, but all attempts to precipitate additional $\text{TiO}_2(\text{X})_n$ from the solution were unsuccessful. With the volatility of reactants at such high temperatures, the loss of reactants may also be responsible for the observed low recovery. Aside from the experimental difficulties encountered, $\text{TiO}_2(\text{X})_n$ prepared without any hydroxyl capping agents was achieved, with IR spectral evidence provided as support. The evidence provided by Colvin is indirect and is limited to analysis of the reaction solution and isolated byproducts, and not the metal oxide itself. Further characterization was also achieved for the surface structure of the material, with evidence for the presence of chloride capping agents.

With the biomimetic catalyst in mind, the decision was made to proceed using $\text{TiO}_2(\text{OH})_n$ prepared via standard hydrolytic methods. Although the desired organic dispersibility was not present, it was thought that modification of the surface with porphyrins may have a substantial effect on governing the colloid-solvent interactions. As Chapter 4 discusses, this turned out to be a valid assumption. TiO_2 prepared via Colvin's techniques was not discarded completely, and was used in a ^1H NMR study with 9-anthracenecarboxylic acid, and some very interesting and novel results were obtained.

Chapter 4

Surface Derivatization of TiO₂

Chapter 4: Surface Derivatization of TiO₂

4.1 Introduction

The goal of the second phase of the described research is the development of a hemin chloride/TiO₂ assembly that can be used as a photodriven catalyst for oxygen insertion reactions. Progress towards this included the sensitization of TiO₂ with several different chromophores and characterization of the bonding interaction between the metal oxide base and substrates.

Regardless of the combination of metal oxide and chromophore types, all sensitization schemes utilize the interaction between some functional group on the dye with the surface of the titanium dioxide. As discussed in Chapter 1, there are several different functional groups that can be used to tether a molecule to the metal oxide surface. These groups include for example, carboxylic acids, hydroxyls, phosphates, and metal cyanides. The presence of carboxylic acid functionality in a multitude of porphyrins made it a natural choice, enabling the potential extension of methods developed here to many different metal oxide/porphyrin combinations.

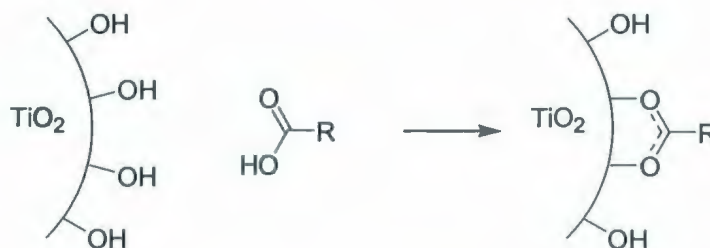


Figure 4.1: Surface derivatization of TiO₂ via a carboxylate linkage.

In reality, there are many more factors to consider. The nature of the attachment site is not only dependent upon the identity of the semiconductor and the chromophores, but is also influenced by solvent molecules near the binding site and those of the bulk solvent.

Previous research by Roberts⁸⁹ examined the kinetics of such an attachment using 9-anthracenecarboxylic acid (9-AcCOOH) and $\text{TiO}_2(\text{OH})_n$. As 9-AcCOOH was attached to the TiO_2 colloids, photon emission from the dye was quenched by interfacial electron transfer into the metal oxide, resulting in a decrease in the observed emission signal. Following this signal over a period of time, two stages were seen. A sharp, quick drop in the strength of the signal as shown in Figure 4.2 was followed by a slower rate of loss that continued for a significant time.

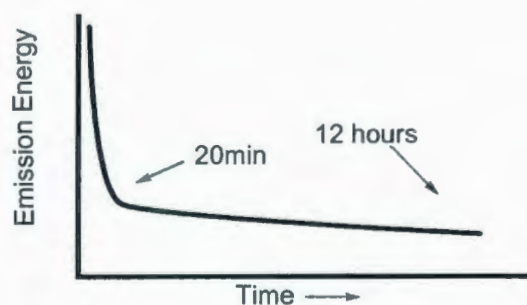
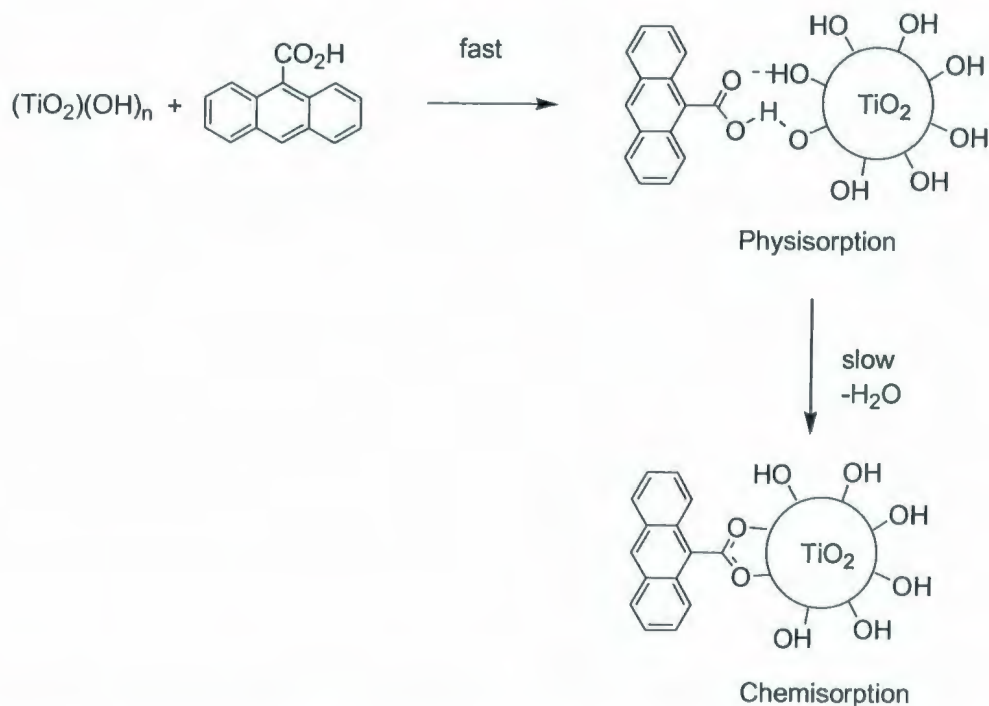


Figure 4.2: A schematic representation of the biphasic kinetics in the adsorption of 9-9-AcCOOH to $\text{TiO}_2(\text{OH})_n$.

It was proposed that the attachment actually goes through a two-step mechanism, whereby the dye initially hydrogen-bonds with the metal oxide surface before attachment, as shown in Scheme 4.1.



Scheme 4.1: Proposed mechanism for the biphasic kinetics of 9-anthracene carboxylic acid tethering to $\text{TiO}_2(\text{OH})_n$.

These intriguing results alluded to just how little is known about the binding sites of these assemblies. The influence of these binding stages on the preparation of surface-sensitized metal oxides can have a significant impact. In addition to surface-sensitization experiments, knowledge gained regarding the interaction of these colloids with various molecules can be extended to other areas of TiO_2 chemistry. For example, the impact of the adsorption stage that a molecule can achieve, whether physisorbed or chemisorbed, may play a significant role in TiO_2 's application as a photodegradation agent used in the breakdown of organic pollutants. Characterization of the native surface structure of TiO_2 and the binding of molecules to that surface structure can only aid in the extension and

expansion of metal oxide chemistry, in general. As such, the analysis of materials used and created within this project was regarded with as much emphasis as the production of the materials themselves.

Given the prior success with the attachment of 9-AcCOOH to the surface of TiO_2 , this dye was chosen for initial attempts at surface derivatization in this project. While the product assembly formed is outside the primary focus of this research, the confirmation of tethering with $\text{TiO}_2(\text{OH})_n$ made it a natural choice to test the possibility of surface sensitization of nonhydrolytically prepared $\text{TiO}_2(\text{X})_n$. While ultimately abandoned as a support structure for the target catalyst, surface derivatization with $\text{TiO}_2(\text{X})_n$ prepared via this nonaqueous approach had yet to be reported in the literature. Experiments were limited to small scale NMR experiments, which demonstrated the first solution-based ^1H NMR spectrum of surface-sensitized TiO_2 colloids. Evidence for the creation of such assemblies is generally reported as visible colour changes retained by TiO_2 films following immersion in a dye solution. IR spectroscopy has been used to analyze these structures, specifically through examination of the carbonyl stretching frequencies. This C-O stretching frequency is extremely sensitive to the influence of nearby electric fields, leading to some ambiguity regarding the nature of the bonding sites. Research in this project focused on the possibility of using NMR to provide evidence for tethering as well as assessing the impact TiO_2 has upon the chemical shifts of attached chromophores.

Following these NMR experiments, focus shifted back to the creation of the target catalysts. Progress towards this assembly began with the development of techniques to attach porphyrins to the colloids. Much of the surface sensitization procedures in the

literature involve the use of $\text{TiO}_2(\text{OH})_n$ films supported on glass surfaces. This heterogeneous approach allows for easy and efficient derivation of TiO_2 surfaces. The slides are immersed in a solution of the dye, are removed, and finally, rinsed. While the preparation and extraction of the assemblies is simplified, the glass supports immobilize the catalyst and thus limit the spectroscopic techniques available to examine the materials. One of the aims of this project was to incorporate the capability for solubility into organic solvents onto the catalyst. Colloidal $\text{TiO}_2(\text{OH})_n$ presented the best possibility of achieving this.

The use of $\text{TiO}_2(\text{OH})_n$ in colloidal form introduces several new considerations that had to be addressed. Heterogeneous reaction conditions could still be used, where solid TiO_2 is introduced into a solution of the desired chromophore. Although this method was explored, initial experiments attempted to use homogeneous solutions, wherein the colloids and the chromophores are present in the same layer. It was thought that this approach would be more likely to yield colloids with higher coverage densities and increase the possibility of solubility of the final assembly in organic solvents. UV-VIS, IR, and ^1H NMR spectroscopies were used to confirm the production of tethered assemblies, as opposed to isolated mixtures.

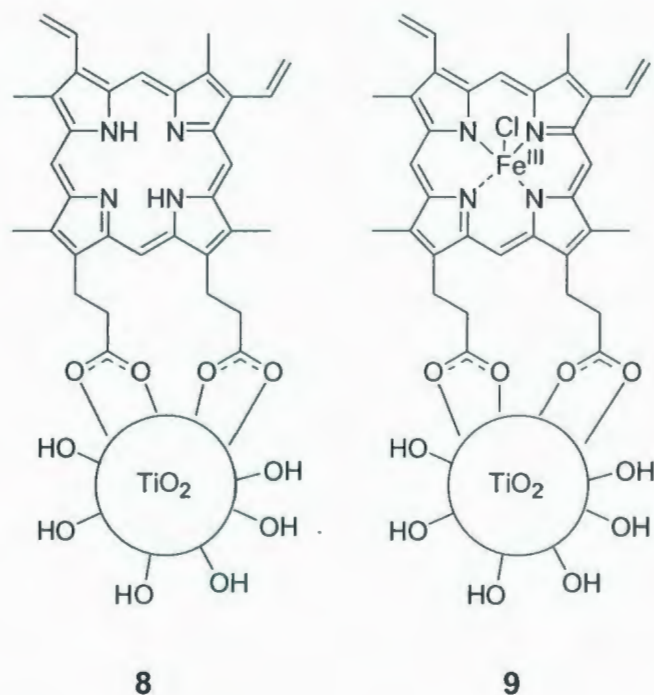


Figure 4.3: Porphyrin/TiO₂ Assemblies.

First attempts to tether a porphyrin to the surface of TiO₂ began with protoporphyrin IX (**8**) (Figure 4.3). Preliminary attempts using this substituent were aimed at finding proper tethering methodology which would provide isolable and useable assemblies that could be carried further into the biomimetic phase of the project. In contrast to the 9-AcCOOH experiments, the foundation for these assemblies was TiO₂ prepared via the hydrolytic approach. As mentioned in the previous chapter, TiO₂(OH)_n was chosen due to the large scale and reliability of the synthesis. Utilization of the TiO₂(X)_n proved unpractical.

Although the absence of the iron in **8** renders the assembly useless in the target catalytic process, it opens the windows to additional forms of spectroscopic methods that

the hemin chloride inhibits access to, such as emission and excitation spectroscopy. In addition, ^1H NMR spectroscopy is simplified in the absence of the paramagnetic metal.

The third chromophore tethered to the surface of TiO_2 was hemin chloride (9). Hemin chloride is the active center in the target catalyst, however, hemin chloride exhibited different solubility than the previously examined protoporphyrin IX, which was in fact a sodium salt, and led to the use of a different tethering technique altogether. In addition to the sensitization of TiO_2 in colloidal form, films generously supplied by G. Meyer of John Hopkins University were used.

The remaining sections in this Chapter describe the methods used, barriers encountered, and the pathways taken to achieve derivatization and characterization of the surface of TiO_2 .

4.2 Results and Discussion

4.2.1 9-Anthracenecarboxylic Acid/ TiO_2 Assembly

Given the smaller scale of the nonaqueous preparation of $\text{TiO}_2(\text{X})_n$, experiments in which 9-AcCOOH was attached were conducted as *in situ* ^1H NMR experiments, with spectra obtained before and after combining reactants. A spectrum was obtained of 9-AcCOOH (7.1 mg) in CDCl_3 . Although the acid exhibited limited solubility in the solvent, a clearly-resolved spectrum was obtained without difficulty. To this sample, $\text{TiO}_2(\text{X})_n$ (10.8 mg) was added. Initially, no significant change in the ^1H NMR spectrum was noted, aside from the introduction of signals due to residual heptadecane within the

TiO₂(X)_n sample. With interest focused primarily on the aromatic region of the spectrum, these signals did not interfere with the experiments, but it did lead to further purification of the TiO₂, as presented in Chapter 3. After 96 hours, the spectrum showed two significant changes. The resolved multiplicity of the initial spectrum was replaced with a set of broadened peaks. While no changes in chemical shifts were noted in these peaks, there was a loss in signal resolution. Secondly, a new set of signals became apparent, and increased in strength over time. Most notably, a clear doublet at δ 9.0 ppm was produced. Less distinguishable peaks were generated within the aromatic region as well, although overlap with the stronger signals presented difficulty in peak assignments for these new signals.

Reversing the order of addition, (9-AcCOOH added to a TiO₂(X)_n /CDCl₃ mixture) yielded nearly identical results. Figure 4.4 shows the expanded aromatic region of the obtained NMR spectra, as well as peak assignments for the untethered 9-AcCOOH. Despite the overlap of peaks, a clear doublet at δ 8.99 ppm and δ 7.96 ppm and a singlet at δ 8.48 ppm are evident. With a closer inspection of the smaller peaks present on the edges of the stronger signals, several other doublets and triplets can be identified, although not as clearly as those without overlap.

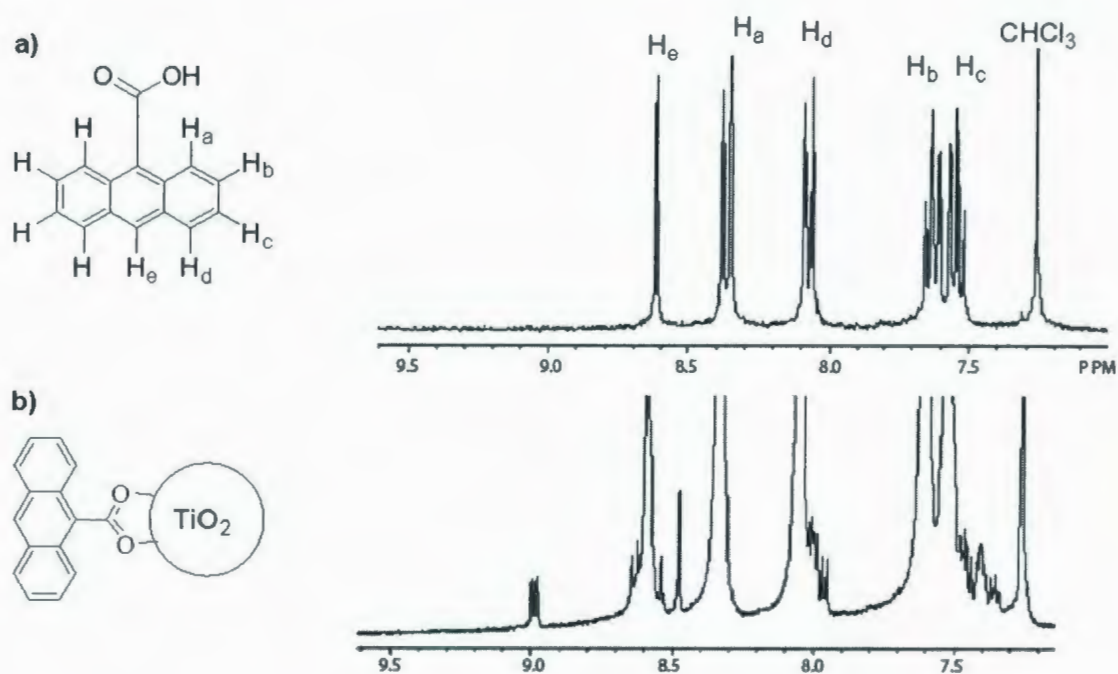


Figure 4.4: ¹H NMR spectra of a) 9-anthracenecarboxylic acid and b) following addition of TiO₂(X)_n. Spectra acquired in CDCl₃(l).

Unfortunately, overlapping of peaks limits the use of peak integration to assist in peak assignments. Regardless, the shift of signals is taken as evidence of the tethering of 9-AcCOOH to the surface of TiO₂(X)_n. Figure 4.5 shows arrows which have been added to the spectrum shown in Figure 4.4 to show the shift that the particular signals of the 9-AcCOOH have undergone, upon its attachment to the metal oxide surface in Figure 4.5.

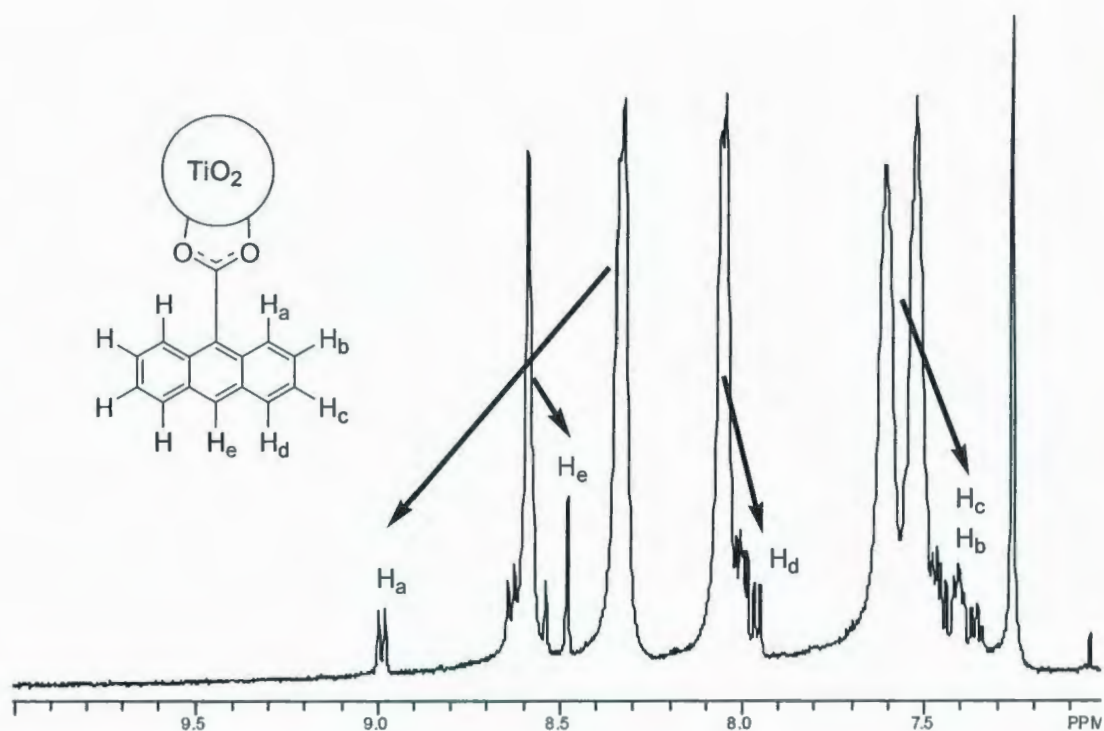


Figure 4.5: ^1H NMR of 9-anthracene carboxylic acid on $\text{TiO}_2(\text{X})_n$ in CDCl_3 .

The peak assignments shown in Figure 4.5 have been made primarily on the basis of the multiplicity of each appropriate signal. Three of the signals move upfield, while the lone doublet at δ 8.99 ppm was shifted downfield, indicating a loss in electron density. To predict the rearrangement of electron density that results from the attachment of a molecule to the surface of TiO_2 would be speculation, at best. The conjugation and aromaticity of the rings would likely transmit the electronic influence of the TiO_2 throughout the system. Compounded to this, would be the steric influence of the electric field around the colloid upon the protons. It is postulated that this would be the primary factor in shifting the H_a signal downfield, while electron density rearrangement through bonding would be more significant to protons H_{b-e} . The location of H_a adjacent to the

tethering carboxylic acid would result in immersion into the face of the TiO_2 colloids, greatly changing its chemical shift relative to other protons on the anthracene ring.

In addition to the peaks discussed here, the spectrum contains several other peaks that are difficult to distinguish, but resemble other doublet and triplets. Two explanations are proposed to account for these peaks. Firstly, it is possible that inconsistencies on the surface could cause an attached molecule to lose its symmetry. This loss would give individual signatures for each H on the anthracene rings. Secondly, and more likely, the NMR sample may not only be a mixture of free and tethered 9-AcCOOH, but may also have different degrees of loading on different colloids.



Figure 4.6: Surface loading differences among colloids.

Given various degrees of surface coverage among different colloids, it would be expected that a variance in chemical shift would be present. Figure 4.6 portrays a simple example of the difference loading density may have on the electronic environment of the

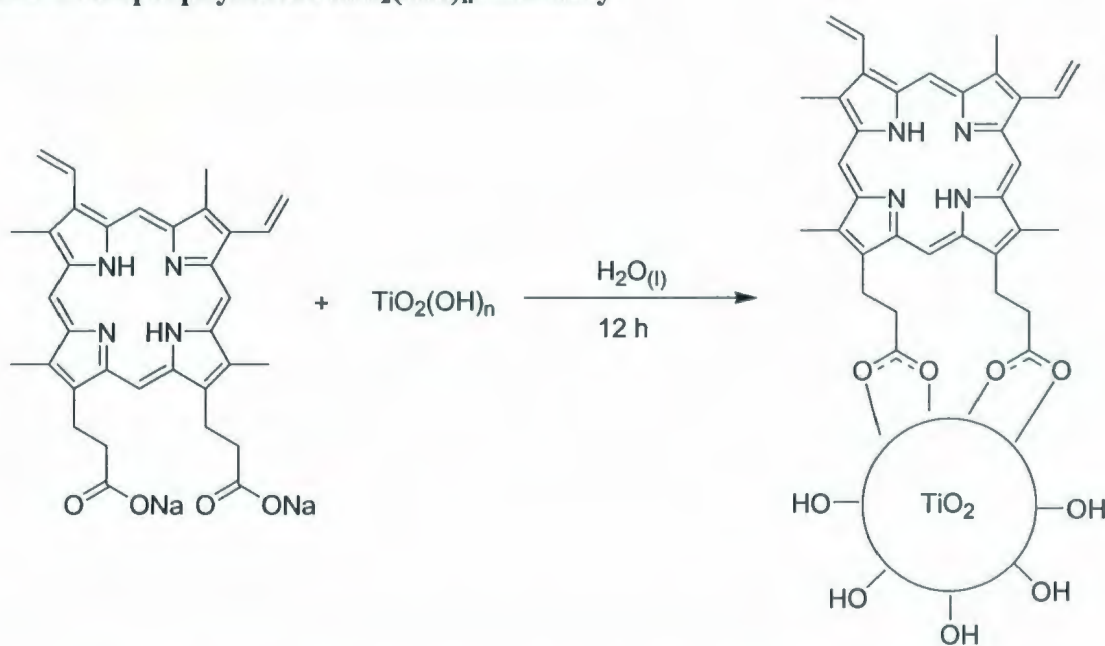
adsorbed molecules. The degree to which these assemblies can be dispersed in the NMR solvent may also be a factor of the coverage concentrations as well.

Apart from the formation of new signals following the addition of TiO_2 to the NMR sample, loss of peak resolution of the original signals was immediately apparent. Initially, it was attributed to the introduction of a solid to the sample tube. The presence of undissolved solid within an NMR sample can cause interference in the acquisition of good spectra. This may also be a cause of the broadening, but the resolution achieved on the weaker signals discussed previously provides evidence to the contrary. Given instrument difficulty in 'locking' or otherwise, these signals would have been affected as well. Formation of aggregates with 9-AcCOOH is also possible in the form of π -coordinated ring systems, H-bonded dimers, or H-bonded polymers, but broadening clearly follows the addition of TiO_2 to the sample. Unless aggregation is initiated by the presence of the colloids, it is more likely that the colloids are interacting with the anthracene molecules, the manner and degree to which is presently unknown. Several possibilities exist. If an excess of 9-AcCOOH exists relative to the availability of binding sites on the surface of TiO_2 , it is possible that physisorption may still be possible. Returning to the concept of surface derivatization densities, it is possible that the smaller peaks examined in detail here represent a minor product with specific coverage density and the major peaks represent not free 9-AcCOOH, but surface-tethered chromophores as well.

Although it seems that this experiment has posed more questions than it has answered, several novel results were obtained. It has been shown that TiO_2 prepared via

Colvin's nonaqueous approach can be surface-sensitized. As of this writing, Colvin's preparation has only been utilized in the production of TiO_2 for the purpose of studying the degree of crystallinity in the nanoparticles formed. The findings obtained in the present study is the first example in extending Colvin's synthesis towards applications similar to that of hydrolytically-prepared TiO_2 . In addition, ^1H NMR spectra have been obtained of 9-anthracenecarboxylic acid attached to the surface of titanium dioxide.

4.2.2 Protoporphyrin IX/ $\text{TiO}_2(\text{OH})_n$ Assembly



Scheme 4.2: Preparation of protoporphyrin IX/ $\text{TiO}_2(\text{OH})_n$ assemblies.

To prepare the first porphyrin/ TiO_2 assembly, water was chosen as the reaction medium. Although PPIX was supplied as a disodium salt and exhibited some solubility in water, the mixture could best be described as a suspension. Briefly, a suspension of PPIX disodium salt (2.9 mg) in water (5.0 mL) was added to an aqueous solution of TiO_2 (56.8 mg in 2.0 mL). The burgundy mixture was left to stir overnight (~18 hrs).

Following centrifugation of the sample, a clear red solution was obtained as a supernatant above a darker burgundy solid.

The supernatant aqueous solution was separated from the solid via pipette. The solvent was removed on a rotary evaporator followed by high vacuum, yielding a black solid (44.2 mg). UV-VIS spectra of the sample in H₂O showed evidence for the presence of TiO₂ with a small amount of porphyrin, as evidenced by Soret bands. In contrast, an IR spectrum of the sample appeared almost identical to that obtained for hydrolytic TiO₂. Further efforts concentrated on the characterization of the burgundy solid obtained from the initial reaction. While it is possible that the aqueous layer may contain tethered porphyrin/TiO₂ assemblies, it was thought that the insoluble burgundy solid held more promise. As discussed in the previous section, the degree of surface loading is suspected to have a dramatic effect on the solubilities of these assemblies. With this in mind, the assumption was made that while this solid shows evidence for both TiO₂ and porphyrin, it is likely a simple mixture of the two, and not tethered assemblies. Following the removal of the aqueous layer from the burgundy solid, water (20 mL) was added and the mixture centrifuged and decanted to remove any water soluble TiO₂ or PPIX that may remain. The remaining solid was transferred to filter paper where it was washed again with water (2 x 10 mL) and allowed to dry.

To ensure a high retention rate from the small amount of solid that had collected in the filter, a solvent extraction was used. Several different solvents were tested in order to find one in which the isolated solid could be dispersed. Cyclohexane, hexane, chloroform, acetone, ethyl acetate, acetonitrile, and ethanol were all unsuccessful. The

only solvent found capable of dissolving the solid was *N,N*-dimethylformamide.

Removal of the majority of the solvent was achieved through rotary evaporation followed by heating the sample under high vacuum. A black oil (9.2 mg) was isolated. While the complete removal of DMF (b.p. 153 °C) following the extraction proved difficult, DMF proved useful for UV-VIS absorption spectra. Using DMF as a solvent allowed for spectroscopic analysis without the requirement of a completely dry sample, although complete removal of the extraction solvent would be ideal. An additional complication introduced through the use of DMF is the limiting of useable wavelengths to those above 280 nm. Figure 4.7 shows the combined spectra obtained for PPIX, the isolated solid, and $\text{TiO}_2(\text{OH})_n$.

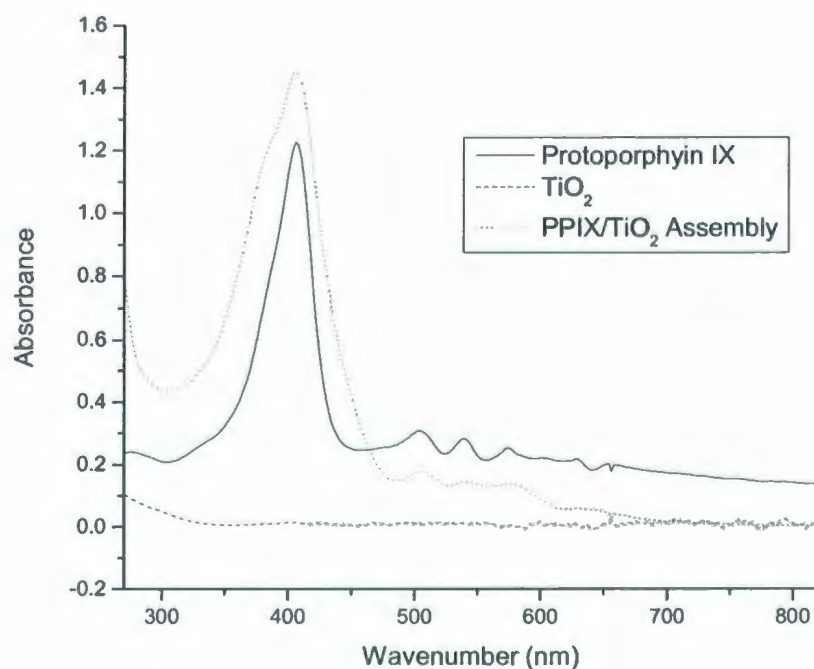


Figure 4.7: UV-VIS spectra of PPIX, $\text{TiO}_2(\text{OH})_n$, and PPIX/ $\text{TiO}_2(\text{OH})_n$ assembly. Obtained in DMF. Spectra unnormalized.

The isolated solid clearly exhibits the characteristic Soret and Q-bands of a porphyrin, with no significant shifts in absorbance wavelength. There does appear to be some difference in the ratio of intensities between the free PPIX, and that isolated from the experiment.

In the analysis and characterization of these materials, one of the main goals is to find evidence that the isolated materials were indeed chromophore/metal oxide assemblies, and not simply mixtures of the two. The UV-VIS spectrum obtained of the suspected PPIX/TiO₂(OH)_n assembly not only confirms the presence of the porphyrin moiety, but also support for TiO₂(OH)_n is provided with the increased absorbance below 300 nm. λ_{max} for the TiO₂ absorbance could not be determined due to overlap with the DMF signal. The question remained as to whether or not this absorbance is a result of sensitized or free TiO₂(OH)_n.

In an effort to confirm the peak assignment for the absorbance below 300 nm, varying amounts of TiO₂(OH)_n were prepared in a cuvette containing DMF, and the UV-VIS spectra of these solutions were measured. Unmodified TiO₂(OH)_n appeared to be extremely insoluble in DMF, and the spectrum shown in Figure 4.7 can be considered to be that of a saturated solution. The absorbance signal obtained was only ~1/8 the strength of that seen in the spectrum of PPIX/TiO₂(OH)_n, in which a much smaller amount of material was used to obtain a satisfactory signal. This is a significant observation. The increased signal strength below 300 nm would not be possible without the interaction with the PPIX, thus providing support for tethering. Furthermore, these spectra support

the role of surface groups in dictating the solubility of $\text{TiO}_2(\text{OH})_n$ colloids. Solubility in organic media has been demonstrated, albeit in an extremely polar solvent.

In an effort to further characterize the PPIX/ $\text{TiO}_2(\text{OH})_n$ assembly, IR spectra were obtained of KBr pellets containing both the isolated assembly, and free protoporphyrin IX. The results are shown in Figure 4.8.

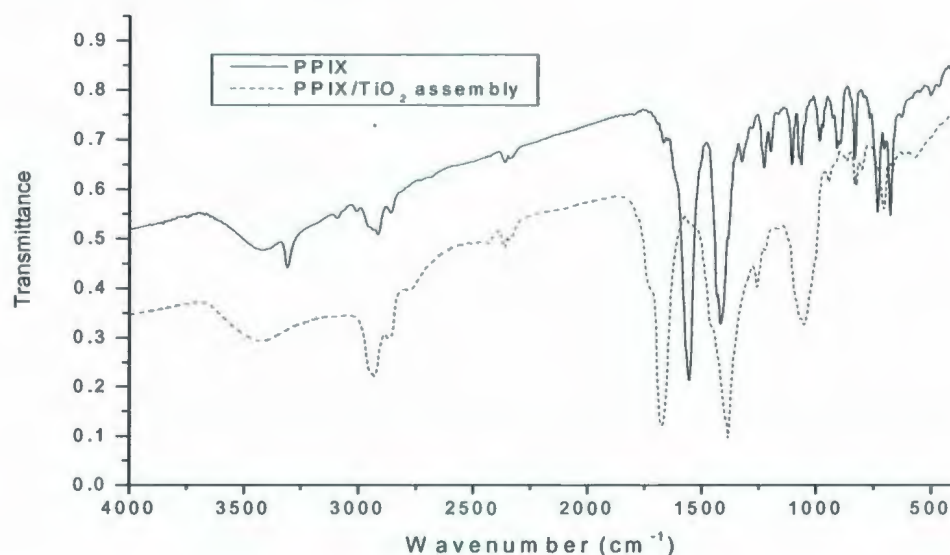


Figure 4.8: IR of free PPIX and PPIX/ $\text{TiO}_2(\text{OH})_n$ assemblies in KBr.

Initially, these spectra were taken as further evidence of tethering. Of particular interest is the apparent shift of the C=O stretch from 1619 cm^{-1} to 1675 cm^{-1} . Given the carbonyl groups role in the tethering of the porphyrin to the surface of the colloids, a change in the vibrational behavior would be expected. Following a more detailed analysis, it appears that many of the stronger peaks could be attributed to DMF, specifically the stronger peaks ranging from 1000 cm^{-1} to 1700 cm^{-1} . This could be expected given the fact the isolated sample remained as an oil, due to the difficulty in

removing DMF. Some information could be obtained from the fingerprint region, but detailed characterization with IR spectroscopy would require further purification and isolation of the assemblies. As is discussed in the remaining chapters, the presence of DMF proved to be a constant interference in several of the analytical techniques used.

Continuing with the success found with the ^1H NMR spectra of 9-AcCOOH, the same method was used to examine the PPIX/TiO₂ assembly. Using DMF-d₇, the following spectrum was collected.

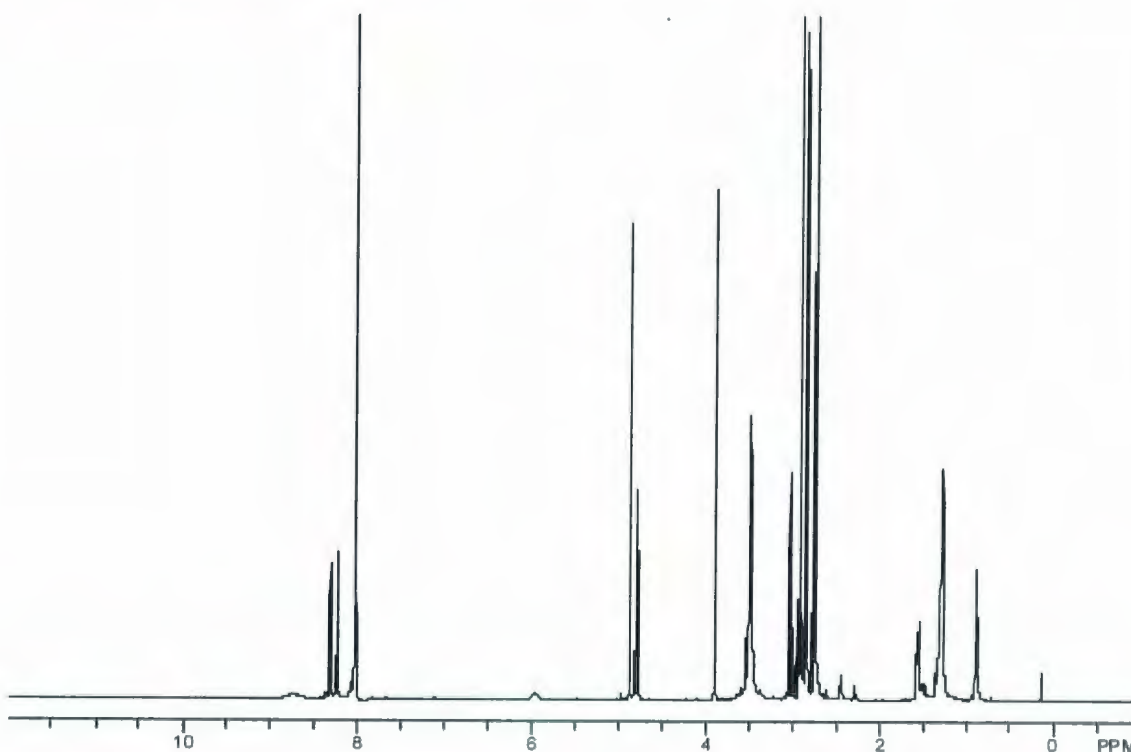


Figure 4.9: ^1H NMR spectrum of PPIX/TiO₂(OH)_n assembly in DMF-d₇.

To draw a comparison to the original untethered form of PPIX, a ^1H NMR spectrum was also collected in DMF-d₇. As a disodium salt, the initial spectrum showed only DMF solvent peaks. A drop of H₂SO₄ increased the solubility of the porphyrin, and

provided an excellent spectrum, aside from the broad signal from the acid at δ 5.2 ppm. It should be noted that the use of deuterated H_2SO_4 would eliminate this interference. Figure 4.10 provides both spectra, with the top spectrum being PPIX, and the lower spectrum showing that obtained for the PPIX/ $\text{TiO}_2(\text{OH})_n$ assembly. In contrast to the ^1H NMR spectra obtained for the 9-AcCOOH/ $\text{TiO}_2(\text{OH})_n$ assembly, the majority of the signals shown in Figure 4.10 shifted upfield, indicating an increase in the shielding of the affected protons. One possible explanation for this difference in chemical shift could be the lack of conjugation through the tethering link. The extra two-carbon separation of the carboxylic linkage group may isolate the conjugated porphyrin system from the electron-withdrawing influence of the $\text{TiO}_2(\text{OH})_n$ colloid, leaving only a spatial electronic interference. It should also be pointed out that the colloids used in this experiment were prepared via the hydrolytic method, while the TiO_2 used in the 9-AcCOOH study was prepared nonhydrolytically. As a result, the capping agents present on the surface of the TiO_2 are different in each case and would offer different chemical environments for the tethered dyes, which consequently may result in different chemical shifts for the respective proton signals.

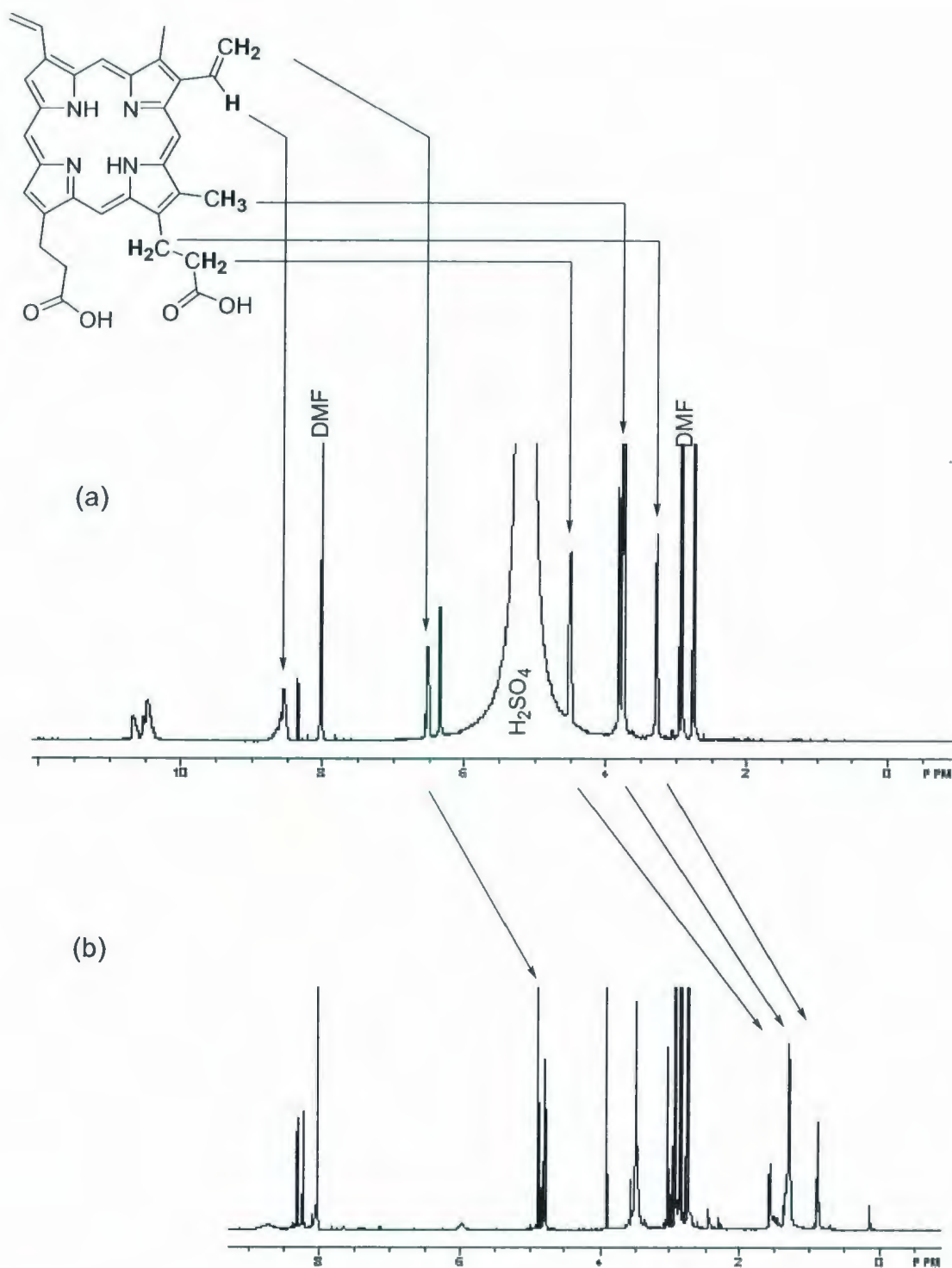


Figure 4.10: ^1H NMR spectra for (a) protoporphyrin IX and (b) protoporphyrin IX/ $\text{TiO}_2(\text{OH})_n$ assembly. H_2SO_4 was added to the protoporphyrin IX disodium salt to aid in solubility in (a).

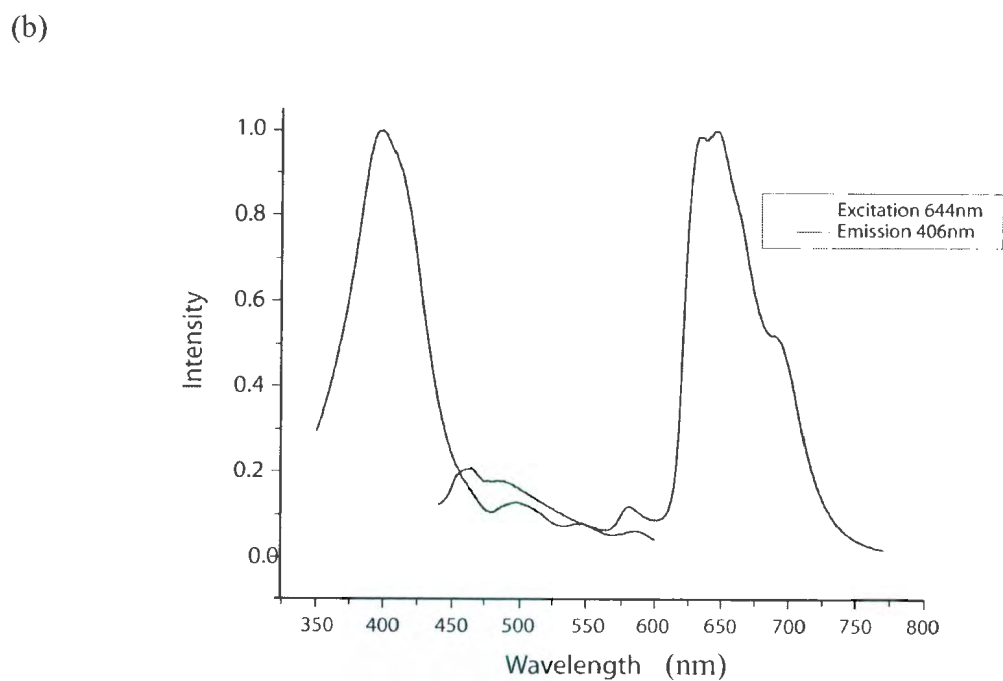
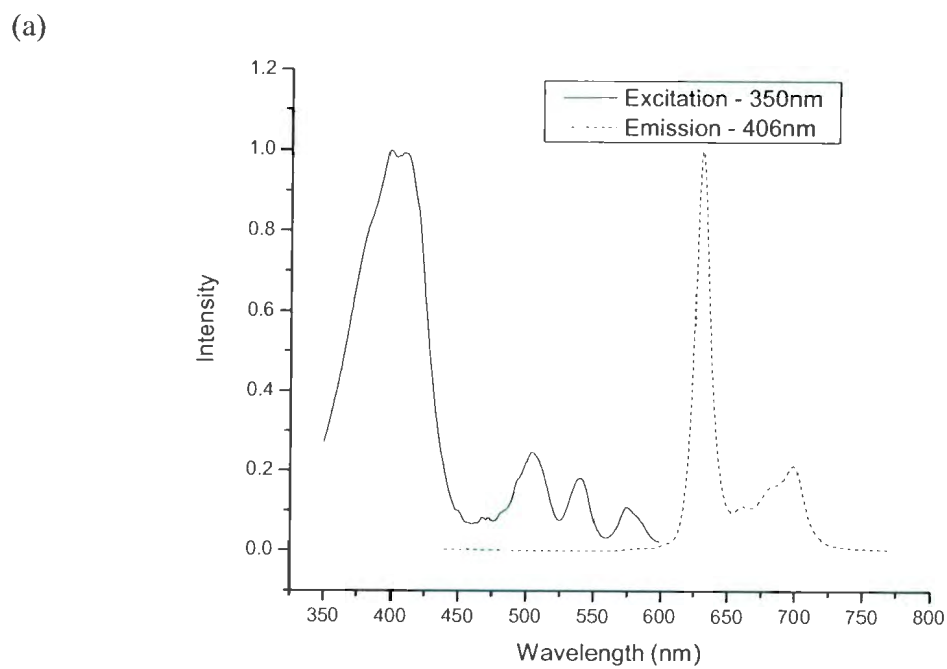


Figure 4.11: Excitation/Emission spectra for (a) PPIX and (b) PPIX/TiO₂(OH)_n, in DMF.

Further characterization of the assemblies included acquisition of emission and excitation spectra, shown in Figure 4.11. In terms of adsorbance, surface attachment appears to have a larger effect on the porphyrin Q-bands (~ 400 – 650 nm) as opposed to the Soret (~ 400 nm) band. Emission spectra show a more dramatic change in the excited state of the porphyrin. Further work involving excitation and emission energetics based on these preliminary results, as well as additional porphyrins, has been completed and reported by Collier.⁹⁰

Several explanations presented in the preceding pages center around arguments concerning the density of surface sensitization that may or may not be found on the surface of the TiO₂ colloids. To gain perspective as to the relative sizes of the colloids when compared to the porphyrins, structures were compared using empirical MM2 methods using CS Chem3D.⁹¹ After obtaining the resulting atomic coordinates, images were rendered using Jmol.⁹² Figure 4.12 portrays protoporphyrin IX attached to a TiO₂ [3 x 3 x 3] cube which represents 1/10th of the 7 nm – 10 nm colloids used in this research. This visual aid helps put into perspective just how many chromophores may be attached to a single colloid. A rough estimate, assuming a single porphyrin per [3 x 3] grid, allots about 600 porphyrin molecules per colloid. In reality, actual loading densities could be much higher or lower.

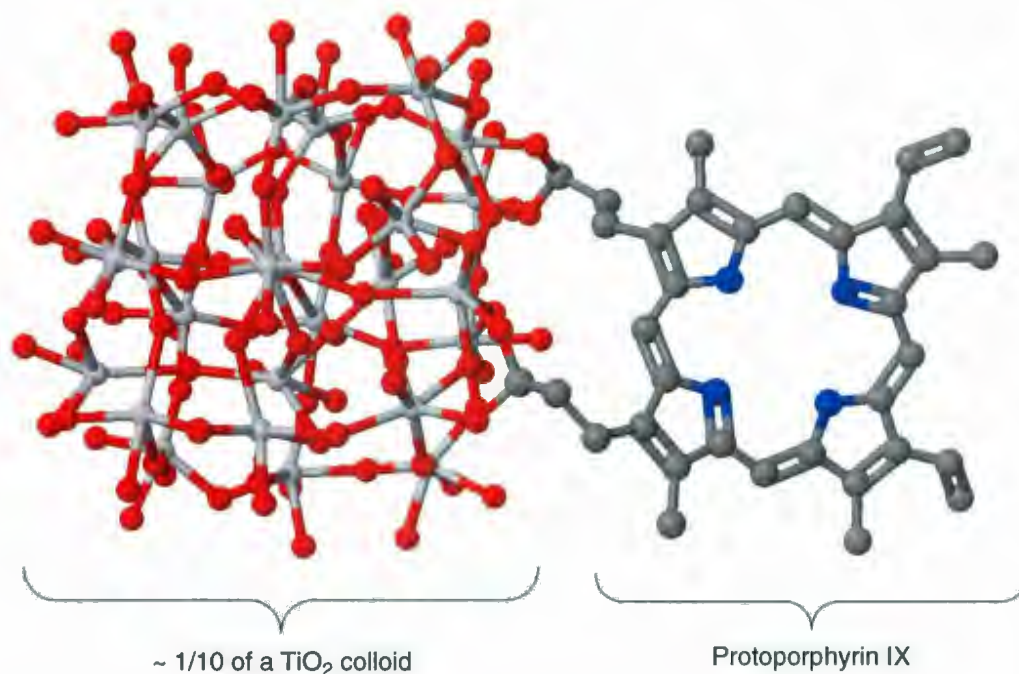
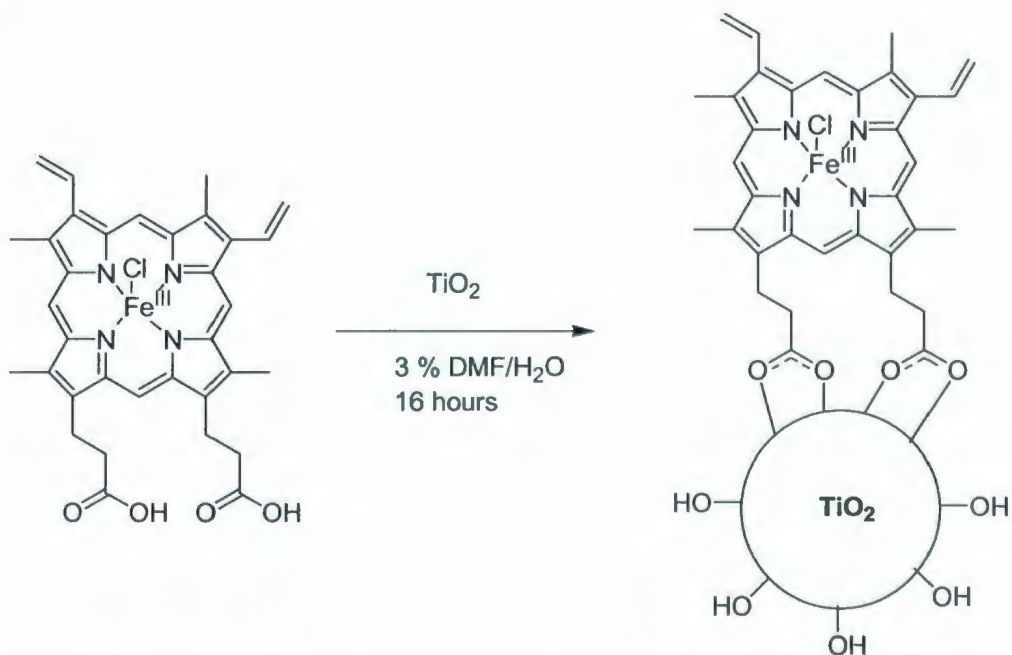


Figure 4.12: Representation of colloidal $\text{TiO}_2(\text{OH})_n$ with attached PPIX.

Initial attempts of surface sensitization of TiO_2 with a porphyrin therefore proved successful. Spectral data from UV-VIS, IR, ^1H NMR, and Excitation/Emission studies provided supporting evidence. It has also been shown that surface groups play a significant role in governing the colloid – solvent interactions, confirming concepts proposed during the metal oxide phase of the research project. These PPIX/ TiO_2 assemblies have a high degree of dispersibility in DMF. While the absence of a metal prevents the use of these assemblies as a catalyst, the experiments demonstrated in this section of the thesis provided substantial procedural and analytical techniques for the preparation, isolation, and analysis of porphyrin/ TiO_2 assemblies.

4.2.3 Hemin Chloride/ $\text{TiO}_2(\text{OH})_n$

Originally, much of the protoporphyrin IX chemistry discussed in the previous section was investigated with the intent of using the developed procedures and inserting the iron into the porphyrin either before or after formation of the porphyrin/ TiO_2 complex. Upon initiating this phase of the project, it was actually found to be more cost effective to purchase the porphyrin in hemin form, specifically hemin chloride. While this eliminates one step in the synthetic route, it also called for the modification of the procedures developed.



Scheme 4.3: Synthesis of Hemin chloride/ TiO_2 assemblies.

The initial experiment was performed in much the same way as previously described. Hemin chloride (21.8 mg) and $\text{TiO}_2(\text{OH})_n$ (111.0 mg) were combined in H_2O

(10 mL). The hemin chloride did not prove to be soluble in the aqueous medium, so a small amount of DMF (4 drops) was added to aid in the mixing of reactants. The mixture was then left to stir for approximately 16 hours at room temperature. A dichloromethane extraction was attempted, but was unsuccessful. The solid in the mixture was isolated via gravity filtration, and the solid was extracted from the filter paper using pure DMF, until subsequent washings became clear and colourless. The solvent was then removed using a combination of reduced pressure followed by high vacuum and heat, yielding a black solid (68.3 mg).

The DMF/water mixture from the mother liquor was removed yielding a black solid (102.3 mg). From the discolouration, it is likely that a small amount of porphyrin or porphyrin/ $\text{TiO}_2(\text{OH})_n$ may have evaded the filter. Follow-up with both UV-VIS and IR spectroscopy showed no evidence for the presence of Soret or Q-bands characteristic of porphyrins. The mother liquor was found to be primarily TiO_2 .

Continuing with the analysis and characterization of the solid isolated from the reaction mixture, UV-VIS spectra were obtained. Figure 4.13 displays a comparison of the Hemin/ $\text{TiO}_2(\text{OH})_n$ assembly and free hemin chloride in a solution of DMF.

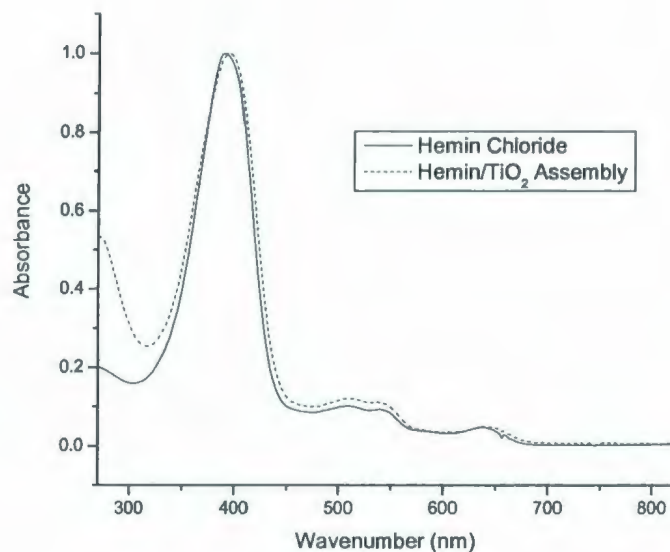


Figure 4.13: UV-VIS of hemin chloride and hemin chloride/TiO₂ assembly in DMF. Normalized to λ_{max} .

An almost identical spectrum to that of PPIX/TiO₂(OH)_n was obtained. While no shift in Soret or Q-bands is noticed, a significant increase in absorption at wavelengths below 300 nm is seen, attributed to the incorporation of TiO₂(OH)_n within the DMF solution. To reiterate the discussion from Section 4.2.2, this absorption has been established to be supportive evidence of tethering between the porphyrin and TiO₂.

Following UV-VIS spectroscopic analysis, an IR spectrum was obtained. While the removal of DMF from the analyte still proved difficult, at this stage of the research isolation methods were refined such that DMF did not interfere with the IR spectra as in those obtained of the PPIX/TiO₂(OH)_n assemblies.

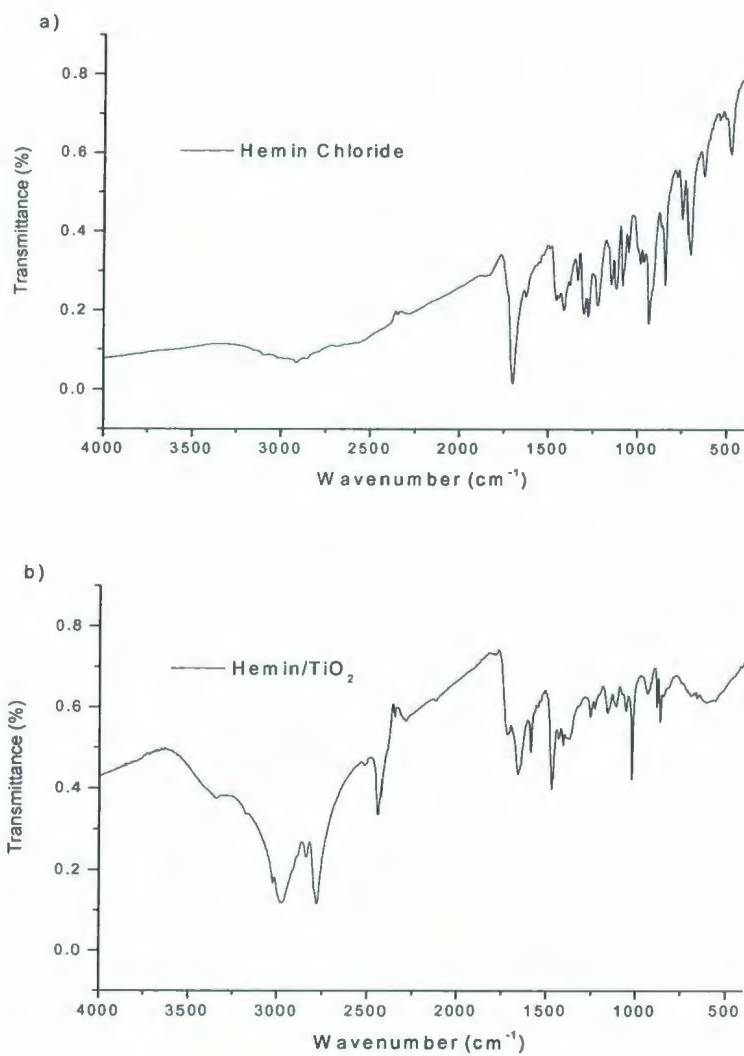


Figure 4.14: IR spectra for a) hemin chloride and b) hemin chloride/ $\text{TiO}_2(\text{OH})_n$ assembly in KBr.

From Figure 4.14 there is a noticeable change in the IR spectrum as the iron porphyrin is tethered to the $\text{TiO}_2(\text{OH})_n$. Rearrangement within the fingerprint region, as well as a sharpening of peaks at higher wavenumbers provides evidence for attachment. Unfortunately, the iron chloride stretch ($\sim 350 \text{ cm}^{-1}$)⁹³ is outside the spectral window.

Further characterization of the isolated materials with ^1H NMR spectroscopy also yielded excellent results, despite the presence of a paramagnetic metal, shown in Figure 4.15.

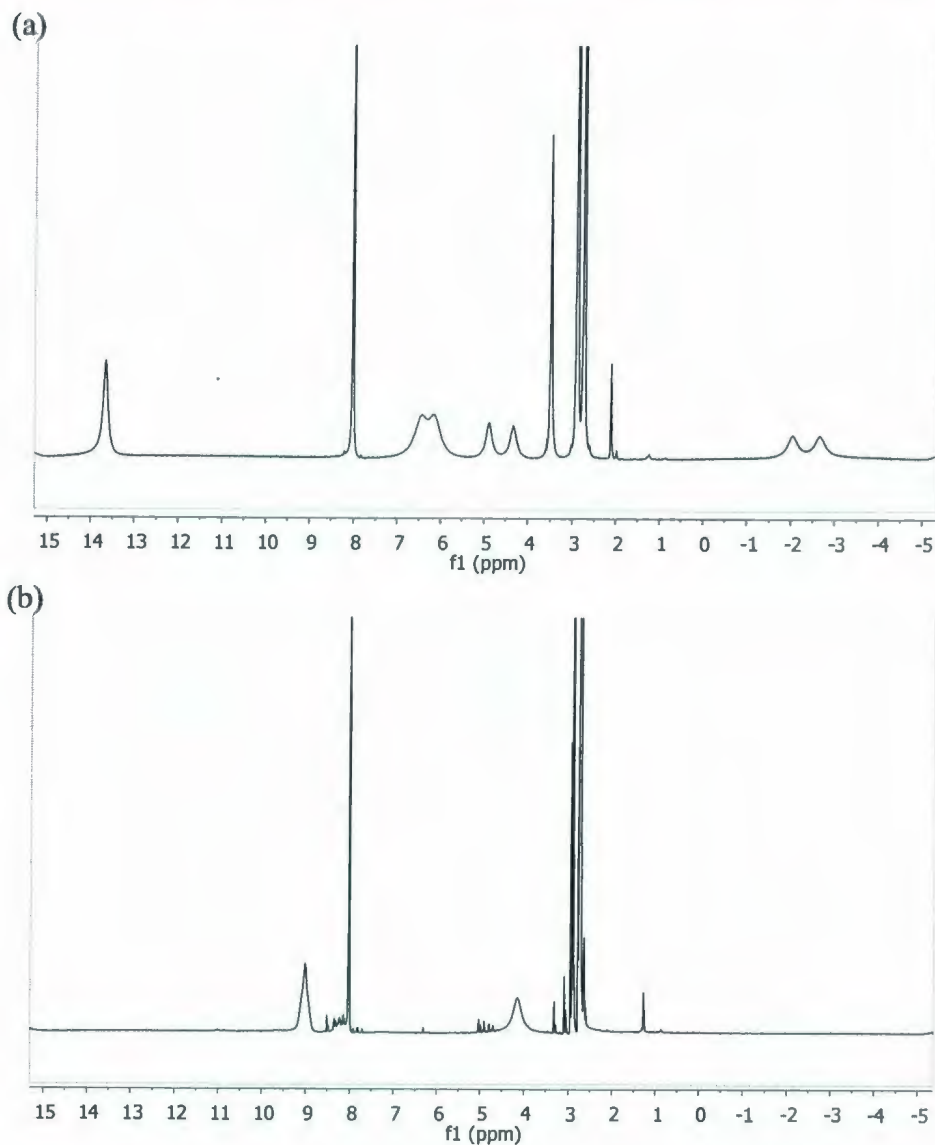


Figure 4.15: ^1H NMR of (a) hemin chloride and (b) hemin chloride/ $\text{TiO}_2(\text{OH})_n$ in DMF-d_7 .

The first spectrum is obtained from hemin chloride in DMF-d_7 . The broadened signals are characteristic of paramagnetic NMR of iron porphyrins.⁹⁴ The more intense

sharp signals are attributed to the solvent. The spectrum obtained of the hemin chloride/TiO₂ assembly is also displayed in Figure 4.15. A noticeable rearrangement of signals is clearly seen. The ¹H NMR spectrum of hemin chloride has been reported in the past by Smith *et al.*⁹⁵ and La Mar *et al.*⁹⁶ reported a NMR study of iron hemin approximately two decades ago. Since then Smith⁹⁴ has dedicated an entire volume of *The Porphyrin Handbook* to the topic of NMR and EPR spectroscopy of porphyrins, where the chemical shifts reported for hemin chloride still reference those original papers. Introduction of a paramagnetic metal center modifies the observed chemical shifts according to equation (3):

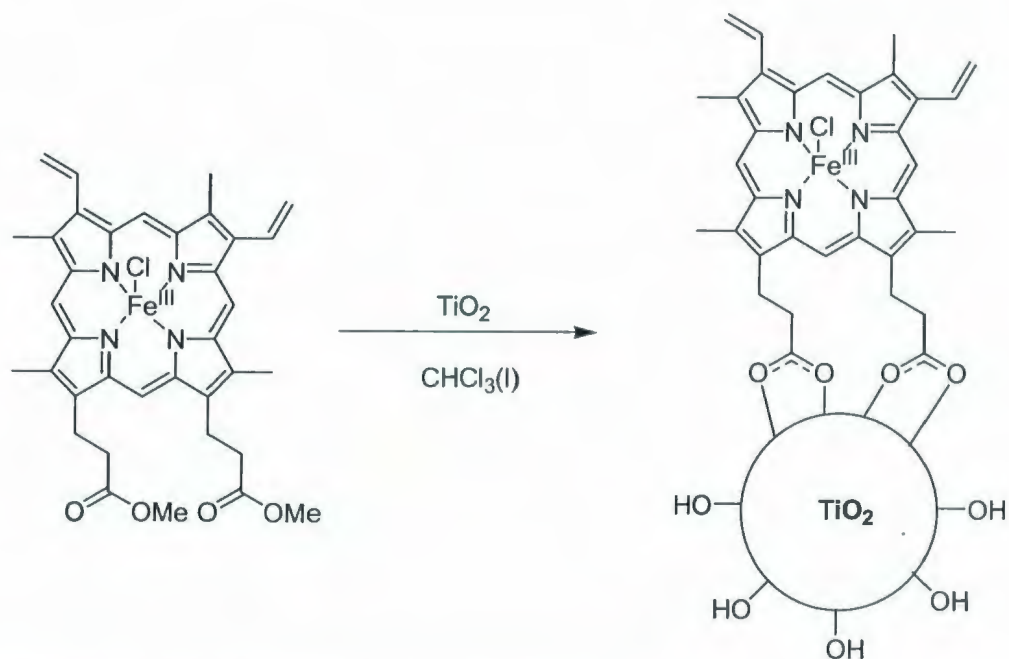
$$\delta_{\text{obs}} = \delta_{\text{dia}} + \delta_{\text{para}} \quad (3)$$

The observed chemical shift is a combination of the diamagnetic and paramagnetic contributions. Paramagnetic shift is also known as hyperfine or isotropic shift. Chemical shifts also vary greatly among different porphyrins with changes in substituents, metal centers, solvents, and temperatures. An in-depth discussion of NMR and EPR spectroscopy of paramagnetic metalloporphyrins is provided by Walker.⁹⁷ Further study following the initial acquisition of both the hemin chloride and hemin chloride/TiO₂(OH)_n spectra has lead us to believe the spectral window may have been too narrow. Depending on the porphyrin in question, signals can range in chemical shift from δ -20 ppm to δ 100 ppm. Depending on the choice of solvent, chemical shift positions of signals can vary by up to δ 50 ppm. While this interpretation of this novel paramagnetic ¹H NMR spectra of a chromophore/metal oxide assembly is limited, it does show the potential for characterization of these assemblies using this technique. Peak

assignment for metalloporphyrins is an involved process that generally incorporates isotopic comparison and temperature-dependent studies. Analysis of a paramagnetic porphyrin attached to the surface of a metal oxide semiconductor would be an intensive undertaking for which time did not permit.

4.2.4 Hemin Chloride Dimethyl Ester/TiO₂ films

Given the difficulties encountered in the use of DMF in the isolation, characterization, and application of the assemblies, attempts were made to switch to a more volatile solvent. Following esterification of the hemin chloride using 5 % v/v H₂SO₄/MeOH, solubility was achieved in chloroform. While this allows the incorporation of a volatile solvent in the tethering process, the insolubility of titanium dioxide presents a heterogeneous interaction. Similar to the procedure used in the surface-sensitization of TiO₂ films and sol-gels, the porphyrin solution is stirred over solid TiO₂. The solid is then filtered from the reaction mixture, and rinsed with the solvent to remove any untethered hemin. The product was isolated as a beige solid, indicating some attachment of the porphyrin to the TiO₂ colloids.



Scheme 4.4: Preparation of hemin chloride/TiO₂ assembly.

While this allowed for a simplification of the isolation process, it is likely that the produced hemin chloride/TiO₂ assemblies have a much lower loading density than the assemblies prepared via a single phase approach. The procedure developed previously utilized primarily aqueous reaction conditions, followed by isolation of a precipitate. From analysis of the isolated mass of the product, the majority of the TiO₂ used remained in the aqueous layer. Using this heterogeneous tethering approach, there is no separation of tethered TiO₂ and untethered TiO₂. Figure 4.16 exhibits the IR spectrum obtained through this method.

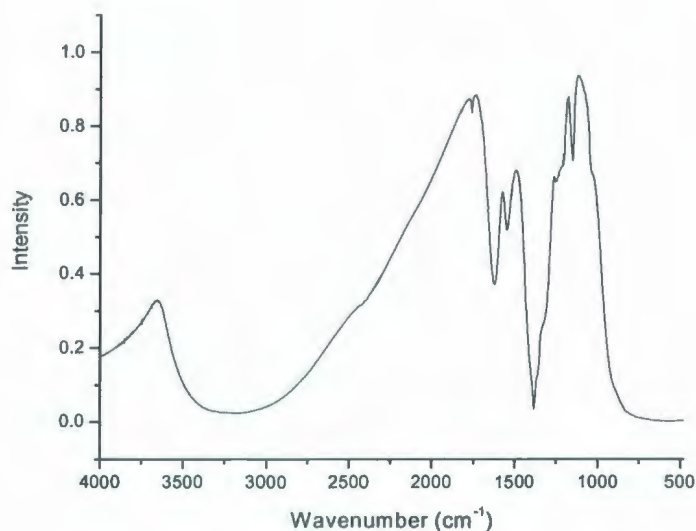
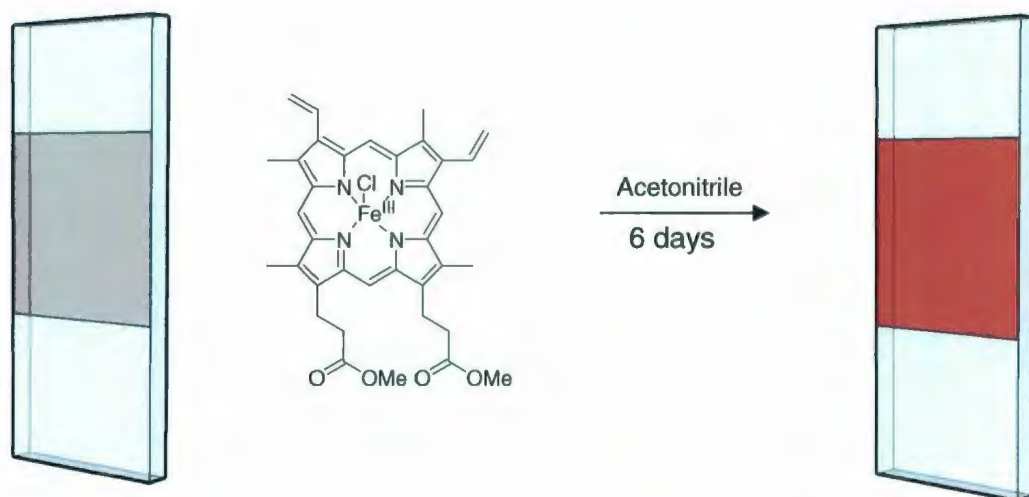


Figure 4.16: IR spectrum of hemin chloride dimethyl ester/TiO₂ assembly in KBr.

By comparison with Figure 3.4, this spectrum exhibits the characteristic IR absorption of TiO₂, with additional peaks appearing in the range of 1200 cm⁻¹ to 1800 cm⁻¹. When compared to Figure 4.14, the IR spectrum of the hemin chloride/TiO₂ assembly, there is a noticeable difference. Although the colour change of the isolated solid provides some evidence of tethering, it is not to the same extent of that achieved using previously developed methods.

With the limited success found using a colloidal approach, hemin chloride dimethyl ester was also used to sensitize TiO₂ films generously supplied by G. Meyer. As described in Chapter 1, the films are prepared via a sol-gel process incorporating Carbowax[®] to give a transparent clear film on a glass slide.



Scheme 4.5: Surface sensitization of TiO_2 films with hemin chloride dimethyl ester

Briefly, a TiO_2 film is immersed in a solution of hemin chloride dimethyl ester in acetonitrile for 6 days (Scheme 4.5). The film is then removed from the solution and rinsed with acetonitrile to remove any residual porphyrin solution. Surface sensitization is indicated by a change in the previously opaque film to a dark red colour. Further verification of surface sensitization is provided by a clearly visible Soret band in the UV-VIS spectrum.

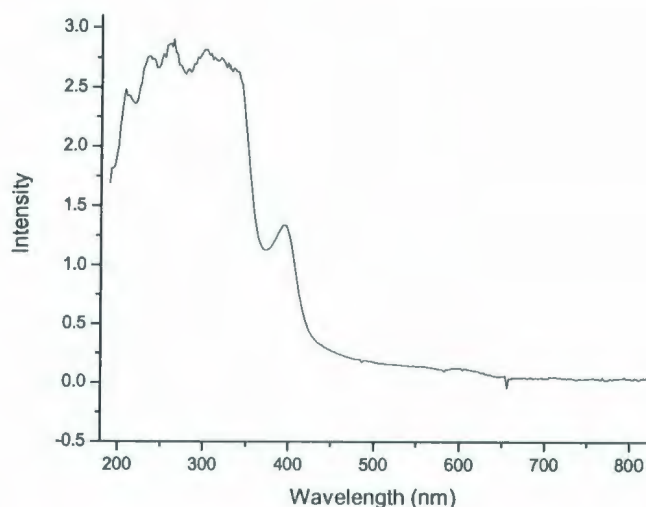


Figure 4.17: UV-VIS spectrum of surface-sensitized TiO₂ films.

To obtain the spectrum in Figure 4.17, the entire glass slide is placed into the UV-VIS spectrometer, resulting in a cutoff of transmittance from 350 nm and below due to the absorbance of the TiO₂ and primarily, the glass slide. While the use of the slides can limit some of the spectroscopic methods applied previously it greatly increases the ease of derivatization and isolation of the materials.

4.3 Conclusions

Through the course of this phase of the research, several different chromophore – metal oxide assemblies were prepared. Several different methods were developed for the preparation, isolation, and characterization of these assemblies.

Specifically, 9-anthracenecarboxylic acid/TiO₂ assemblies have been prepared and analyzed through ¹H NMR spectroscopy. Although these experiments were a departure from the primary focus of this project, valuable information was gained in

terms of characterization procedures and the surface structure of TiO_2 . These spectra are also the first reported evidence for the surface derivatization of the TiO_2 prepared via nonhydrolytic methods. To date, research that incorporates the synthetic methods reported by Colvin focus primarily on the physical properties of the nanoparticles produced, such as the degree of crystallinity, and not the application of the material in ways described in this Chapter. While the use of $\text{TiO}_2(\text{X})_n$ was abandoned in favor of hydrolytic processes this represents a significant result.

Several different porphyrin-sensitized colloidal TiO_2 assemblies were prepared through several different methods. Using an aqueous solution of hydrolytically-prepared TiO_2 with a small amount of porphyrin in DMF to provide a single-phase tethering environment proved to be the most effective means of preparing the assemblies. Compared to the heterogeneous approach described in Section 4.2.4, the use of a solution in which both reactants are soluble yielded much higher loading densities. In the future, development of methodologies to quantify the degree of surface sensitization will hopefully shed more light on these assertions. The level of surface modification appears to govern the solubility of the assemblies exhibited by the inclusion of hydrolytically-prepared TiO_2 into organic solutions. This supports the idea that capping agents play a key role in governing the solvent interactions of the colloids. Novel ^1H NMR spectra of the protoporphyrin IX/ TiO_2 assemblies were obtained with excellent resolution. Paramagnetic ^1H NMR spectra of the hemin version were also obtained.

Chapter 5

Biomimetic Catalysis

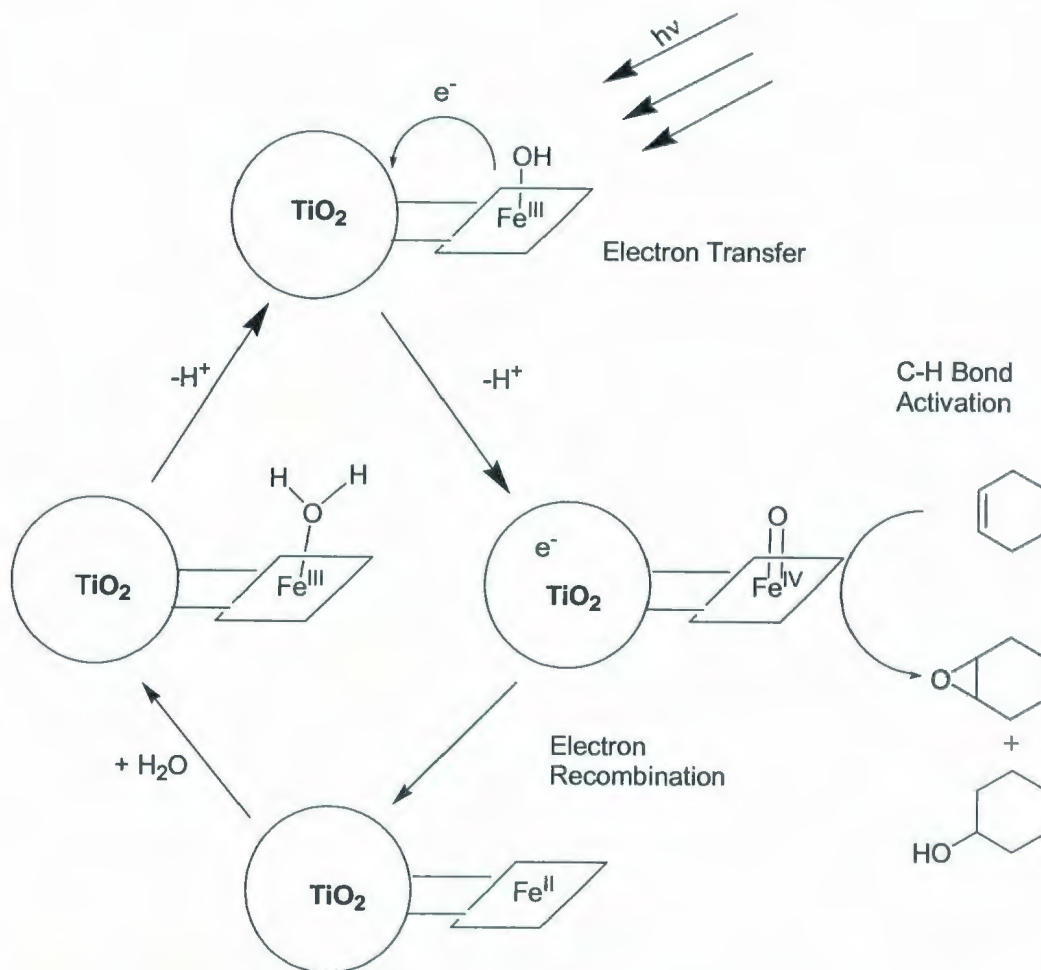
Chapter 5: Biomimetic Catalysis

5.1 Introduction

The successful development and systematic characterization of porphyrin/TiO₂ assemblies described in Chapter 4 has laid the ground-work required for utilization of these assemblies for photo-induced oxo-functionalization of unsaturated substrates. These proof-of-concept experiments in which hemin chloride/TiO₂ is activated photochemically should give rise to the biomimetic analogues of horseradish peroxidase and cytochrome P450. The requisite background literature, as well as some of the methods used to model these activities, was described in Chapter 1. This Chapter addresses the application of the assemblies to achieve catalytic insertion of oxygen into cyclohexene, a common substrate used to test P450 models.

The proposed mechanism for oxo-functionalization and the design of the nanoscale molecular assemblies is predicated on the mechanism shown in Scheme 5.1. Briefly, the cycle begins with the attachment of water to the iron center of the porphyrin and is the oxygen source, instead of the terminal oxidants used in peroxide shunt mechanism utilization in various P450 models. Excitation of the porphyrin/TiO₂ followed by electron injection into the TiO₂ should yield the Fe(IV)=O compound needed to mimic the active site of metalloenzymatic oxo-transfer catalysts. Oxygen insertion onto cyclohexene may then be followed by electron recombination from the TiO₂ back to the porphyrin. The expected products depend on the nature of the active catalyst

mechanisms of oxo-transfer: cyclohexene oxide via a route that proceeds via a Fe(IV)=O^+ radical cation, or cyclohexanol via Fe(IV)=O .



Scheme 5.1: Proposed mechanism for the catalytic insertion of oxygen through photochemical activation of porphyrin/ TiO_2 assemblies.

It should be noted that Scheme 5.1 shows a very general pathway. Experiments described in this chapter can be considered proof-of-concept, where the focus was photochemical excitation of these assemblies in the presence of cyclohexene followed by identification of the resulting products. The mechanism for oxygen insertion is often

inferred from the distribution and stereochemistry of products. Detailed kinetic investigations using laser flash photolysis protocols are outside the scope of this study.

The role of TiO_2 in the catalytic cycle is three-fold. Mechanically, the colloids provide an attachment point for the porphyrin, essentially immobilizing the active site. One of the difficulties encountered when attempting to model P450 chemistry is the formation of μ -oxo dimers (Figure 5.1) upon absorption of a photon. Immobilization thereby prevents ambiguity in understanding the mechanism by elimination of the contribution arising from photocleavage of the μ -oxo diiron complex.

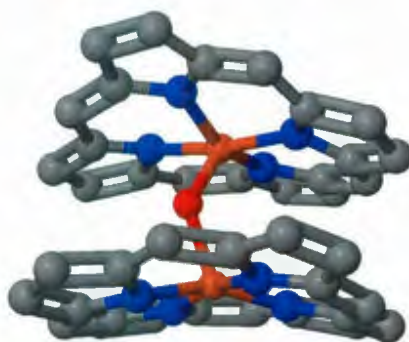


Figure 5.1: Porphyrins can form μ -oxo dimers which can inhibit oxygen insertion reactions.

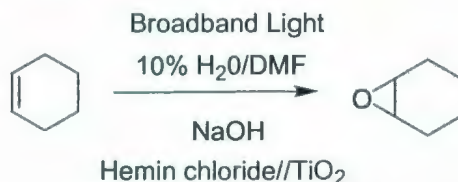
Adsorption to the nanoscale colloids offers an opportunity to compare the reactivity of biomimetic assemblies at the interface between a colloidal particle and the bulk solvent, to that inside a protein matrix. The interfacial region has been proposed to be highly hydrated and is poorly understood. Electron injection has been postulated to yield large electric fields at the point of injection. The impacts of these forces have yet to be clearly delineated. A third proposed role served by the colloidal semiconductor is that

of an electron sink. In other dye-sensitized systems, excitation with light yields an excited-state porphyrinic transient that has the ability to inject an electron into the high density of non-occupied acceptor orbitals of the semiconductor. (See Section 1.2.1) In the case of iron porphyrins, the result is oxidation of the metal and initiation of the catalytic cycle. These issues were previously described in Chapter 1, including some of the interesting and novel solutions other researchers have found to this problem.

5.2 Results and Discussion

5.2.1 Catalysis via Colloidal $\text{TiO}_2(\text{OH})_n$ Supports

Using the colloidal hemin chloride/ TiO_2 assemblies described in Section 4.2.3, the epoxidation of cyclohexene was attempted. Briefly, hemin chloride/ TiO_2 (1.0 mg) was combined with cyclohexene (41.8 mg) in DMF (9.0 mL) in a quartz cuvette to give a burgundy suspension. $\text{NaOH}(\text{aq})$ (1.0 mL, 9×10^{-4} mol/L) was added. Addition of the $\text{NaOH}(\text{aq})$ initiated the precipitation of a brown solid, which redissolved after the mixture was stirred. The solution was exposed to broad-band white light excitation using a 450 W Xenon arc lamp (Scheme 5.2).



Scheme 5.2: Epoxidation of cyclohexene with hemin chloride/ TiO_2 assembly.

UV-VIS spectra of the reaction mixture were taken before irradiation, at 3 hours, and after 22 hours. The results are shown in Figure 5.2.

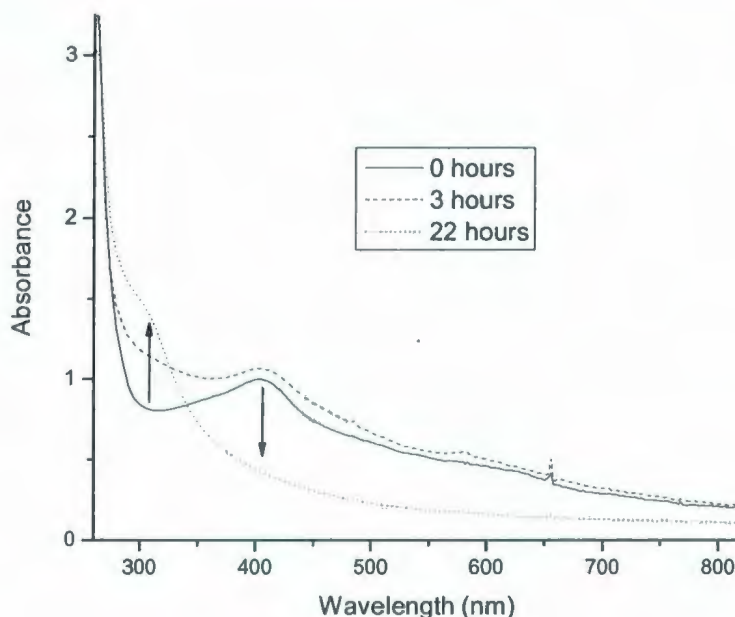


Figure 5.2: UV-VIS spectra of hemin chloride/ $\text{TiO}_2(\text{OH})_n$ with cyclohexene and NaOH in DMF/ H_2O at various time intervals.

Significant changes are evident in the UV-VIS absorption spectra observed over the duration of the experiment; specifically, an increase in the signal at ~ 300 nm accompanied by a decrease in the Soret band of the porphyrin at ~ 404 nm. Loss of the Soret band indicates degradation of the PPIX ligand. No changes were observed in control solutions stored in the absence of light for the same time period.

Initial analysis of the epoxidation attempt indicates that irradiation resulted in the decomposition of the hemin chloride/ TiO_2 assembly. This may indicate that a catalytic mechanism is not present, or that it exists in competition with decomposition. The use of

broadband light may be the source of decomposition of the catalyst. White light excitation of the porphyrin satellite on the surface of the colloid may have been in competition with band gap excitation within the TiO_2 . It should be noted that there is a cooled transparent optical filter which prevents the heating of the sample and significant attenuation of UV light. Given that the absorption onset for TiO_2 is ~ 355 nm, coupled with extended photolysis, an exciton may be photochemically generated within the colloid base of the catalytic structure. Exciton formation yields a bound $[\text{e}^-, \text{h}^+]$ pair which must dissociate to give e^- in the conduction band and h^+ in the valence band. The oxidizing power of the hole is well known and yields hydroxide radicals upon migration to the surface.

Regardless of the assembly's potential as a catalyst, analysis shifted towards finding evidence of oxygen insertion onto the cyclohexene substrate. GC-MS yielded the spectrum depicted in Figure 5.3.

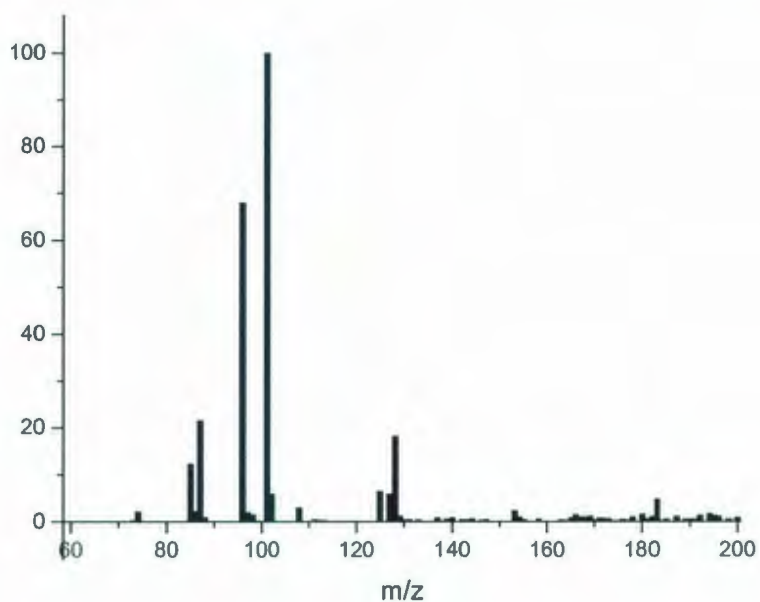


Figure 5.3: GC-MS of reaction solution following 22 hours of irradiation.

The obtained spectrum shows evidence for the attachment of oxygen to the cyclohexene. The peak at $m/z = 101$ indicates cyclohexanol. With the UV-VIS spectrum indicating a deterioration of the porphyrin, caution was used in the analysis of the MS spectrum. The products of that decomposition are unknown, thus it is acknowledged that the spectrum could be easily misinterpreted.

To further analyze the reaction mixture, GC-FID was used. Initial spectra obtained using the GC-FID was rendered uninformative due to the presence of DMF. The solvent signal in the chromatograph was broad and intense, making identification of any underlying signals impossible. To determine if a better temperature profile would achieve resolution of the signals, a standard was prepared consisting of cyclohexene, cyclohexene oxide, and cyclohexanol in DMF. This solution was also used as a standard with which to compare the retention times found in the reaction mixture. Initial attempts to achieve signal separation of the test sample involved testing of various temperature programs of the GC-FID. This included varying temperatures of the injector, column, and detector. Modification of the temperature profiles achieved moderate success towards the resolution of the test signals, although it was still not ideal, as seen in Figure 5.4.

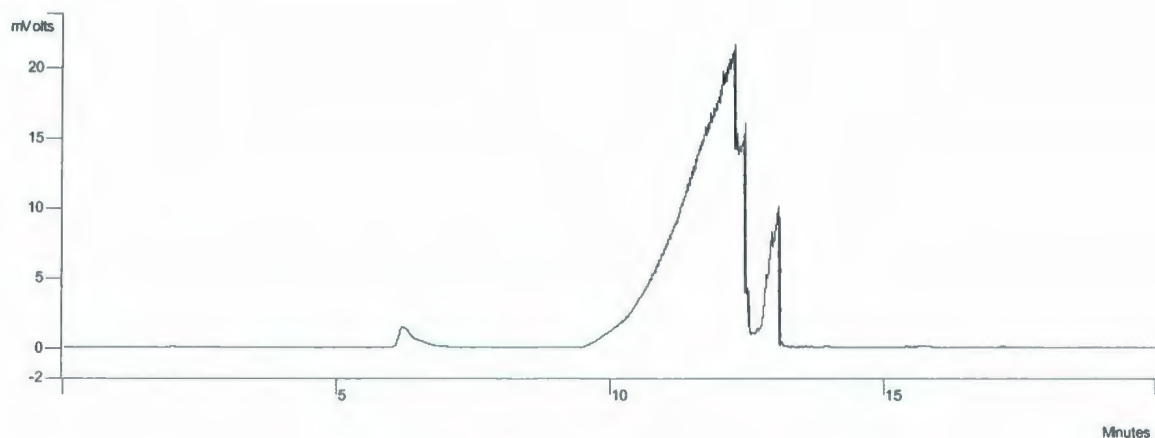


Figure 5.4: GC-FID chromatograph of cyclohexene, cyclohexene oxide, and cyclohexanol in DMF.

Aside from varying the temperature profiles of the instrument, it was thought that resolution of the analyte signals would be enhanced if the amount of DMF in the injected samples could be decreased. The method chosen was extraction of the analytes from the reaction mixture into a solvent that would pose less interference in the GC-FID spectrum. Hexane was used for extraction of the analytes from the reaction mixture, with its relatively low boiling point and immiscibility with DMF. Before attempting the extraction, additional test samples were prepared to determine if the analyte FID signals would be distinguishable from the hexane, as shown in Figure 5.5.

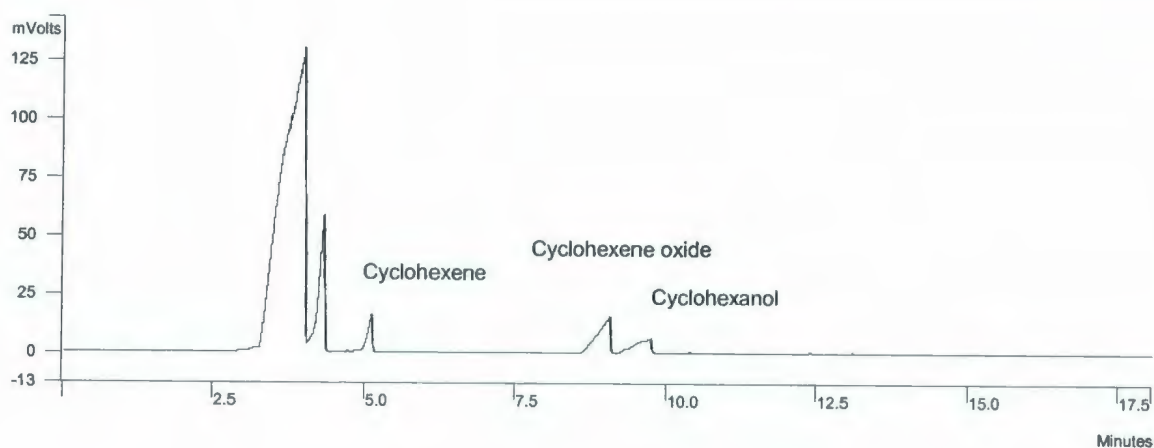


Figure 5.5: GC-FID chromatograph of hexane solution of cyclohexene, cyclohexene oxide, and cyclohexanol.

In order to decrease the solubility of the organic analytes and encourage their uptake into the hexane layer, a small amount of water was added to the DMF. Figure 5.6 shows a significant reduction in the DMF signal, resulting in enhanced resolution and identification of the analyte signals. Following resolution, sample conditions were repeated using each standard individually in order to accurately assign the peaks. Although the DMF signal was still present, it was small and sharp enough not to interfere with the detection of the signals for cyclohexene, cyclohexanol, and cyclohexene oxide, as seen in Figure 5.6.

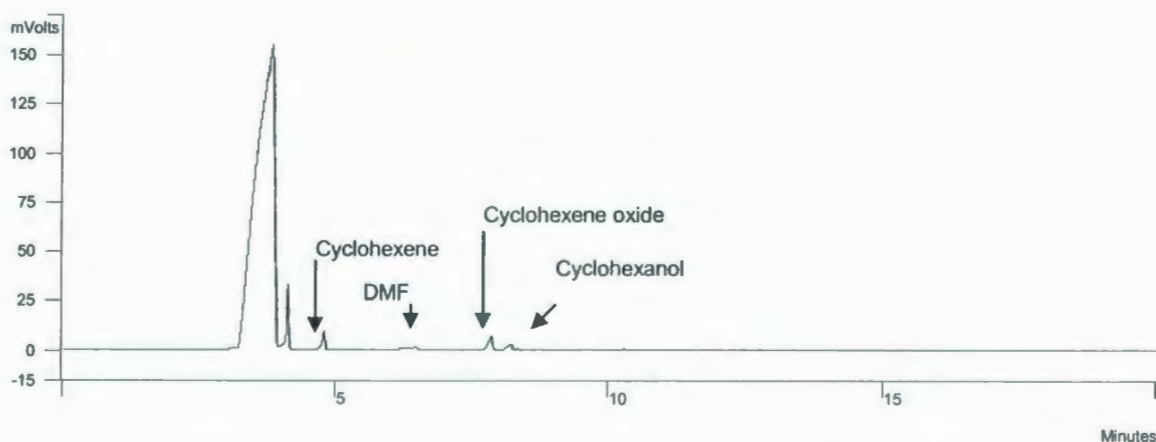


Figure 5.6: Hexane extraction of DMF standards solution showed a significant improvement in GC-FID peak resolution.

The procedure for the collection of the chromatograph in Figure 5.6 is as follows:

Hexane (2 mL) is added to a sample of the reaction mixture (3 mL). Water (2 mL) is added, and the mixture capped, shaken, and allowed to separate. Using a glass syringe, a small amount of the hexane layer (2 μ L) is extracted and injected into the GC-FID.

Injector temperature was held constant at 200 $^{\circ}$ C. The column was held at 60 $^{\circ}$ C for 3 minutes. The temperature was then increased at a rate of 15 $^{\circ}$ C/min to a temperature of 100 $^{\circ}$ C and held for 2 minutes. At that point, the temperature of the column was increased by 25 $^{\circ}$ C/min to 160 $^{\circ}$ C where it was held constant for another 2 minutes.

Finally, the temperature was increased to 210 $^{\circ}$ C at a rate of 25 $^{\circ}$ C/min and held at that temperature for 2 minutes.

Under these conditions, the reaction solution yielded the GC-FID chromatograph shown in Figure 5.7:

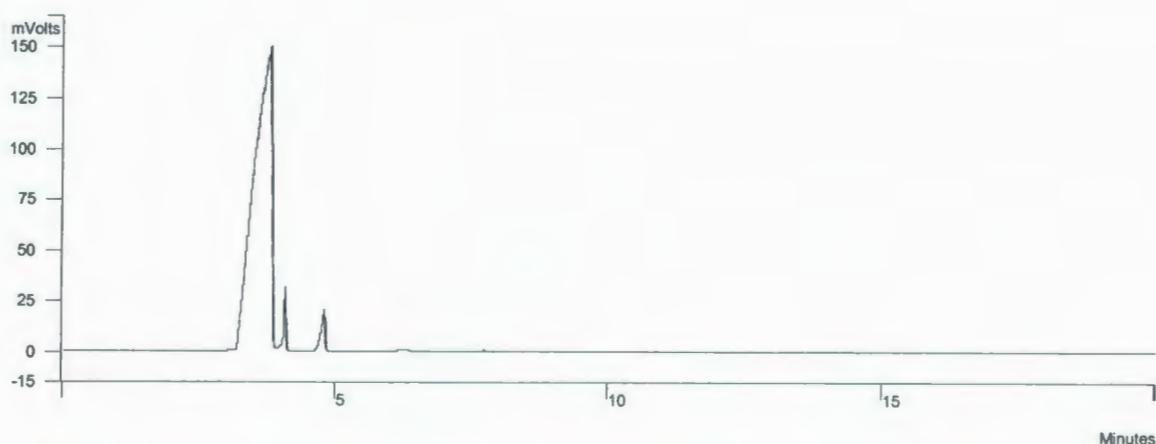


Figure 5.7: GC-FID chromatograph of hexane extraction of reaction solution.

Peaks for hexane and cyclohexene are clearly evident. A magnified view between 4 and 8 minutes is shown in Figure 5.8.

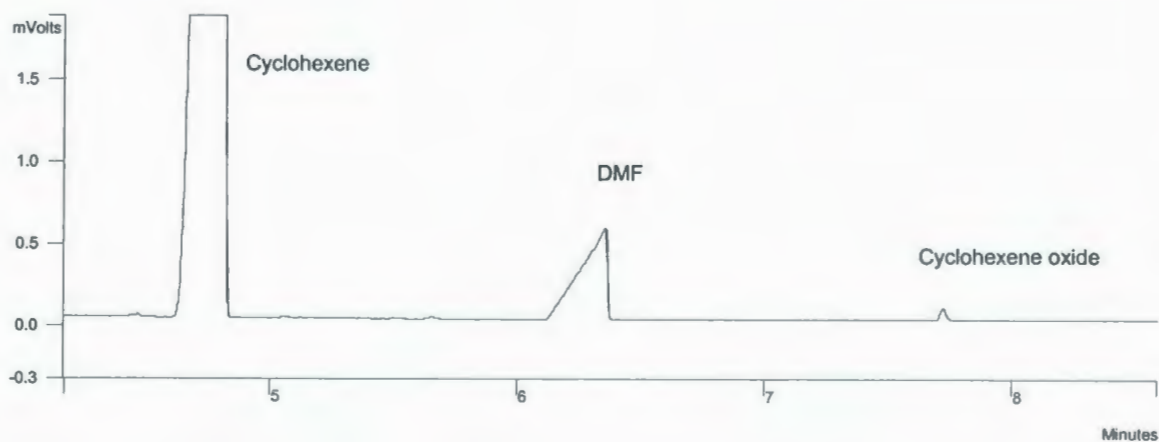


Figure 5.8: Magnified view of GC-FID chromatograph of hexane extraction of reaction mixture.

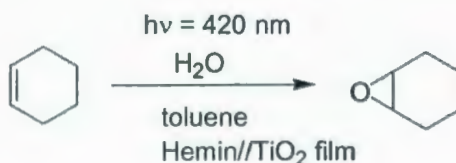
At ~ 7.8 minutes, a small peak indicates the presence of cyclohexene oxide. The low intensity of the signal may indicate that only a small amount of cyclohexene oxide was formed, but it should be noted that the detection of FID drops significantly for a

molecule containing oxygen, compared to that of simple hydrocarbons. Therefore a comparison between the peak heights cannot be used as a gauge of percent yield. It does, however, indicate that a significant amount of cyclohexene remains unreacted in the reaction solution. Quantification of these results would involve the preparation and application of a calibration curve.

These results show promise for the photochemical insertion of oxygen the hemin chloride/TiO₂ assemblies prepared in this project. These experiments were intended to provide proof-of-concept. It is acknowledged that there are many factors surrounding this reaction that need to be modified and studied, as described in Chapter 7. The exclusion of oxygen over the 22 hour photolysis time was not attempted. Sensitization of ³ΣO₂ to form ¹ΔO₂ is well-known and is the basis of photodynamic therapy especially using iron porphyrins.⁹⁸

5.2.2 Catalysis via TiO₂ film supports

Section 4.2.4 describes the sensitization of TiO₂ glass slides with hemin chloride dimethyl ester. While the use of these slides was a minor focus, the sensitized films were also used in an attempted catalytic reaction similar to that discussed in the previous section, with a few details changed (Scheme 5.3).



Scheme 5.3: Biomimetic catalyst via glass supported TiO₂ films.

Toluene was chosen as an alternative solvent. In the previous experiment DMF was required for the solubility of the colloidal catalyst. Given the nature of the TiO₂ supports used in this approach, the use of DMF was not necessary. Using the PTI fluorimeter, the absorbance spectrum of the hemin chloride/TiO₂ films was obtained (Figure 4.13), and the excitation wavelength set to correspond to the Soret band of the porphyrin (420 nm). The use of light restricted to the absorbance region of the porphyrin would avoid excitation of the TiO₂ and the deterioration of the catalyst seen in the colloid-based attempts. A UV-VIS spectrum was also obtained of the toluene solution after emersion of the slides. No absorbance providing evidence for the porphyrins remaining attached to the surface of the films was seen in the Soret band regions.

Cyclohexene (3 μ L) was added to a quartz cuvette containing toluene (3 mL). A glass slide containing a film of TiO₂ in Carbowax[®] previously derivatized with hemin chloride dimethyl ester was placed diagonally in the quartz cuvette. The assembly was then irradiated at 420 nm for a total of 278 min. Small portions of the toluene solution were removed at various time intervals throughout the experiment for analysis. The experiment was halted at various times to analyze the slide assembly by UV-VIS as irradiation progressed. The toluene solution was analyzed for reactants and products using the GC-FID.

As the experiment proceeded it was visually apparent that the burgundy film was turning colourless at the site of irradiation. UV-VIS spectra, shown in Figure 5.9, exhibited a bleaching of the Soret band absorbance, indicating either a detachment of the adsorbed porphyrin or its decomposition.

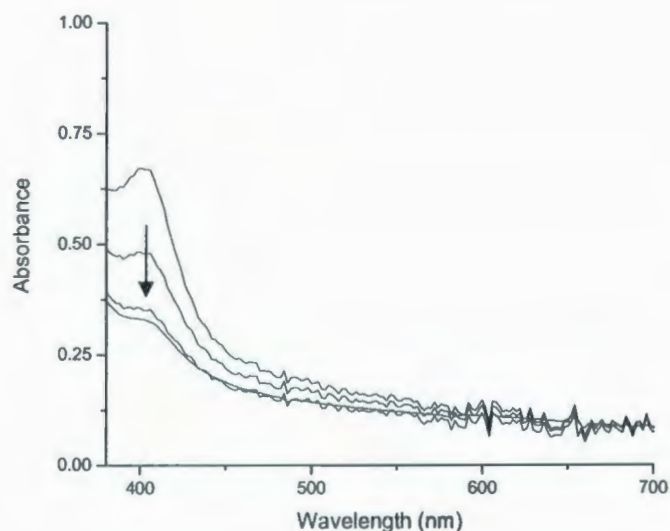


Figure 5.9: UV-VIS spectra of hemin chloride/TiO₂ slides irradiated at 420 nm.

Spectra obtained of the toluene reaction solution did not show any Soret bands, which lends support to the assertion the porphyrin may be decomposing on the surface of the film, a result similar to that seen previously. A significant problem to overcome is the stabilization of the catalyst over the time period of the photolysis.

The reaction solution was analyzed with GC-FID to find evidence for oxygen insertion using the methods described in Section 5.2.1. A standard sample was prepared using cyclohexene, cyclohexanol, and cyclohexene oxide in toluene in amounts mirroring the reaction conditions. Several combinations of analytes and solvents were examined to correlate proper peak assignments with retention times, as well as various temperature profiles. Figure 5.10 represents the best resolution of peaks achieved, as well as their respective assignments. It should be noted that the figure is an expanded view of areas of

interest. The solvent peak, toluene, yields a much more intense signal relative to the analytes.

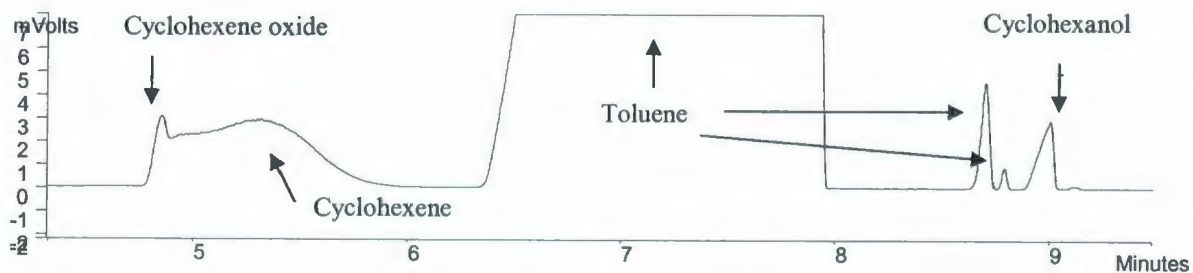


Figure 5.10: GC-FID chromatograph of standards cyclohexene, cyclohexanol, and cyclohexene oxide in toluene.

Following the development of the GC-FID protocols that achieved successful resolution and identification of peaks, the reaction solution was analyzed, and yielded the chromatograph shown in Figure 5.11.

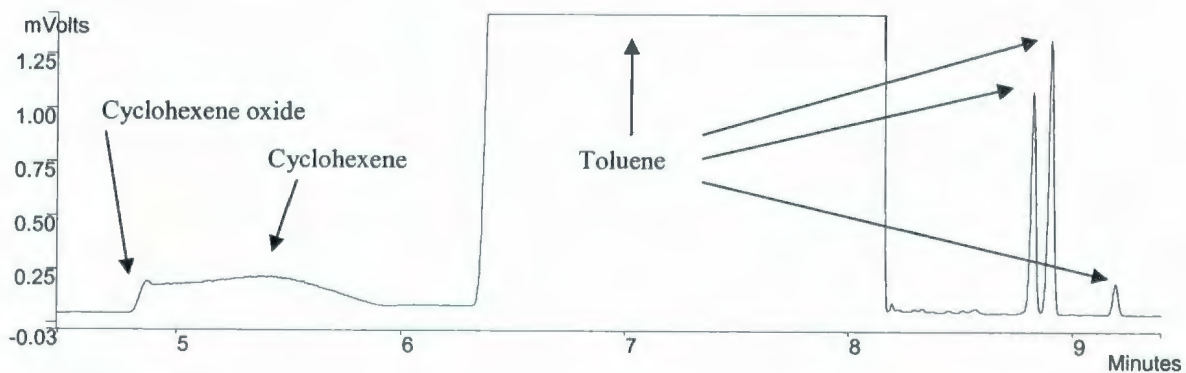


Figure 5.11: GC-FID chromatograph of reaction solution following irradiation at 420 nm.

Figure 5.11 suggests the presence of cyclohexene oxide within the reaction solution, verified by comparison to GC-FID of various combinations of the standards. Cyclohexanol is absent from the reaction solution, and a significant amount of cyclohexene remains.

5.3 Conclusions

This chapter presented the primary goal of this research project: to develop porphyrin/metal oxide assemblies that could be utilized in the photocatalytic insertion of oxygen. Success was achieved in the role of oxygen insertion, but with a degradation of the materials seen in both approaches.

The colloidal approach via broad band-light excitation met with partial success. GC-FID provided evidence for the epoxidation of cyclohexene, but UV-VIS analysis showed a loss of intensity of the Soret band. Initially, it was proposed that the use of broad spectrum of light resulted in band gap excitation of the TiO_2 , which in turn contributed to a breakdown of the attached porphyrin. The second approach using TiO_2 films with a focused wavelength of light provided similar results, discounting the previous assumptions. These results indicate that excitation of the porphyrin in achieving oxygen insertion, but in a way in which the porphyrin is consumed.

Many issues remain to be addressed. These experiments have been approached as proof-of-concept, whereby the primary goal was the detection and verification of oxygen insertion. Isolation and quantification of the products remains to be achieved, as well as

recovery of the assemblies. Modification of the reaction conditions such as solvent, temperature, etc. may provide better results.

These promising results represent an excellent starting point for further development of porphyrin/TiO₂ catalytic materials with mechanistic characterization of photo-induced oxo-transfer reactions.

Chapter 6

Self-Supporting TiO₂ Membranes

Chapter 6: Self-supporting TiO₂ membranes

6.1 Introduction

The majority of this thesis describes the development of colloid-based porphyrin assemblies. The donation of TiO₂ films by G. Meyer of John Hopkins University allowed for the investigation of alternate routes. The ease of sensitization of these films compared to the extractions required via colloidal methods encouraged an interest towards the development of other free-standing TiO₂ materials. The final phase of this research project was directed toward the fabrication of self-supporting TiO₂ membranes. Methods to produce membranes used similar approaches to those used for KBr pellets which are employed in IR applications. More specifically, powdered material was subjected to high pressure within a die normally used for IR pellets. The goal for this phase of the research described in this Chapter was mechanical in nature, in essence to produce membranes with sufficient structural integrity to allow for useful application of pellets. Several different methods were used through a trial-and-error approach with the incorporation of various materials intended to enhance the strength of the membranes (Figure 6.1).

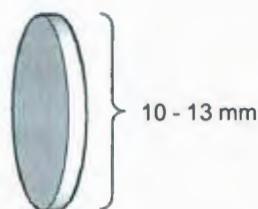


Figure 6.1: TiO₂ self-supporting membranes.

Following the successful production of these membranes, preliminary experiments towards surface sensitization of a single side of these membranes was also achieved. The ability to selectively attach different dyes to opposite sides of the membranes may lead to several novel applications of surface-sensitized metal oxides semiconductors. While outside the scope of this project, further studies by the Thompson group will work towards exploitation of such materials into biphasic chemical reactions.

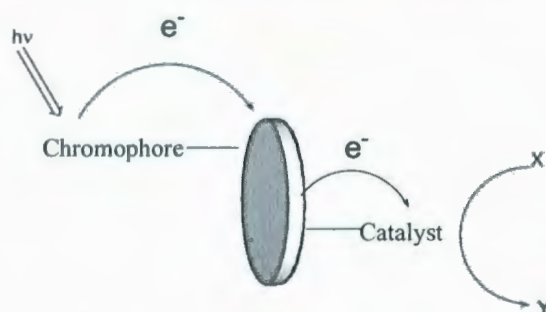


Figure 6.2: Proposed application of membranes in biphasic chemistry.

Figure 6.2 represents one example of an application of these materials. The ability to selectively sensitize opposite surfaces of the TiO_2 disc may allow for the use of separate chromophore/catalyst combinations. This is in contrast to the assemblies developed in earlier phases of this project whereby the light-harvesting chromophore and the reactive entity are one and the same. The ability to tune the chromophore to maximize photon capture while selecting a catalyst that is focused towards the desired application would greatly maximize the efficiency of these catalysts. Light can be

selectively introduced to a specific side without interference with the active site on the opposing face of the membrane.

This chapter presents various methods for the fabrication of membranes and also preliminary experiments toward the surface sensitization of a single side.

6.2 Results and Discussion

6.2.1 Fabrication

The fabrication of membranes is described below on a per experiment basis in chronological order. To the best of the author's knowledge, these materials have not been previously reported, and the presentation of results allows for a systematic critical evaluation of the protocols employed. Each experiment is categorized based on the materials incorporated into the membranes.

TiO₂

The first approach taken toward the fabrication of TiO₂ membranes followed the usual procedures employed in the preparation of KBr discs used for solid phase IR analysis. TiO₂ prepared via hydrolytic means was powdered using a mortar and pestle. The white powder was added to the 13 mm diameter KBr press. 5 tons of pressure was applied under high vacuum for 2 minutes. The pressure was increased to 10 tons for another 5 minutes. It was found that 104.6 mg of TiO₂ was insufficient to form a stable disc, while larger amounts (110.5 mg, 150.5 mg, and 182.8 mg) provided TiO₂ membranes that could easily be removed from the press without cracking. This

procedure was successful in providing TiO₂ membranes, but not of sufficient strength. A simple stress test (shaking inside a sample vial) indicated that the membranes were brittle and would not have the structural integrity needed for practical applications. A major problem encountered by Fitzmaurice in the development of membranes introduced in Section 1.2.2 was the fragility of the assemblies.

TiO₂ + 5 % Nafion[®] solution

To increase the structural integrity of the membranes it was proposed that Nafion[®] may serve that purpose. A paper by Tanaka *et al.*⁹⁹ reports the enhancement of photocatalytic degradation of paraquat achieved by the coating of TiO₂ with Nafion[®]. Initial attempts followed a similar approach towards the incorporation of Nafion[®] into the membranes. A 5% Nafion[®] solution (~1 mL) was added to powdered TiO₂ and allowed to dry. Membranes were prepared as previously described, yielding pellets of roughly the same quality. It should be noted that pressure was limited to ~2 tons in order to retain the structure of Nafion[®]. While no substantial improvement of membrane strength was noted, it was still possible to prepare membranes using TiO₂ with Nafion[®].

Focus shifted towards the coating of a prefabricated membrane with a film of Nafion[®]. In this approach, a coating of Nafion[®] solution was placed on a single side of the membrane and allowed to dry. The membranes immediately disintegrated after the addition of the solution. As received, Nafion[®] is dissolved in a solution of lower aliphatic alcohols and water (40%). The addition of an aqueous solvent to the membranes resulted in redispersion of the colloids. To avoid this, Nafion[®] films were

prepared by allowing the solution to evaporate. The film was dissolved in methanol, ethanol, and isopropanol. Using methanol, a clear colourless solution was produced. Ethanol and isopropanol yielded clear colourless gels. The solutions were placed on top of different membranes and allowed to dry. A visible film formed on the surface of all three membranes, with the ethanol edition appearing slightly better than the others. While these methods provide another means to incorporate Nafion[®] onto the surface of the membranes, no substantial improvement in their strength was seen when compared to those prepared using pure TiO₂.

TiO₂ + Nafion[®] 112 disc

With moderate success using Nafion[®] solutions, research continued into methods to attach Nafion[®] to the membranes. Nafion[®] 112 films were generously donated by Dr. P. Pickup of Memorial University of Newfoundland. These clear orange films are available in the form of sheets. With the IR press plunger as a guide, the sheets could be cut into small discs. Figure 6.3 illustrates the setup of the press and components.

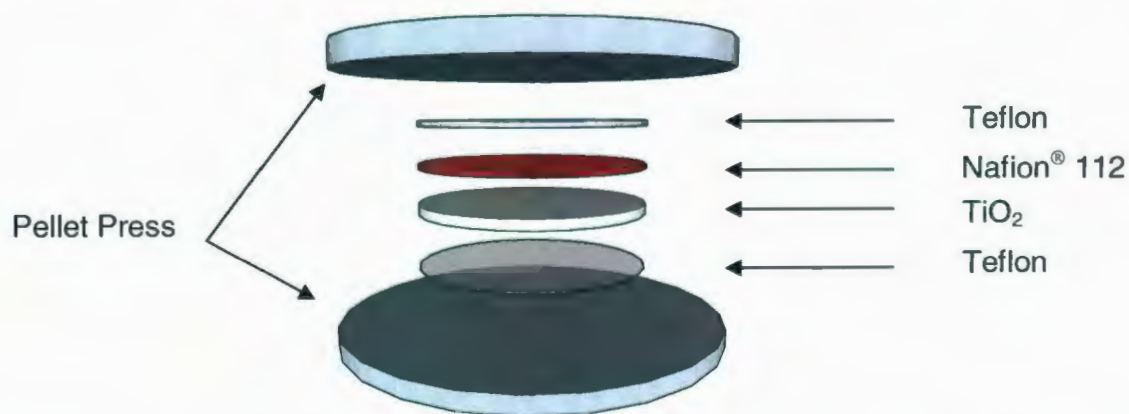


Figure 6.3: Arrangement used to incorporate Nafion[®] 112 film onto TiO₂ membranes.

Teflon discs were cut to size in order to protect the polished die within the press from tarnishing. Carbon paper was also tried, but could not easily be separated from the Nafion 112[®] following high pressure. Using prefabricated membranes (13 mm press, with 10 tons of pressure) the membranes were returned to the pellet press with a disc of Nafion[®]. Pressure was increased to 2 tons for ~15 minutes. Partial attachment of the film was attained, but the film could easily be detached. Better results were achieved when a Nafion 112[®] disc was placed within the press followed by the addition of powdered TiO₂. That is, when Nafion[®] film is incorporated into the initial fabrication process of the membranes, much better attachment is seen. Quantities of TiO₂ (110 mg – 160 mg) yielded membranes of similar quality to those previously prepared, even under lower pressures. Following the simple stress test, these membranes however also showed only a moderate improvement, with the TiO₂ still crumbling away from the Nafion[®] film.

TiO₂ + Nafion[®] 112 + heat

The introduction of heat into these methods was possible with the use of a hydraulic press modified with heat plates. For these attempts, a 10 mm brass pellet press was used. A few test membranes showed that the procedures developed previously could be applied using this setup, with 110 mg of TiO₂ yielding satisfactory membranes. The upper pressure limit for the brass press was unknown, so the applied pressure was limited to 2 tons. The hydraulic press was preheated to 80 °C and the brass die assembled as previously described, with powdered TiO₂ atop a 10 mm Nafion[®] disc. (It should be noted that experiments in which the order was reversed, decreased the quality). Pressure

was increased to 2 tons for ~ 15 minutes. Pressure and heat were then removed, and the pellet press was allowed to cool to room temperature before the membranes were removed. This approach yielded the strongest assemblies to date. The Nafion[®] film showed a much stronger bond to the membrane than previously found. The membrane resisted shattering, with moderate breaking near the edges of these discs while still retaining form.

TiO₂ + Nafion[®] 112 + Carbowax[®] + heat

The introduction of heat into the pressing process for the fabrication of these membranes not only provided an increase in strength with two distinctly different faces, but led to the incorporation of Carbowax[®] into the membranes. Chapters 4 and 5 describe the use of TiO₂ films attached to glass slides as prepared by Meyer's group. Carbowax[®] (poly(ethylene glycol)) is incorporated into the TiO₂ films to allow for better adherence to the slides. Its presence does not interfere with the photochemistry of the metal oxide.^{100,101} With a melting point of 57 – 61 °C, the procedures allowed for easy addition of Carbowax[®]. Initial attempts used excessive amounts of Carbowax[®] (31 mg). Once melted and pressure applied, the liquid was simply expelled from the press. To determine the amount of Carbowax[®] required to act as a binding agent within the TiO₂ membranes, calculations were carried out to obtain the volume of pore space within the pellet, assuming a composition of spheres of 10 nm diameter and comparing volumes to that of cubes of the same dimensions. It was determined that << 1 mg would be sufficient. Further experiments limited the amount of Carbowax[®] to a few grains, inserted into the

assembly between the Nafion[®] film and the powdered TiO₂. To allow for complete dispersion of the TiO₂, these membranes were kept at 80 °C with 2 tons of pressure for ~ 2 hours. A schematic of the setup is shown in Figure 6.4.

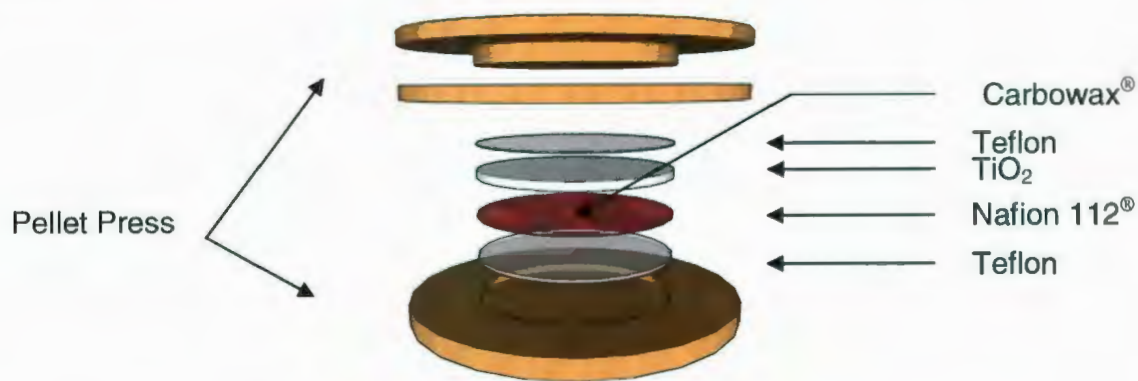


Figure 6.4: Incorporation of TiO₂, Teflon, Nafion[®], and Carbowax[®] to form membranes under pressure and heat.

The pellets obtained via this were significantly stronger than previously. The Nafion[®] appeared to be bound to the TiO₂ membrane much more completely. The Carbowax[®] not only acted as a binding agent within the TiO₂ but also as a glue to attach the Nafion[®] films. The results (Figure 6.5) were easily reproducible with careful attention to the even distribution of the Carbowax[®] and powdered TiO₂.



Figure 6.5: TiO₂/Nafion[®] membranes.

6.2.2 Surface Derivatization

After procedures that yielded consistently strong TiO₂/Nafion[®] membranes had been developed focus shifted towards the attachment of porphyrins to the surface. As mentioned in the introduction to this Chapter, one of the reasons for the development of these membranes is the possibility of photochemical catalyst whereby light is absorbed on one side of the membrane and electrons are transferred to the opposite side. In order to achieve this, it was required to demonstrate that sensitization of a single side of the membrane could be achieved. Hemin chloride dimethyl ester in dichloromethane was selected as the test chromophore. With this porphyrin, previous experiments using both colloidal and film-based approaches allowed for surface sensitization without the difficulties posed with the volatile solvents required when using non-ester porphyrins.

The first attempt involved complete immersion of a TiO₂/Nafion[®] membrane to test whether or not attachment would take place. With the absence of optical transparency, UV-VIS or IR spectroscopy could not be used as in previous experiments to verify coordination of the dye to the surface. In this case, tethering had to be verified visually by a discolouration of the membranes that would be sustained following washing with the solvent. The membrane was immersed into a solution of hemin chloride dimethyl ester (1 mg) in dichloromethane (5 mL) the membrane and left overnight. The membrane became slightly discoloured, and so it was decided to leave it for another night (~ 40 hours total). The additional soaking time increased the dark red colour of the membrane. Repeating the experiment with a higher concentration of porphyrin solution

(6.7 mg in 2 mL) and extended times (6 days) yielding a significantly darker colouring. In each case both sides, pure TiO₂ and Nafion[®], showed discolouration, indicating that tethering is possible through the Nafion[®] membrane as well.

To attach the porphyrin to a specific side of the membrane, several different methods were attempted. Each approach involved the use of solution concentrations similar to those reported above. Given the increase in surface loading with extended soaking times, the goal was to allow sustained contact with the porphyrin solution. Various techniques were used to suspend the pellet over the porphyrin solution with only the pure TiO₂ in surface contact, such as for example, placing the pellet atop the mouth of a completely filled sample vial. However, extended soaking times could not be achieved due to evaporation of the solvent resulting in a decrease in the level of the solution, thereby removing the membrane from contact. Attempts to prevent the loss of solvent by placing the vials within a sealed and solvent-saturated environment were unsuccessful as well.

A simpler method was developed to allow for the tethering of porphyrins to the membranes. Glass wool or cotton was placed within a sample vial, followed by a sufficient quantity of porphyrin dichloromethane solution required to saturate the fibrous material without covering it completely. The membrane was then placed on top with the pure TiO₂ side in contact with the glass wool or cotton. Both approaches yielded discoloured membranes, retained following washing with dichloromethane. Using cotton, the red colouring appeared much more even than the membrane prepared using

glass wool. The cotton serves a dual role to support the membranes, and also absorb the porphyrin solution to retain contact, regardless of solvent evaporation.

These experiments, while qualitative in nature, serve as evidence for the selective sensitization of a single side of the TiO₂/Nafion[®] membranes.

6.3 Conclusions

This Chapter presents the first steps toward the development of materials capable of cross-membrane electron transfer in biphasic chemical environments. Research was limited to the development and surface derivatization of the membranes.

Many different combinations of mass, heat, pressure and materials were studied to produce membranes with sufficient strength for practical applications. Using powdered TiO₂ (110 mg), Carbowax[®] (<< 1mg), and Nafion 112[®] film membranes were prepared using both heat (80 °C) and pressure (~2 tons). Single-side surface-sensitization was also achieved through a simple setup using a cotton support in a dichloromethane porphyrin solution.

Any extension of this project will focus on demonstrating that the membranes retain the photochemical properties of TiO₂ in both colloidal, and film forms. Replication of established TiO₂ photochemistry and interfacial electron transfer reactions will be necessary. If successful, the next step would include surface modification with different species on opposite sides of the membrane to determine if electron (or positive hole) transfer from one surface to the other is possible. The ability to integrate a photon harvest assembly with a separate electron-accepting active site on the same TiO₂ support

holds great potential for the development of new materials. Ultimately, future research would work towards the practical application of these membranes to provide separate chemical environments for donor and acceptor pairs allowing for transmission of electrons from one side to the other. A proposed apparatus is shown in Figure 6.6.

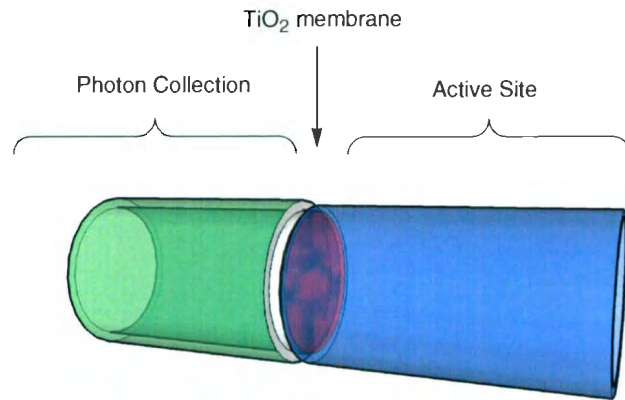


Figure 6.6: Proposed application of TiO₂/Nafion[®] membranes.

Chapter 7

Conclusions and Future Work

Chapter 7: Conclusions and Future Work

7.1 Introduction

The results of this project are categorized into two broad themes: photoinitiated catalysis and materials engineering. Much of the work reported here represents the initial investigations for the Thompson research group of Memorial University of Newfoundland into biomimetic catalysis using surface attachment on TiO_2 . Refinement of these experiments and extension of the results beyond proof-of-concept is needed. This final Chapter will briefly summarize some of the achievements from each research phase along with specific areas that hold potential for further investigation.

7.2 Conclusions and Future Work

7.2.1 Phase 1: Nanocrystalline Materials

For the preparation of the nanoscale anatase TiO_2 a well-established hydrolytic preparation was compared to a relatively new approach using a nonhydrolytic synthesis. Both methods presented positives and negatives. Hydrolytic synthesis provided high yields of stable anatase TiO_2 but this product was only dispersible in aqueous media. Nonhydrolytic routes held promise for organic solubility but were accompanied by extremely volatile reaction conditions that provided low yields of an unstable product. While hydrolytically-prepared $\text{TiO}_2(\text{OH})_n$ was ultimately chosen for the remaining phases a substantial amount of information regarding the surface science of $\text{TiO}_2(\text{X})_n$ was provided through analysis of Colvin's reported synthesis.

Nanoscale anatase TiO_2 was prepared in relatively high quantities through the hydrolysis of titanium(IV) isopropoxide. Further treatment of the solid in a vacuum desiccator proved useful in addressing the issue of residual nitric acid, used to lower the pH of the reaction solution. TiO_2 prepared via this approach was used in the preparation of porphyrin/metal oxide assemblies and proof-of-concept experiments for photo-induced biomimetic oxygen insertion. Hydrolytically-prepared TiO_2 was also utilized in the fabrication of free-standing membranes. Without the success of the reaction on larger scales the production of membranes through a primarily trial-and-error approach would not have been possible. Current research within the Thompson group is focusing on the use of ^1H NMR spectroscopy for the further characterization of surface hydroxyl groups on hydrolytic TiO_2 and the exchangeability of these protons.

In the beginning stages of this project a large amount of time and resources were dedicated to the production of TiO_2 using Colvin's nonhydrolytic approach. Refinement of experimental details was the initial focus, followed by isolation techniques and characterization of the product. The goal of much of the characterization was to determine if the TiO_2 is produced without hydroxyl capping agents and if this is maintained following isolation from solution. While these goals were achieved, many questions remained. Evidence was found for the presence of chloride capping agents, but it is still possible that TOPO may be coordinated to the surface, as well. The solubility reported by Colvin was lost following extraction of the $\text{TiO}_2(\text{X})_n$ from the reaction mixture and degradation was evidenced by the progression of the white precipitate to form a back solid, after isolation. Exploration into the susceptibility of the isolated

material to the adsorption of atmospheric water would prove useful in dictating further required isolation procedures and the experimental techniques required to increase the usefulness of this approach.

Modification of capping agents on the surface of colloidal TiO_2 was also attempted, but did not prove successful. Nonetheless, the replacement of the hydroxyl surface groups with simple compounds holds potential as a relatively simple approach to control the colloid-solvent interactions that dictate solubility. These concepts were only briefly addressed within this project, as the attachment of larger porphyrin molecules achieved solubility in organic media. Interconversion of these capping agents may allow for solubility in other more volatile organic solvents which would greatly simplify extraction and analytic methods.

Valuable information was gained about the fabrication of these materials and their resulting surface structures.

7.2.2 Phase 2: Surface Derivatization of TiO_2

Using hydrolytically- and nonhydrolytically-prepared TiO_2 in both colloidal and film forms several new materials were prepared and characterized. 9-Anthracene-carboxylic acid was attached to the surface of TiO_2 prepared using Colvin's procedures. This combination was also used to probe the usefulness of ^1H NMR spectra as an analytical tool to probe the surface-substrate interface with good results. Methods were developed for the tethering of protoporphyrin IX and hemin chloride to the surface of

colloidal hydrolytic TiO₂. UV-VIS, IR, and Emission/Excitation spectroscopy were used to analyze the assemblies. In addition, novel ¹H NMR spectra of these assemblies were obtained. Dispersion of the assemblies in organic solvent was also achieved, highlighting the importance of surface groups in dictating the solvent interactions of TiO₂.

One of the main omissions from this thesis is the study of the excited-state dynamics of these porphyrin/TiO₂ assemblies due to instrumentation difficulties at the time of research. Since then, these assemblies have been characterized using further emission/excitation and flash photolysis spectroscopy by Collier.⁹⁰ Flash photolysis experiments of the hemin chloride/TiO₂ assemblies prepared using the methods outlined here show evidence for injection and are consistent with the generation of an Fe(IV)=O radical cation, similar to Compound I.

¹H NMR spectroscopy results have shown the potential of this technique in probing the metal oxide substrate interactions. NMR spectroscopy of porphyrins, metallated or not, can be complicated in the best of circumstances. Adsorption of simpler molecules would allow for better identification of electronic effects, which will translate into a better understanding of signal chemical shifts within larger molecules. Many questions still remain as to the nature of the tethers, and the orientations with which the molecule attaches. The diagrams presented here generally show porphyrins attached at the carboxylic acid linkage and extending perpendicular to the colloid face. It is more likely that the porphyrins will exist in a bent conformation, parallel to the colloidal plane. There also exists a possibility of axial ligation between the Fe species and the surface of TiO₂. Collier⁹⁰ reports evidence for electron injection between iron(III) 5,10,15,20-

tetraphenyl-21H,23H-porphine and TiO_2 , for which a tethering carboxylic group or otherwise does not exist. It was proposed that the attachment occurs via a Fe-O-Ti linkage. The possibility exists with the assemblies described here that both the carboxylate and iron linkages may be present simultaneously. Additional work is needed to determine these possibilities.

Furthermore, the results reported here are primarily qualitative in nature. Focus was placed on the development of procedures to prepare and isolate the assemblies. As mentioned previously, the loading densities of the chromophores on the surface of the metal oxides have not been examined quantitatively. The importance of these groups in determining the solvent interactions has been demonstrated. The specific density threshold required to achieve solubility is unknown. In catalytic applications, there may be an optimum surface concentration. It is not known if an excess of dye on the surface may actually interfere with the catalytic activity of the assemblies.

Aside from porphyrin-based assemblies, the development of new materials for extended charge separation is one avenue of interest that can utilize many of the techniques developed here. Figure 3.1 briefly introduced this concept of building polymer-type linkages between several TiO_2 colloids. The mobility of the colloidal approach is one benefit over the more popular film-based techniques currently published in the literature.

7.2.3 Phase 3: Biomimetic Catalysis

The primary goal of this project, to accomplish photo-induced oxygen insertion using iron porphyrins attached to the surface of nanoscale titanium(IV) dioxide, was achieved and verified using GC-FID and GC-MS. Both colloidal- and film-based approaches were used. From initial experiments, these processes did not prove to be catalytic in nature. Degradation of the porphyrin/metal oxide resulted following irradiation with both broad-band irradiation and Soret band excitation.

It is important to note that these experiments represent the first steps towards biomimetic catalysis. Now that evidence has been shown that the reaction can proceed using these materials, future work will focus on refinement of reaction conditions. Catalytic activity may be possible with the introduction of a sacrificial acceptor, either in solution or adsorbed to the surface. Variations in solvent, substrate and other variables may lead to more success. Evidence has been provided for the formation of oxygenated products, but further work is needed to isolate these products and determine the actual yields. Ultimately, upon further advancements, focus will shift toward the elucidation of mechanistic pathways and reaction orientations. Many questions also remain as to the role of the oxygen source. In these experiments, H₂O was assumed to be the oxygen supply, while molecular oxygen was not specifically excluded from the reaction mixtures. Increasing the availability of O₂ within the reaction mixture may promote a mechanism that more closely mirrors that of P450 and HRP.

As previously discussed, TiO₂ acts as an electron-acceptor and an immobilizer to prevent the formation of μ -oxo dimers that may result after excitation of the porphyrins.

Given the work reported in Chapter 1 and published by Nocera *et al.*,⁷⁸ whereby pacman porphyrins are cleaved by light, consideration should be given to utilizing these dimers instead of working to prevent them. Cleavage is seen following absorption of a photon to yield Fe(IV)=O and Fe(II) on the separated porphyrins. Figure 7.1 below demonstrates how the μ -oxo dimers may be incorporated into the catalyst.

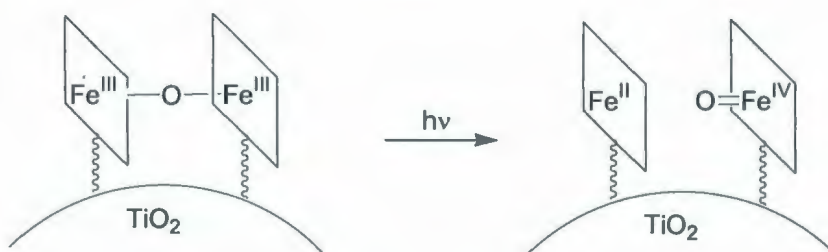


Figure 7.1: Incorporation of μ -oxo porphyrin dimers onto the surface of TiO_2

Formation of the dimers followed by attachment to the surface of TiO_2 with irradiation may actually prove to be more of a benefit than a hindrance as initially thought. Coordination of molecular oxygen to the remaining Fe(II) may possibly yield an additional species capable of oxygen insertion. The use of these dimers may also prevent axial ligation of the iron centers to the surface of TiO_2 .

These initial experiments represent the starting point for the development of nanoscale assemblies for catalytic oxygen insertion. Ongoing study has the potential to diverge into many different pathways. It was the purpose of this research to show that potential and provide a foundation on which further work can be built.

7.2.4 Phase 4: Self-Supporting TiO₂ Membranes

The final phase of this project deviated somewhat from the first three. Mechanical in nature, the development of macroscopic free-standing TiO₂ membranes using hydrolytically-prepared nanoscale TiO₂ posed some interesting challenges. With an approach similar to that used in the preparation of KBr pellets used for IR spectroscopy, preliminary membranes proved to be too fragile. Through much trial and error, the incorporation of a Nafion112[®] film with Carbowax[®] on a single side of the membrane using increased heat and pressure proved to be an excellent combination to produce TiO₂ membranes with enough structural integrity to be used in practical application. Furthermore, surface derivatization of a single side of the membranes was demonstrated using several simple techniques.

Continuation of this research would first involve further characterization of the physical and chemical properties of these membranes. SEM would yield a clearer picture of the surface of the membranes. While it is assumed that these membranes retain the photochemical properties of nanoscale TiO₂ verification of this fact would need to be assessed through evaluation of the membranes' electrochemical properties.

Surface derivatization of a single side has been demonstrated. A similar procedure used on the alternate face of the TiO₂ membrane may allow for attachment of a different donor or acceptor molecule. The integration of Nafion[®] on one side lends support to the membranes but it is unclear as to the influence this film will have on the adsorption of molecules to the surface. Nafion[®] does exhibit permeability but it may yet pose an obstacle. The use of this material was limited to its structural features. Further

assessment of its impact on the TiO₂ will need to be performed. As mentioned in Chapter 6, studies have demonstrated that Nafion[®] can enhance the photochemical activity of TiO₂. It is not clear what impact it will have in the surface sensitization of the metal oxide.

Once dual surface sensitization has been achieved, the work of Fitzmaurice *et al.*⁴⁹ or similar should be repeated to determine if these membranes exhibit the ability to mediate transmembrane electron transfer between molecules on opposing faces. If this can be completed, the development of apparatus similar to that schematically shown as Figure 6.6 in order to allow for distinctly different chemical environments for the donor and acceptor molecules can proceed. From that point, an almost limitless combination of possibilities for further photochemical activity exists. The light-harvesting array can be fine-tuned to allow for optimum efficiency in the conversion of light to electrons while the active site on the adjacent side of the membrane can be adjusted to suit the chemical application required. Ultimately, these materials would separate the current dependencies which surface-sensitized metal oxides have, whereby the chromophore is the active site.

References

- (1) Trentler, T.; Denler, T.; Bertone, J.; Agrawal, A.; Colvin, V. *J. Am. Chem. Soc.* **1999**, *121*, 1613-1614.
- (2) Renz, Carl. *Helv. Chim. Acta* **1921**, *4*, 961-968.
- (3) Dubrovinsky, L.S., *Nature* **2001**, *410*, 653-654.
- (4) Pang, C.; Lindsay, R.; Thornton, G. *Chem. Soc. Rev.* **2008**, *37*, 2328-2353.
- (5) Diebold, U. *Sur. Sci. Rep.* **2003**, *48*, 53-229.
- (6) Liu, S.; Gan, L.; Liu, L.; Zhang, W.; Zeng, H. *Chem. Mater.* **2002**, *14*, 1391-1397.
- (7) Cozzoli, P.; Kornowski, A.; Weller, H. *J. Am. Chem. Soc.* **2003**, *125*, 14539-14548.
- (8) Arabatzis, I.; Falaras, P. *Nano Lett.* **2003**, *3*, 249-251.
- (9) Linsebigler, A.; Lu, G.; Yates, J. *Chem. Rev.* **1995**, *95*, 735-758.
- (10) Fox, M.; Nosaka, Y. *J. Phys. Chem.* **1988**, *92*, 1893-1897.
- (11) Graetzel, M.; Hagfeldt, A. *Chem. Rev.* **1995**, *95*, 49-68.
- (12) Kittel, C. *Introduction to Solid State Physics* John Wiley & Sons, Inc.: New York, NY **1996**, 202.
- (13) Rothenberger, G.; Moser, J.; Graetzel, M.; Serpone, N.; Sharma, D. *J. Am. Chem. Soc.* **1985**, *107*, 8054-8059.
- (14) Gopel, W.; Rucker, G. *Phys. Rev. B.* **1983**, *28*, 3427-3438.
- (15) Bahnemann, D.; Hilgendorff, M.; Memming, R. *J. Phys. Chem. B.* **1997**, *101*, 4265-4275.
- (16) Zhang, J. *J. Phys. Chem. B.* **2000**, *104*, 7239-7253.
- (17) Thompson, T.; Yates, J. *Chem. Rev.*, **2006**, *106*, 4428-4453.
- (18) Bullen, H.; Garrett, S. *Surfactant Science Series* **2003**, *108*, 255-274.

- (19) Guth, T.; Schrauzer, G. *J. Am. Chem. Soc.* **1977**, *99*, 7189-7193.
- (20) Bard, A. *J. Phys. Chem.* **1982**, *86*, 172-177.; *J. Photochem.* **1979**, *10*, 59-75.; *Science* **1980**, *207*, 139-144.
- (21) Choi W. *Catal. Surv. Asia*, **2006**, *10*, 16-28.
- (22) Bahnemann, D.; Hoffmann, M.; Martin, S., Wonyong, C. *Chem. Rev.*, **1995**, *95*, 69-96.
- (23) Taoda, H. *Res. Chem. Intermed.* **2008**, *34*, 417-426.
- (24) Adams, D.; Brus, L.; Chidsey, C.; Creager, S.; Creutz, C.; Kagan, C.; Kamat, P.; Lieberman, M.; Lindsay, S.; Marcus, R.; Metzger, R.; Michel-Beyerle, M.; Miller, J.; Newton, M.; Rolison, D.; Sankey, O.; Schanze, K.; Yardley, J.; Zhu, X. *J. Phys. Chem. B* **2003**, *107*, 6668-6697.
- (25) Ernstorger, R.; Gundlach, L; Willig, F. *Prog. Surf. Sci.* **2007**, *82*, 355-377.
- (26) Graetzel, M.; O'Regan, B. *Nature* **1991**, *353*, 737-740.
- (27) Gerfin, T., Graetzel, M., Walder, L. in *Molecular Level Artificial Photosynthetic Materials, Progress in Inorganic Chemistry*; Meyer, G.J.(Ed); Karlin, K. (Ed); John Wiley & Sons, Inc.: New York, NY **1997**, *44*.
- (28) Chen, L.; Nedeljkovic, J.; Poluektov, O.; Rajh, T.; Thurnauer, M. *J. Phys. Chem. B.* **1999**, *103*, 3515-3519.
- (29) Lowell, D.; Konovalova, T. *J. Phys. Chem. B* **1999**, *103*, 4672-4677.
- (30) Blackbourn, R.; Hupp, J.; Johnson, C. *J. Am. Chem. Soc.* **1991**, *131*, 1060-1062.
- (31) Hupp, J.; Lemon, B. *J. Phys. Chem. B* **1999**, *103*, 3797-3799.
- (32) Curtiss, L.; Dimitrijevic, N.; Liu, J.; Rajh, T.; Saponjic, Z.; Scherer, N.; Turnauer, M.; Vega-Arroyo, M.; Zapol, P. *Nano Letters* **2004**, *4*, 1017-1023
- (33) Boschloo, G.; Goossens, A.; Koehorst, R.; Savenije, T.; Schaafsma, T. *J. Phys. Chem. B* **2000**, *104*, 2371-2377.
- (34) Lindstrom, C.; Zhu, X. *Chem. Rev.* **2006**, *106*, 4281-4300.

- (35) Ardo, S.; Meyer, G. *Chem. Soc. Rev.* **2009**, *38*, 115-164.
- (36) Burrell, A.; Campbell, W.; Jolley, K.; Officer, D. *Coord. Chem. Rev.* **2004**, *248*, 1363-1379.
- (37) Ito, T.; Meyer, G.; Obare, S. *J. Am. Chem. Soc.* **2006**, *128*, 712-713.
- (38) Meyer, G.; Pinlac, R.; Stromberg, J.; Wnuk, J. *Nano Letters* **2006**, *6*, 1284-1286.
- (39) Iseda, K.; Hayashi, E.; Kato, K.; Tanemura, S.; Taoda, H.; Watanabe, T. *Proceedings of the Fifth International Symposium on New Glass* **1995**, 143-146.
- (40) Cheuk, K.; Daoud, W.; Leung, S.; Tung, W.; Qi, K.; Xin, J. *Chem. Mater.* **2008**, *20*, 1242-1244.
- (41) Anderson, M.; Giselman, M.; Xu, Q. *J. Membr. Sci.* **1988**, *39*, 243-258.
- (42) Anderson, M.; Hill, C.; Moosemiller, M. *Sep. Sci. Tech.* **1989**, *24*, 641-657.
- (43) Anderson, M.; Qunyin, X. *J. Mater. Res.* **1991**, *6*, 1073-1081.
- (44) Agoudjil, N.; Benkacem, T. *Desalination*, **2007**, *206*, 531-537
- (45) Du, A.; Leckie, J.; Lee, P.; Sun, D.; Zhang, X. *J. Membr. Sci.* **2008**, *313*, 44-51.
- (46) Porter, J.; Zhaung, S. *Desalin.*, **1996**, *107*, 203-215.
- (47) Fujishima, A.; Honda, K. *Nature* **1972**, *238*, 37-38.
- (48) D'Arcangelis, S.; Farzad, F.; Heimer, T.; Meyer, G.; Stipkala, J. *Inorg. Chem.* **1996**, *35*, 5319-5324.
- (49) Fitzmaurice, D.; Hoyle, R.; Sotomayor, J.; Will, G. *J Phys. Chem. B* **1997**, *101*, 10791-10800.; Fitzmaurice, D.; Hoyle, R.; Sotomayor, J.; Will, G. *J. Mat. Chem.* **1998**, *8*, 105-110.
- (50) Klingenberg, M. *Arch. Biochem. Biophys.* **1958**, *75*, 376-386.
- (51) Planche, L. *Bull. Pharmacie* **1810**, *2*, 578-580.

- (52) Gajhede, M.; Messerschmidt, A, *et al.* (eds.) *Handbook of Metalloproteins* **2001**, *1*, 195-210.
- (53) Veitch, N. *Phytochem.* **2004**, *65*, 249-259.
- (54) Omura, T. *Biochem. Biophys. Res. Commun.* **1999**, *266*, 690-698.
- (55) Ortiz de Montellano, P. (Ed.) *Cytochrome P450: Structure, Mechanism, and Biochemistry* **2005** NY: Kluwer Academic/Plenum Publishers
- (56) Lewis, D. *Guide to Cytochromes P450: Structure and Function* **2001** NY: CRC Press
- (57) Denisov, I.; Markris, T.; Sligar, S.; Schlichting, I. *Chem. Rev.*, **2005**, *105*, 2253-2278.
- (58) Mittler, R. *Trends Plant Sci.* **2002**, *7*, 405-410.
- (59) Garcia-Canovas, F.; Gilabert M.; Rodriguez-Lopez J.; Thorneley R.; Tudela J. *Biochem.* **2000**, *39*, 13201-13209.
- (60) Iwaki, M.; Rich, P. *Biochem. (Moscow)*, **2007**, *72*, 1047-1055.
- (61) Han, X.; Peng, B.; Xu, S. *Biosens. Bioelec.* **2007**, *22*, 1807-1810.
- (62) Kimura, T.; Kobayashi, S.; Minoru, N.; Schapp, A. *Biochem.* **1987**, *26*, 5019-5022.
- (63) Kuo, J.; Ortiz de Montellano, P.; Savenkova, M. *Biochem.* **1998**, *37*, 10828-10836.
- (64) Ortiz de Monetallano, P.; Ozaki, S. *J. Am. Chem. Soc.* **1995**, *117*, 7056-7064.
- (65) Hayasaka, S.; Konuma, M.; Ozaki, S.; Watanabe, S. *Chem. Commun.* **2001**, 1654-1655.
- (66) Arimoto, R. *Curr. Top. Med. Chem.* **2006**, *6*, 1609-1618.
- (67) Coon, M.; Hollenberg, P.; Newcomb, M. *Arch. Biochem. Biophys.* **2003**, *409*, 72-79.
- (68) Groves, J. *Inorg Biochem.* **2006**, *100*, 434-447.

- (69) Groves, J.; Ortiz de Montellano, P. (Ed.) *Cytochrome P450: Structure, Mechanism, and Biochemistry* **2005** NY: Kluwer Academic/Plenum Publishers
- (70) Filatov, M.; Schroder, H.; Schwarz, H.; Shaik, S. *Chem. Eur. J.* **1998**, *4*, 193-199.
- (71) Groves, J.; Myers, R.; Nemo, T. *J. Am. Chem. Soc.* **1979**, *101*, 1032-1033.
- (72) Brauman, J.; Collman, J.; Lee, V.; Uffelman, E.; Zhang, X. *Science*, **1993**, *261*, 1404-1411.
- (73) Claude, C.; Wagenknecht, H.; Woggon, W. *J. Inorg. Biochem.* **2001**, *83*, 289-300.
- (74) Leifels, T.; Meyer, D.; Sbaragli, L.; Woggon, W. *Biochem. Biophys. Res. Comm.*, **2005**, *338*, 372-377.
- (75) Berzins, A.; Cannon, J.; Chang, C.; Geibel, J.; Mincey, T.; Traylor, T. *J. Am. Chem. Soc.* **1979**, *101*, 6716-6731.
- (76) Harris, D. *Curr. Opin. Chem. Bio.* **2001**, *5*, 724-735.
- (77) Visser, S. *J. Biol. Inorg. Chem.* **2006**, *11*, 168-178.
- (78) Chang, L.; Nocera, D.; Pistorio, B.; Rosenthal, J. *J. Org. Chem.* **2005**, *70*, 1885-1888.
- (79) Gray, H.; Low, D.; Winkler, J. *J. Am. Chem. Soc.* **1996**, *118*, 117-120.
- (80) Berglund, J.; Gray, H.; Pascher, T.; Winkler, J. *J. Am. Chem. Soc.* **1997**, *119*, 2464-2469.
- (81) Bilio, A.; Cohen, M.; Farmer, P.; Gray, H.; Immoos, C.; Van der Veer, W. *Inorg. Chem.* **2004**, *43*, 3593-3596.
- (82) Peterson, J.; Smith, T.; Thordarson, P. *Chem. Comm.* **2007**, 1899-1901.
- (83) Asbury, J.; Hirendra, G.; Lian, T. *J. Phys. Chem. B* **1998**, *102*, 6482-6486.
- (84) Smith, K. *Porphyrins and Metalloporphyrins* **1975**, 835, Elsevier Scientific Pub. Co., New York.

- (85) Bawendi, M.; Murray, C.B.; Norris, D. J. *J. Am. Chem. Soc.* **1993**, *115*, 8706-8715.
- (86) Vioux, A. *Chem. Mater.* **1997**, *9*, 694-698.
- (87) Michael Hughes, D.W. Thompson Research Group, Unpublished
- (88) Anderson, N.; Asbury, J.; Hao, E.; Lian, T. *J. Phys. Chem. B* **2002**, *106*, 10191-10198.
- (89) Jenene Roberts, D.W. Thompson Research Group, Unpublished
- (90) Collier, A. *B. Sc. (Hons) Thesis*, Memorial University of Newfoundland, St. John's, NL, Canada, 2007
- (91) CS Chem3D Ultra, v. 7.0.0, CambridgeSoft Corporation, 2001.
- (92) Jmol: an open-source Java viewer for chemical structures in 3D.
<http://www.jmol.org/>
- (93) Alben, J. *Infrared Spectroscopy of Porphyrins*, Academic Press, Amsterdam, **1978**, 323.
- (94) Guillard, R. (Ed); Kadish, K. (Ed) ; Smith, K. (Eds) *The Porphyrin Handbook: Volume 5*, Academic Press, NY **2000**.
- (95) Budd, D.; Langry, K.; La Mar, G.; Nayyir-Mazhir, R.; Smith, K. *J. Am. Chem. Soc.* **1979**, *101*, 6091-6096.
- (96) Anderson, R.; Chatfield, M.; La Mar, G.; Licoccia, S.; Mansfield, K.; Smith, K. *J. Am. Chem. Soc.* **1989**, *111*, 6087-6093.
- (97) Walker, A. in *The Porphyrin Handbook: Volume 5*, Guillard, R. (Ed); Kadish, K. (Ed) ; Smith, K. (Eds), Academic Press, NY **2000**, 81-184.
- (98) Dougherty, T. (Ed); Henderson B. (Ed) *Photodynamic Therapy* Marcel Dekker Inc., NY **1992**, 1-15.
- (99) Tanaka, K.; Vohra, M. *Environ. Sci. Technol.* **2001**, *35*, 411-415.
- (100) D'Arcangelis, S.; Farzad, F.; Heimer, T.; Meyer, G.; Stipkala, J. *Inorg. Chem.* **1996**, *35*, 5319-5324.

- (101) Anderson, M.; Graetzel, M.; Moser, J.; O'Regan, B. *J. Phys. Chem.* **1990**, *94*, 8720-8726.



